Carbon Nanotube Thin Films: Fabrication, Properties, and Applications

Liangbing Hu,* David S. Hecht, and George Grüner*

Department of Physics, University of California Los Angeles, Los Angeles, California 90095

Received September 2, 2009

Contents

1. Introduction

Nanoscale materials, defined as having at least one dimension less than 100 nm, have received steadily growing interest due to their unique properties and application potential, oftentimes superior to their bulk counterparts. Typical examples include zero-dimensional nanoparticles,[1] one-dimensional nanowires,[2−7] and two-dimensional (2D) graphenes.[8−18] Because of the quantum confinement of electrons in one or more dimensions, novel electrical, optical, and magnetic properties can be achieved in nanostructures. Currently, carbon nanotubes (CNTs) hold the most promise among nanoscale materials. Nanotubes can be thought of as sheets of graphene bent into a cylindrical shape and exist both as a single-walled nanotube (SWCNT) and as a multiwalled nanotube (MWCNT). Depending on the chirality along the graphene sheet, either semiconducting or metallic electronic states are created.[10] Both experiments and theory have shown that SWCNTs possess high mobility (on the order of 100 000 $cm^2\ V^{-1}\ s^{-1}$),[19] high conductivity (up to 400 000 $S\ cm^{-1}$), and, for semiconducting nanotubes, tube diameter-dependent band gap ($E_{gap} \approx 1/R_{tube}$).[20,21]

Physical properties and device integration of individual nanoscale materials have been widely studied, while thin films of nanoscale materials is an emerging research area, with the advantage of statistical averaging for better reproducibility.[22] Collective behavior of nanostructures can provide unique physical properties and enhanced device performance. A 2D network, often referred to as a thin film, made of randomly distributed CNTs can be regarded as a novel material. Because of the mixture of metallic and

Liangbing Hu got his B.S. in applied physics from the University of Science and Technology of China (USTC) in 2002. He did his Ph.D. in experimental physics with Prof. George Gruner at UCLA, with focus on the charge transport and optoelectronic properties of carbon nanotube thin films. In 2006, he joined Unidym as a cofunding scientist. Unidym is a Bay Area startup company focusing on commercialization of transparent and conductive carbon nanotube thin films. At Unidym, Liangbing's role was mainly in the development of carbon nanotube ink, roll-to-roll coating, encapsulation and device integrations in touch panels, LCDs, flexible OLEDs, and printed solar cells. He has published over 30 papers in the carbon nanotube thin film area, and over 10 issued patent or patent applications. Currently, Liangbing is a postdoctoral research fellow with Prof. Yi Cui at Stanford University, focusing on nanomaterial and nanostructures for energy storage applications such as supercapacitors and Li-ion batteries.

* To whom correspondence should be addressed. E-mail: hlb@physics.ucla.edu (L.H.), gruner@physics.ucla.edu (G.G.).

10.1021/cr9002962
Published on Web 07/22/2010

David S. Hecht received his B.S. degree in physics from UCSD in 2001, and subsequently worked at Quantum Magnetics, developing sensitive biomedical and military magnetometers. He went on to do his M.S. and Ph.D. research at UCLA under Prof. George Gruner, studying the electro-optic properties of carbon nanotube films, including a 3 month internship at the IPRI in Wollongong, Australia. Following his graduation in 2007, David joined Unidym, a Bay Area startup company, as a cofounding scientist. At Unidym, David is commercializing a roll-to-roll printed CNT film on plastic as an ITO replacement for touch panels, LCDs, EPDs, solar cells, and OLEDs.

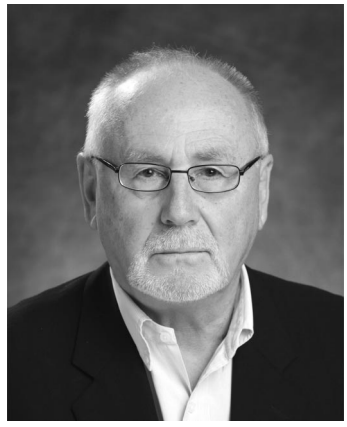

George Gruner is Distinguished Professor of Physics at the University of California Los Angeles. He has published over 400 papers and two books. He is one of the most highly cited scientists worldwide. He has more than 30 patent applications to his credit, and has launched and has been involved in several startup companies. His current interests focus on energy-related applications of nanotechnology.

semiconducting nanotubes, CNT thin films show a semiconductor−metal transition as the film thickness increases.[23,24] There are numerous studies on nanotube thin films and device applications. For example, CNT thin films with density close to the percolation threshold show semiconductor behavior and can be used as the active layer in thin film transistors and sensors.[7,25−30] Films with thickness in the range of 10−100 nm show high optical transparency and electrical conductivity and can be used as a replacement for indium−tin−oxide (ITO) electrodes.[7,31−38] Micrometer-thick CNT films are nanoporous and used as electrodes for supercapacitors, fuel cells, and battery applications.[39−50] Research focus and specific applications depend on the nanotube density, as listed in Figure 1. In this Review, a nanotube thin film is defined as a random or oriented network with nanotubes as the major component. More specifically, the nanotubes are laid horizontally on the surface of a substrate. Films of vertically oriented nanotubes or nanotube composites are not covered in this Review.

In the first section, we will focus on nanotube thin film fabrication methods. Chemical vapor deposition (CVD) growth and solution-based coating methods are discussed. In the second section, we review several patterning methods such as plasma etching, PDMS stamp patterning, and laser ablation. We will also discuss the chemical doping and engineering of CNT films. In the third section, we review extensively the electronic, optoelectronic, transport, and mechanical properties of nanotube thin films. In the last section, we will review the device applications of nanotube thin films as electronic materials in three major application areas including thin film transistors, transparent electrodes, and as nanoporous electrodes for energy storage.

2. Fabrication of Carbon Nanotube Thin Films

2.1. Direct Growth

CNTs have been produced by three major methods: arc-discharge, laser ablation, and chemical vapor deposition (CVD). There has been substantial research regarding CNT synthesis, purification, and characterization.[3,28,51−58] CVD is the most common method for direct growth of CNT thin films. In the CVD method, catalyst nanoparticles on substrates are used as seeds for CNT growth. The key parameters that control the growth kinetics are the hydrocarbon carrier gas, the growth time and temperature, and the catalyst composition. Although vertically aligned CNTs have unique properties and device applications, such as in field emission devices and supercapacitors,[51,59−62] they will not be covered in this Review. CVD can grow CNT films either randomly distributed or aligned. Aligned nanotubes are useful for high mobility devices and molecular electronics where control over positioning is important. Aligned CNT films can be fabricated using patterned catalysts, electric or magnetic fields during the CVD process, directional gas flow, or use of a substrate with defined lattice structure .[3,57,63−65] Zhou et al. demonstrated CVD grown CNTs aligned on sapphire or silicon substrates (Figure 2a).[65] Recently, Baughman et al. reported a novel, simple, and scalable process to draw aligned CNT films from vertically aligned forests (Figure 2b).[66] Devices with aligned CNT film components have poor statistical reproducibility. On the other hand, films with randomly distributed CNTs are more reproducible and are more practical for applications (Figure 2c).[67] The density of CNT thin films is critical for device applications due to the mixture of metallic and semiconducting CNTs. For example, the density needs to be above, but close to, the percolation threshold for CNT thin film transistors. Slight changes in tube density in these films can dramatically affect the on/off ratio. The CVD method can produce macroscopic quantities of CNTs or submonolayer densities. The density is normally controlled by the catalyst density and growth time. As compared to a solution-based process, the direct growth method leads to films with individually separated tubes with fewer defects and better CNT−CNT contact, which leads to highly conductive films. Figure 2d shows a comparison between transparent electrodes made using either CVD grown films or solution fabricated films. The performance for direct CVD grown films is based on the reported sheet resistance (R_s) and film surface coverage. However, films directly grown on a substrate may have significant amounts of residual catalyst, imprecise density control, and substrate incompatibility for device integration. Furthermore, CVD is a high vacuum, high temperature process and is not

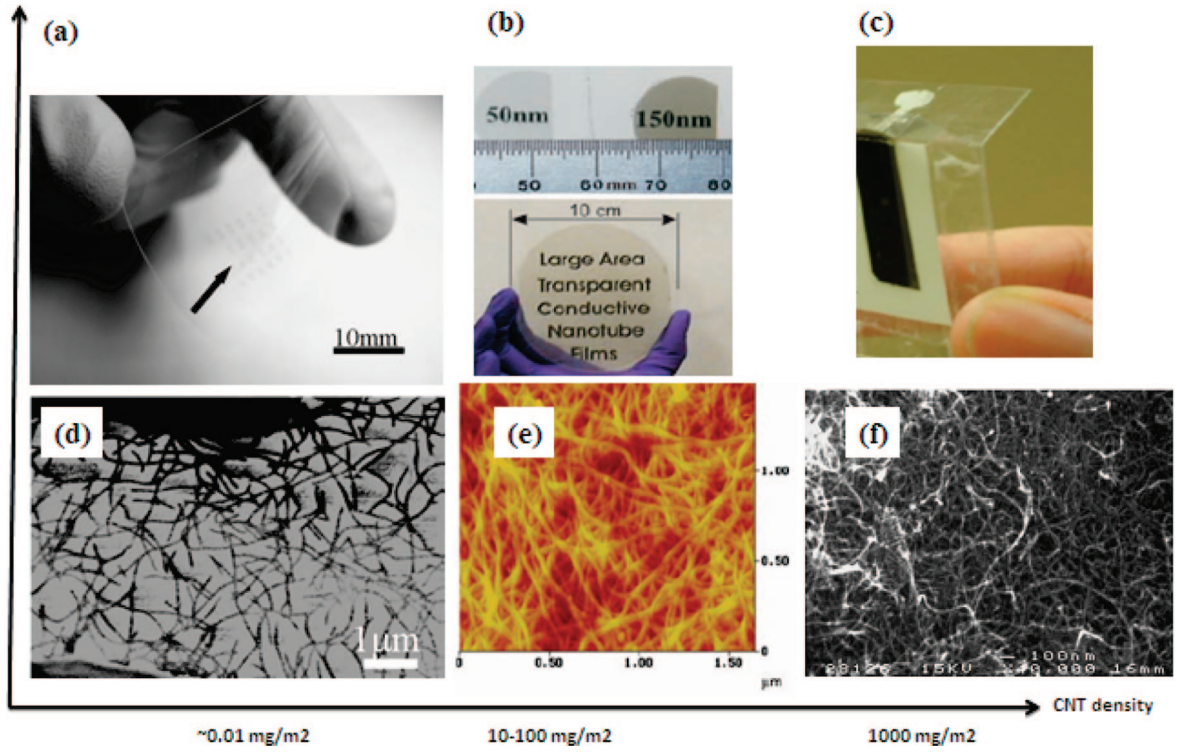

Figure 1. CNT thin films and their application in three different density regions. (Reprinted with permission from refs 156 and 317. Copyright 2006 Wiley-VCH Verlag, American Institute of Physics, and Science.) (a) CNT thin film transistor on plastic substrate. (b) Transparent and conductive CNT film on glass substrate. (c) A plastic supercapacitor with porous CNT electrode. (d) Scanning electron microscope (SEM) of percolating CNT network in (a). (e) Atomic force microscope (AFM) image of transparent CNT film in (b). (f) SEM of porous CNT films for supercapacitor devices.

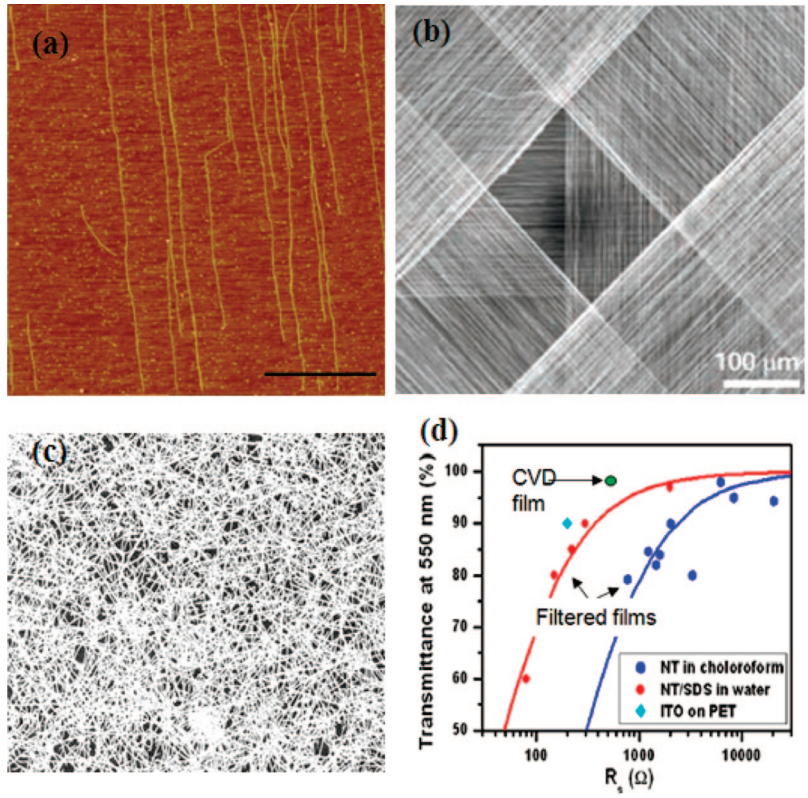

Figure 2. (a) Aligned CNTs on an *a*-plane sapphire substrate. (b) Aligned CNT film by a simple and scalable draw process. (c) Randomly oriented CNT thin film as transparent electrode. (d) Performance comparison between films made by direct CVD growth and films made using two solution-based processes. The direct CVD method leads to transparent and conductive film with better performance. (Reprinted with permission from refs 65 and 66. Copyright 2006 American Chemical Society and 2005 Science, respectively.)

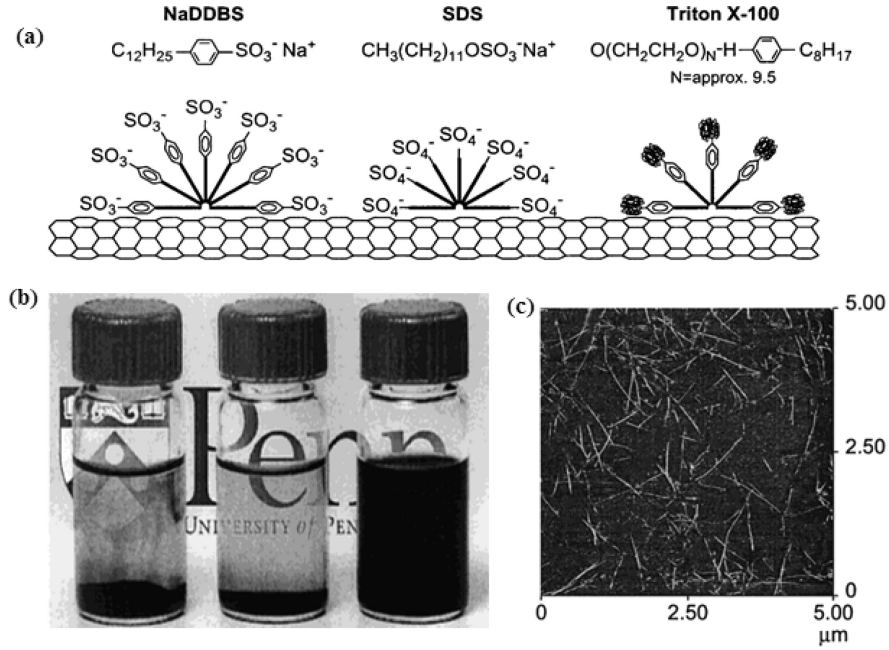

Figure 3. (a) Schematic representation of how surfactants may adsorb onto the nanotube surfaces. (b) 6 mL vials containing aqueous dispersion of SDS-HiPCO (0.5 mg/mL), Triton X-100-HiPCO (0.8 mg/mL), and NaDDBS- HiPCO (20 mg/mL). (c) Tapping mode AFM image of Triton X-100-stabilized CNTs on a silicon surface. (Reprinted with permission from ref 70. Copyright 2003 American Chemical Society.)

compatible with substrates used in the emerging plastic electronics field.

2.2. Solution-Based Deposition

Recently, solution-based film coatings have found widespread interest in both industry and academia. As compared to direct growth methods for film deposition, a solution-based process has several advantages. It is a low temperature (<100 °C) process, compatible with plastic substrates; it does not need a high-vacuum system, which reduces costs significantly; and the deposition occurs at high speeds up to 200 ft/min using roll-to-roll techniques. For CNT thin film applications, significant work has been published. To achieve CNT thin films with high conductivity, several factors are crucial: CNT material quality, CNT ink stability and degree of CNT dispersion, choice and surface activation of substrate, coating and drying details, removal of dispersion aids after coating, and incorporation of additional binder materials to improve the adhesion and stability. In this section, we will review the extensive work in CNT solution preparation, rheological properties, and various film deposition methods.

2.2.1. Nanotube Dispersion

Because of their large aspect ratio, CNTs are subject to large van der Waals forces, which cause them to stick together, forming large bundles (often referred to as ropes). Therefore, one of the major challenges in fabricating a CNT film is to separate the tubes, without using covalent chemistries or other harsh conditions, which could lower their electrical conductivity. While there has been tremendous research and several reviews on the dispersion of CNTs, here we focus on CNT dispersion methods that enable thin film fabrication. We divide the CNT dispersion work into four major categories: (1) surfactant as dispersion aids (including anionic, cationic, and nonionic surfactants); (2) polymers as dispersion aids; (3) direct dispersion of pristine or functionalized CNTs in organic solvents and water; and (4) other dispersion aids such as DNA, protein, and starch. In general, dispersion aids should be removed after coating due to their insulating nature. This can be difficult because often materials that are best at separating CNTs are those that interact most strongly with the tubes and are therefore most difficult to remove. Direction dispersion in solvent avoids the need to remove dispersion aids; however, it normally leads to much larger bundles, especially for high CNT concentrations.

Using surfactant to disperse CNTs for film fabrication is the most widely used route due to its ability to individualize CNTs at high concentrations, and its ability to be rinsed off in subsequent washing of the film.[34,68−72] Also, most surfactants are water-soluble, leading to aqueous-based CNT dispersions. This is important for fields such as biochemistry and biomedical engineering, in which organic solvents cannot be used due to incompatibilities with living organisms. To avoid affecting the inherent electrical, mechanical, and chemical properties of CNTs, surface functionalization through chemical bonds is not preferred; fortunately, surfactants interact noncovalently with CNTs. There are three classes of surfactants: anionic (negative charge in water), cationic (positive charge in water), and nonionic (neutrally charged in water). The hydrophobic end of a surfactant will attach to CNTs, while the hydrophilic end helps pull the CNTs into solvents such as water. It has been found that the π-like stacking of benzene rings benefits the binding of surfactant and CNTs. The headgroup, chain length, and surfactant weight are found to affect the dispersion ability of the surfactant. Among surfactants, Triton X-100, sodium dodecyl sulfate (SDS), and sodium dodecylbenzene sulfonate (NaDDBS) are the most widely studied (pioneered by A. G. Yodh et al.).[70] Figure 3 shows a schematic representation of how surfactants may adsorb onto the nanotube surface. The CNT stabilization depends on the surfactant molecules that lie on the tube surface parallel to the cylindrical axis. These surfactants lead to a high fraction of individualized CNTs after dispersion, resulting in higher CNT film conductivity. In particular, NaDDBS leads to 63% individual CNTs in

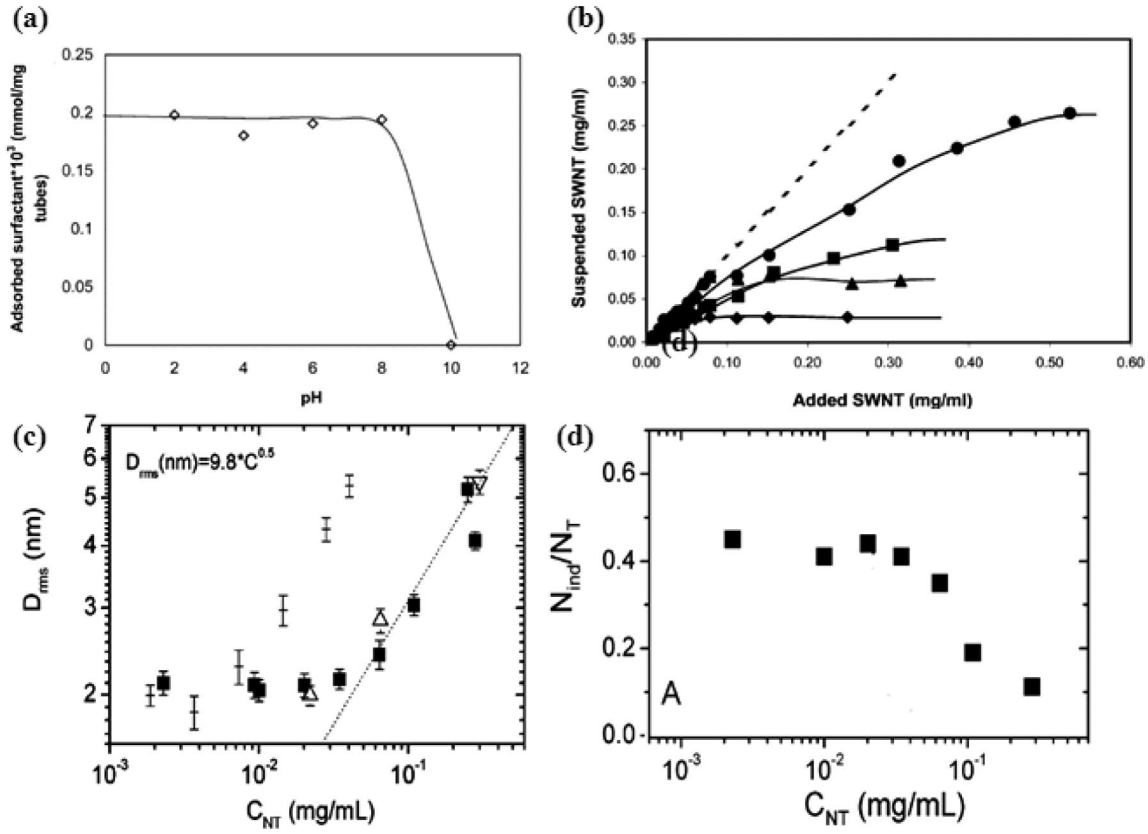

Figure 4. (a) Effect of pH on adsorption of NaDDBS on CNTs at 0.025 cmc. (b) Concentration of suspended CNTs at various initial CNT concentrations for various NaDDBS concentrations and sonication times (◆, 0.1 cmc with 1 min sonication; ▲, 1.0 cmc with 1 min sonication; ■, 0.1 cmc with 20 min sonication; and ●, 1.0 cmc with 20 min sonication). (Reprinted with permission from ref 69. Copyright 2003 American Chemistry Society.) (c) The measured diameter distributions (D_{rms}), plotted against CNT concentration. (d) The number fraction of individual CNTs vs CNT concentration. (Reprinted with permission from ref 74. Copyright 2003 American Chemistry Society.)

solution at concentrations up to 20 mg/mL (measured by AFM scans on films drop cast onto silicon from solution). Figure 3 also shows vials containing aqueous dispersion of SDS, Triton X-100, and NaDDBS with CNTs.

Resasco et al.[69] and Yodh et al.[70] have extensively studied the interaction between surfactants and CNTs. The phenomenon depends on the chemical characteristics of CNTs, the surfactant, and the solvent nature. The major forces are the Coulombic attraction between the charged surfactant heads, the hydrophobic bonding between the surfactant tails and the CNT surface, and the CNT−aromatic ring interactions. Therefore, understanding the surface charge of CNTs is important for studying their interactions with surfactants. There are three states for surfactants in dispersions: free surfactant, micelles, and adsorbed onto CNTs. The absorption of surfactant onto a CNT surface depends on the surfactant, CNT concentration, and the system charge nature (pH value). Resasco et al. proposed that initially surfactant lies parallel to the surface, and as the surface coverage increases, but before forming a monolayer, the surfactant molecules stand up in a "tails on" configuration until the adsorption reaches equilibrium. The absorption of surfactants on the CNT surface highly depends on the pH values (Figure 4a), the sonication time, and the surfactant critical micelle concentration (cmc). They also optimized the use of surfactant by determining the minimum concentration needed to suspend a given fraction of CNTs under different sonication conditions and CNT concentrations. Achieving individualized CNTs is critical for surfactant-based dispersions, because the electronic performance of films highly depends on the bundling of CNTs. For example, for thin film transistors using a CNT film as the semiconductor layer, bundling of CNTs will cause a gate screening effect by metallic CNTs in the bundle. For transparent conductors using CNTs, high conductivity is important. For bundles of CNTs, electric current only flows on the outermost tubes in a bundle, while the inner tubes do not contribute significantly to the current.[73] Coleman et al. used an AFM to analyze the percentage of individual CNTs in a dispersion.[74] They found that the percentage of individual CNTs depends on the concentration, with the average bundle diameter (D_{rms}) $\approx$ 2 nm for concentrations of $C_{NT} < 0.05$ mg/mL. The number of bundles and bundle size in solution increases with increasing concentration (Figure 4c). The fraction of individualized CNTs decreases with concentration. CNTs tend to bundle together at higher concentrations (Figure 4d). A typical CNT concentration in surfactant is <1 mg/mL for most studies.

Sonication is required for surfactant-assisted CNT dispersion. Dispersion occurs by the formation of gaps or spaces at the bundle ends in the high shear environment of the ultrasonicated solution.[68,75] The adsorbed surfactant diffuses into this space along the bundle length, thereby separating the CNTs. Figure 5a shows this "unzipping" mechanism.[73,76] The characteristic time for the "unzipping" process is estimated on the basis of the surfactant adsorption rate, the CNT length, and the surfactant headgroup effective area to be approximately 1 s. The initial activation via sonication is rate limiting, and the latter "unzipping" process proceeds relatively much faster. Of course, sonication will generate heat in the solution and increase the temperature dramatically, which can affect the dynamics of the unzipping process or the ultrasonic acoustics; therefore, temperature control is

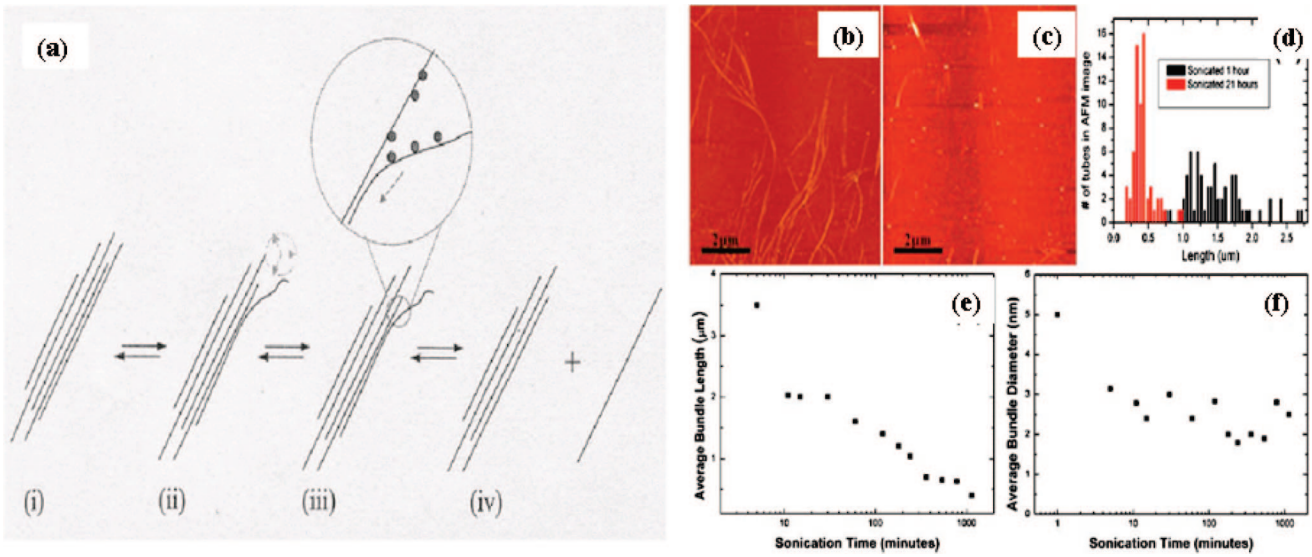

Figure 5. (a) Proposed mechanism of CNT isolation from bundles (i). Ultrasonic processing "frays" the bundle end (ii), which then becomes a site for additional surfactant adsorption. This latter process continues in an "unzippering" fashion (iii) that terminates with the release of an isolated, surfactant-coated CNT in solution (iv). (Reprinted with permission from ref 75. Copyright 2003 American Scientific Publishers.) (b−f) Effect of sonication time on CNT bundle length and diameter. (b,c) AFM of CNTs adsorbed on silicon wafers after 1 and 21 h of sonication time. (c) Histogram of bundle length distribution taken from several AFM images. (d) Plot of average bundle length and (e) average bundle diameter for various sonication times as measured from AFM images.[33] (Reprinted with permission from ref 33. Copyright 2006 American Institute of Physics.)

important. Sonication can also damage nanotubes by causing defects on the ends and the walls of CNTs and even cutting the tubes.[3] The defects and shortening of tubes can dramatically decrease the conductivity of final films. Figure 6b−f shows that the CNT length varies with sonication time.[33] Here, a 300 W probe sonicator is used on 50 mL of CNT solution with arc discharge CNTs and SDS surfactant. The length of the tubes decreases exponentially with sonication time from 4 μm initially, to 0.4 μm after about 21 h of sonication, and the diameter of the bundles decreases sharply from 5 to 3 nm in the first 5 min of sonication, and then remains constant between 2 and 3 nm subsequently.[33] The optimal sonication time depends on the CNT preparation and functionalization, the surfactant choice, CNT and surfactant concentration, the sonication power and amplitude, solution volume and temperature, and pH value.[77]

Bundling dynamics of CNT aqueous suspensions with 1% SDS have been investigated by a simple optical method based on the absorption of monochromatic light.[78] The resonant scattering of CNT bundles exhibits signature peaks. The bundling phenomenon happens immediately after termination of sonication and continues to increase for up to ~10 h. Figure 6a shows the schematic of the measurement setup used to monitor this bundling process with three laser beams at different vertical positions in the CNT dispersion. The diameter of the bundle size is calculated on the basis of the absorption of the dispersion and Mie scattering theory. Figure 6b shows that the bundling process occurs quickly and steadily for up to 10 h after sonication, and the bundles eventually reach almost micrometer sizes. Another method for studying bundling effects in CNT solutions is to take aliquots and deposit them on a flat silicon or mica substrate for AFM imaging. AFM images of the CNT diameter size from the sample solution at different times can indicate bundling dynamics.[70] Because individual CNTs are desired for high conductivity CNT films, one has to consider this bundling effect. Shortening the time between solution preparation and film fabrication, or continued bath sonication of the CNT dispersion prior to deposition, will help prevent bundling of CNTs in solution. Formulation parameters such as temperature, pH, and additives would also influence the dispersion stability. For example, it has been found that the stability of the dispersion is largely determined by the electrostatic repulsion due to the surface charge.[34]

The ζ-potential, an abbreviation for electrokinetic potential in a colloidal system, is the potential difference between the dispersion medium and the stationary layer of fluid. Because it is a good measure of colloidal stability, different ionic surfactants can be evaluated for their ability to stabilize CNTs in solution. Herman et al.[79] and Haddon et al.[34] have studied the charge distribution and zeta potential of CNT dispersions, particularly for surfactant-assisted dispersions. Positively charged CNTs are obtained by wrapping with the cationic surfactant cetyl trimethyl ammonium bromide (CTAB) and nearly neutral tubes are obtained by wrapping CNTs with nonionic surfactants such as Triton X-100. Figure 6c shows the variation of the ζ-potential distribution of SDS-solubilized nanotubes with SDS concentration. With increasing amounts of SDS, more SDS is adsorbed onto the nanotube sidewalls. The ζ-potential increases with SDS concentration until a value of about −80.3 mV is reached at 1.5% SDS concentration. Figure 6d plots the conductivity of the nanotube solution as a function of the SDS concentration. The solution conductivity monotonically increases with the surfactant concentrations. Therefore, the ζ-potential distribution varies with the surfactant type (Figure 6e). Also, the packing of surfactants on SWCNT sidewalls (and thus the net charge of the SWCNT) can be tuned by varying the length of the surfactant alkyl chain (Figure 6f). Understanding the ζ-potential dependence on surfactant type and concentration will lead to improvements in dispersion quality and stability.

The evaluation of dispersion quality relies on optical probing of dispersions or CNT film examination post deposition. A desired dispersion has individualized CNTs or small bundle sizes. Individualized CNTs have sharp optical transitions, which can be probed spectroscopically. Absorption in the visible and near IR range, along with Raman and

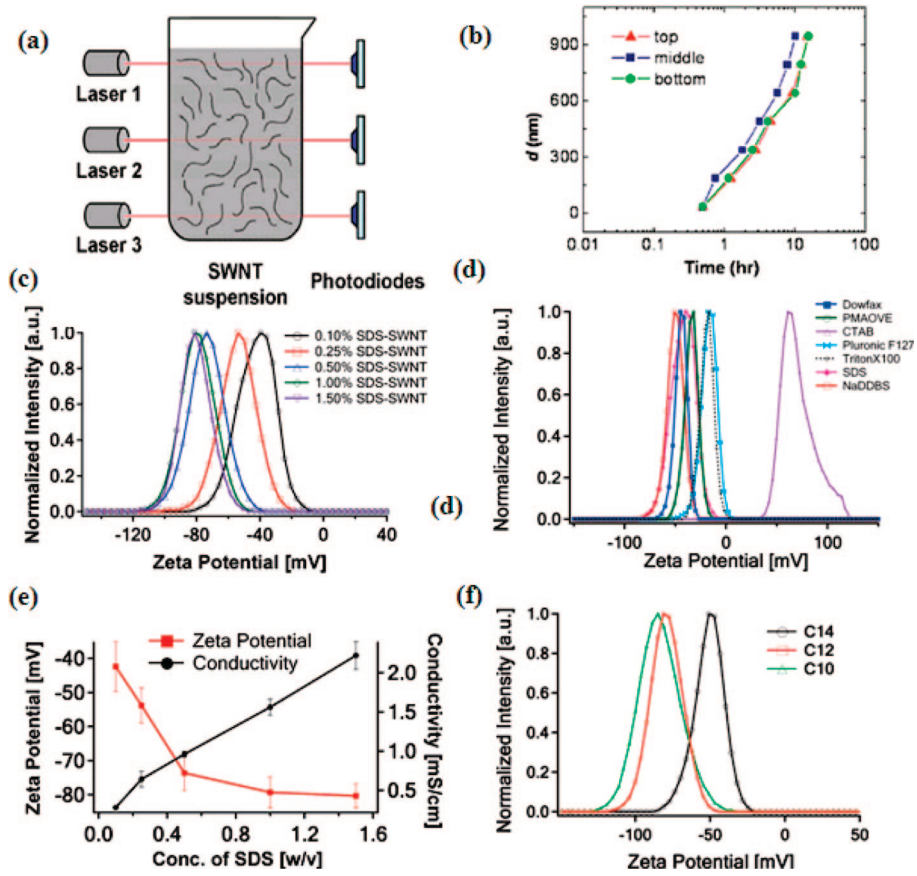

Figure 6. (a) Schematic of the measurement apparatus. The laser wavelength is 655 nm. Measured absorbance of CNT suspension at three different levels as a function of time after termination of the sonication. (b) Bundle diameter as a function of time. (Reprinted with permission from ref 78. Copyright 2007 American Institute of Physics.) (c) The ζ-potential distribution of SDS-wrapped CNTs for different anionic surfactant SDS concentrations. (d) Plot of the peak maximum of the ζ-potential distribution and the conductivity of the CNT solutions vs SDS concentration. (e) The ζ-potential distribution curves for individualized CNT wrapped by different surfactants. (f) The ζ-potential as a function of chain length for sodium alkyl sulfates with 10, 12, and 14 carbon atoms. (Reprinted with permission from ref 79. Copyright 2008 American Chemistry Society.)

fluorescence spectroscopy, are often used to characterize the dispersion quality.[3,34,68−70,72,74,76−81]

CNT dispersions can also be made without surfactant, using organic solvents.[47,74,82−92] One advantage of dispersing tubes without surfactant is to minimize unwanted residue in the fabricated film. The study of solvent-based dispersions focuses on both pristine and functionalized CNTs. There are at least two competitive forces involved: (1) the attractive van der Waals forces between CNTs and (2) the interactions between CNT bundles and the solvent. Hansen solubility parameters are useful in explaining the dispersion state. Because CNT surfaces are nonpolar and hydrophobic, the principal factor determining the dispersion states of CNTs in solvents is the individual Hanson parameters rather than the total Hanson parameter. The individual Hanson parameters include the dispersion component (δ_d), the polar component (δ_p), and the hydrogen-bonding component (δ_h).[34] Chung et al. related the Hansen solubility parameters of various solvents to their ability to disperse CNTs (Table 1).[34] *N*,*N*′-Dimethylformamide, chloroform, and 1-methyl-2-pyrrolidone lead to good CNT dispersions. Chung's results indicate that the solubility does not depend on the total solubility parameter (δ_t) of the solvent, because solvents with the same δ_t show different dispersion states. They found that the individual Hansen solubility parameters rather than the total solubility parameter explain the interactions between CNTs and solvents. The significance of each component depends on the CNT material preparation and purification. For example, acid refluxed CNTs with −COOH groups can be dispersed in butanol/toluene and xylene/ethanol mixtures, which are knows to be poor solvents for pristine CNTs.[40] In a separate study by Tour et al., they found that the best solvents for dispersing CNTs were 1,2-dichorobenzene (95 mg/L), chloroform (31 mg/L), and *N*-methylpyrrolidinone (10 mg/L).[93]

Polymer wrapping of pristine or functionalized CNTs is a common method for CNT dispersion, especially for CNT−polymer composite applications.[94−101] There are excellent reviews on this topic.[57,102] Polymers can assemble onto pristine CNTs through nondestructive $\pi-\pi$ interactions, which preserve the intrinsic properties of CNTs. The wrapping agents are typically conjugated polymers or pyrene containing polymers.[99,100,103] Surface functionalization of CNTs can selectively tune the interactions and guide the polymer coating on CNTs for specific applications. For CNT thin film applications, polymer-assisted dispersion is not preferred due to the large size of polymers and the difficulty in removing the polymers after film fabrication. Some methods have been proposed to remove polymers after CNT thin film coating such as annealing or unwrapping the polymers; however, these methods are not practical. For example, burning polymers requires high temperatures not compatible with plastic substrates. Because polymers are flexible, and the shape of the polymer in solution depends on the solvent and the pH value, interaction competition could lead to different wrapping scenarios.[94,97,104] Other

Table 1. Dispersion of CNTs in Various Solvents with Different Hansen Parameters[a]

organic solvents	δ_d ($MPa^{1/2}$)	δ_p ($MPa^{1/2}$)	δ_h ($MPa^{1/2}$)	δ_t ($MPa^{1/2}$)	molecular weight (g/mol)	structure	dispersion state
N,*N*′-dimethylformamide	17.4	13.7	11.3	24.8	73.10	$HCON(CH_3)_2$	dispersed
chloroform	17.8	3.1	5.7	19.0	119.38	$CHCl_3$	dispersed
1-methyl-2-pyrrolidone	18.0	12.3	7.2	22.9	99.13	$HN((CH_2)_3CO)$, cyclo	dispersed
2-propyl alcohol	15.8	6.1	16.4	23.5	60.10	$(CH_3)_2CHOH$	swollen
1-pentyl alcohol	16.0	4.5	13.9	21.7	88.15	$CH_3(CH_2)_4OH$	swollen
tetrahydrofuran	16.8	5.7	8.0	19.4	72.11	$(CH_2)_4O$, cyclo	swollen
toluene	18.0	1.4	2.0	18.2	92.14	$C_6H_5CH_3$	swollen
o-methoxyphenol	18.0	8.2	13.3	23.8	124.14	$2\text{-}(CH_3O)C_6H_4OH$	swollen
dichloromethane	18.2	6.3	6.1	20.3	84.93	CH_2Cl_2	swollen
benzene	18.4	0.0	2.0	18.6	78.11	C_6H_6	swollen
dimethyl sulfoxide	18.4	16.4	10.2	26.7	78.13	$(CH_3)_2SO$	swollen
styrene	18.6	1.0	4.1	19.0	104.15	$C_6H_5CH{=}CH_2$	swollen
methyl methacrylate	13.7	9.8	6.1	17.9	100.12	$H_2C{=}C(CH_3)CO_2CH_3$	sedimented
methanol	15.1	12.3	22.3	29.6	32.04	CH_3OH	sedimented
hexane	15.3	0.0	0.0	15.3	86.18	$CH_3(CH_2)_4CH_3$	sedimented
acetone	15.5	10.4	7.0	20.0	58.08	CH_3COCH_3	sedimented
water	15.6	16.0	42.3	47.8	18.02	H_2O	sedimented
ethanol	15.8	8.8	19.4	26.5	46.07	C_2H_5OH	sedimented
acrylonitrile	16.4	17.4	6.8	24.8	53.06	$H_2C{=}CHCN$	sedimented

[a] Reprinted with permission from ref 34. Copyright 2005 Elsevier.

materials have been studied for dispersing CNTs such as DNA and proteins (for biological applications) and Nafion (for biofuel cell applications).[63,105−108] Also, extremely functionalized CNTs can be dispersed in water, which is beneficial due to the environmentally friendly and biocompatible nature of water. Functionalization in extreme acids can generate enough functional groups to facilitate the solubility of CNTs in water.[102] However, dramatic amounts of induced defects and noncovalent functionalization hinder the intrinsic high mobility of carriers along CNTs, which is not preferred. DNA-assisted dispersion is of particular significance due to its biological implications. Well-resolved absorption peaks indicate individualized CNTs in dispersion.[108] DNA-based dispersion links one of the central molecules in biology to a technology very important to nanomaterials.

2.2.2. Rheological Properties

For solution-based thin film fabrication, rheology is crucial. For different coating methods, the solution viscosity requirements are quite different. Air turbulence introduced by high web speeds and possible mechanical jitter during roll-to-roll coating could cause film uniformity problems during the film drying process. The liquid thin film is exposed to various stresses, which can induce secondary flows leading to contact line recession, film thinning, and rupture. To avoid these problems, the viscosity should exceed a certain lower limit. Surface tension is another critical solution parameter for coating. For example, in the Mayer rod drawdown method where a CNT ink is coating a PET surface, a surface tension lower than 35−40 mN/m and viscosity in the range of 0.01−1 Pa s at a typical coating speed of 2 cm/s and characteristic wavelength of 2 mm is required.[109] Roll-to-roll coating is well developed, and the rheology requirements are different for different coating methods.[110−115] Wetting agents can be used to lower the surface tension of inks to match the substrate surface energy, or viscosity additives used to increase the viscosity. The rheological properties of CNT dispersions, especially for polymer-assisted dispersions with varying CNT loading, have been widely studied.[3,45,57,116−118] Similar to the percolation-like behavior for electrical conductivity, the rheological properties show a dependence on CNT loading. There are more studies on the rheological properties of polymer-assisted CNT dispersions, but the focus is not for CNT thin film fabrication. Pasquali et al. discuss CNT thin film fabrication-related studies of CNT dispersions.[119,120] In this study, mixtures of NaDDBS and Triton-X 100 are used to tune viscosity (Figure 7a). Triton-X 100, a nonionic surfactant, was found to dramatically increase the viscosity of the NaDDBS-based CNT inks. The authors proposed possible explanations on the basis of similar prior observations in closely related systems. The addition of a neutral or oppositely charged surfactant or salt to another pure surfactant solution raises the viscosity significantly.[121,122] There has been significant work on dispersion agents to enhance CNT coating.[115] These coating agents can tune the dynamic viscosity and the contact angle to achieve better wetting. Another important property of dispersions is the surface tension, which will affect the interaction between CNTs and the substrate, the microstructure of the final CNT thin film, the drying process, and the washing for surfactant-assisted dispersions. Resasco et al. found that the surface tension increases with CNT concentration at lower NaDDBS concentration and decreases with increasing NaDDBS concentration (Figure 7b).[69] To optimize coating of CNT dispersions on substrates such as glass or plastic, one can either modify the substrate by chemical or plasma treatment to raise the surface energy or reformulate the CNT dispersion by adding additives to lower surface tension.

2.2.3. Coating Methods

Once a stable CNT dispersion is made, deposition of these tubes onto a substrate proves a significant challenge. As compared to direct CVD growth, solution-based deposition is preferred for obvious reasons. The low temperature process allows deposition onto arbitrary substrates, can be easily scaled to large areas, and no vacuum is needed, which significantly reduces cost. The basic concept of a solution-based deposition process is to uniformly lay down the CNT solution followed by uniformly drying the solution without causing agglomeration.[109] Therefore, solution/substrate interactions need to be considered. In some cases, an additional step of removing surfactant or polymer is necessary. There are numerous solution-based methods, which have been tried for CNT thin film deposition, as well as a short review on CNT assembly with a focus on direct CVD growth.[101] Here,

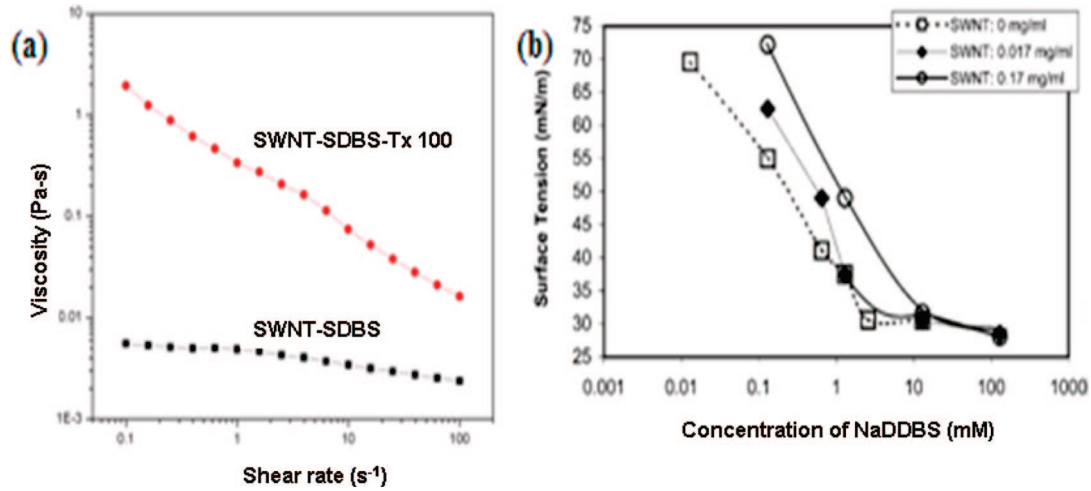

Figure 7. (a) Viscosity vs shear rate for CNT−NaDDBS dispersion and CNT−NaDDBS−TX100 dispersion. The CNT is 0.1 wt %, NaDDBS is 1 wt %, Triton X-100 is 3 wt %. (b) Surface tension measurement of NaDDBS solutions in the present of CNTs at 30 °C. (Reprinted with permission from refs 119 and 69. Copyright 2006 and 2003 American Chemical Society, respectively.)

we will discuss the principles of various methods with some detailed examples.

The "logs-on-a-river" concept, known as the "Langmuir−Blodgett (LB)" method, is based on the hydrophobic behavior of CNTs.[46,123,124] Good surface spreading of CNTs on water is the key. The deposition can be achieved in a layer-by-layer fashion through either a horizontal lifting or a vertical dipping method. Figure 8a shows the floating of CNTs on water. In this study by Matsumoto et al., a chloroform solution of CNTs (1 mg/50 mL) was spread on the surface of water. Quartz or glass substrates were used.[125] The surface was tuned hydrophilic by cleaning them in a KOH/ethanol solution and hydrophobic by dipping them in 1,1,1,3,3,3-hexamethyldisilazane. They found that both types of surfaces can be used to obtain uniform deposition; the hydrophobic surface tends to retain a better transfer ratio up to a larger number of deposition layers. As in the regular LB method for one-dimensional materials, the in-plane compression leads to a certain degree of orientation of the CNTs on the surface. Figure 8c shows the resulting films by two methods. Polarized UV−vis−NIR spectra show anisotropic absorption by aligned LB films. The LB method is extremely useful for fabricating monolayer or submonolayer films. However, for fabricating CNT thin films with more than a monolayer, the process is too slow. Gruner et al. have developed a method using the LB concept but combining it with the filtration method.[126] A CNT thin film is first deposited on a filter by a traditional filtration method.[127] CNTs are then floated off the filter, and the film is picked up by an arbitrary substrate. In this method, the CNTs are randomly distributed and the thickness of the film is easy to control, so the process is quick for generating thick CNT films. However, the control of the backfilling water is tricky, and the film integrity is easily broken when the process is not under good control. Also, the film fabrication area is limited to the size of the filtration assembly.

Self-assembly (SA) is a method to quickly and cheaply form thin films on a surface. SA depends on the interactions between the CNTs and the surface. Silane or polymer treatment of substrates helps the interactions between CNTs and the substrate.[128] When a substrate is placed in a dispersion, CNTs will randomly strike the surface and may or may not adhere depending on the chemical groups, which causes this process to be slow. This interaction can be guided by chemical preparation of CNTs or the surface, by charging the surface locally, or by microfluidic guidance.[51,57,129−137] Rao et al. uses molecular marks on a substrate to guide the self-assembly of individual CNTs. In the surface functionalization step, either polar chemical groups (such as amino ($-NH_2$) or carboxyl ($-COOH$)) or nonpolar groups (such as methyl ($-CH_3$)) can be used to modify the surface.[133] As the substrate is placed in the dispersion, CNTs are attracted toward the polar regions and self-assembled to form the prepatterned structures (Figure 8d). This process can be scaled up easily using a well-developed high throughput process such as photolithography, stamping, or, in the future, parallel dip-pen nanolithography. Another SA method is to charge the substrate and allow the Coulomb interactions to guide the assembly of CNTs onto the charged area.[134] The local surface potential strongly influences the deposition behavior, offering control over pattern resolution. The process is outlined in Figure 8e. In this study, 100 nm of poly(methyl methacrylate) (PMMA) on p-doped silicon wafers was used as electret layers. The CNTs deposited exclusively onto positively charged patterns on the sample, and the negatively charged patterns yielded no attachment of nanotubes. Although the position of SA is guided by electrostatic Coulomb forces, final attachment of particles is dominated by van der Waals forces. The apparent negative surface charge on the nanotubes presumably arises from the surfactant. Therefore, the choice of surfactant is critical for this process. Also, SA can lead to multilayer structures as well (Figure 8f and g).[137] The films are built with alternating layers of negatively charged CNTs and positively charged polyelectrolyte-poly(dimethyldiallylammoniumchloride) (PDDA). The growth of SWCNT thin films can be controlled at the nanometer scale.

Manohar et al. and Poa et al. have used dip coating methods to fabricate transparent and conductive CNT thin films on various substrates.[57,138] Dip coating is a simple process and provides great potential to scale up for large-scale coating. The pick-up of the solution depends on the solution viscosity, the interaction between substrate and the dispersion, and the coating speed. Afterward, the drying process is critical to achieve high-quality films. It has been shown that Triton X-100 leads to uniform CNT films via dip coating, while charged surfactants such as SDS, LDS, or CTAB do not yield highly uniform and or strongly adhering films on PET.[138] The substrate can be treated with

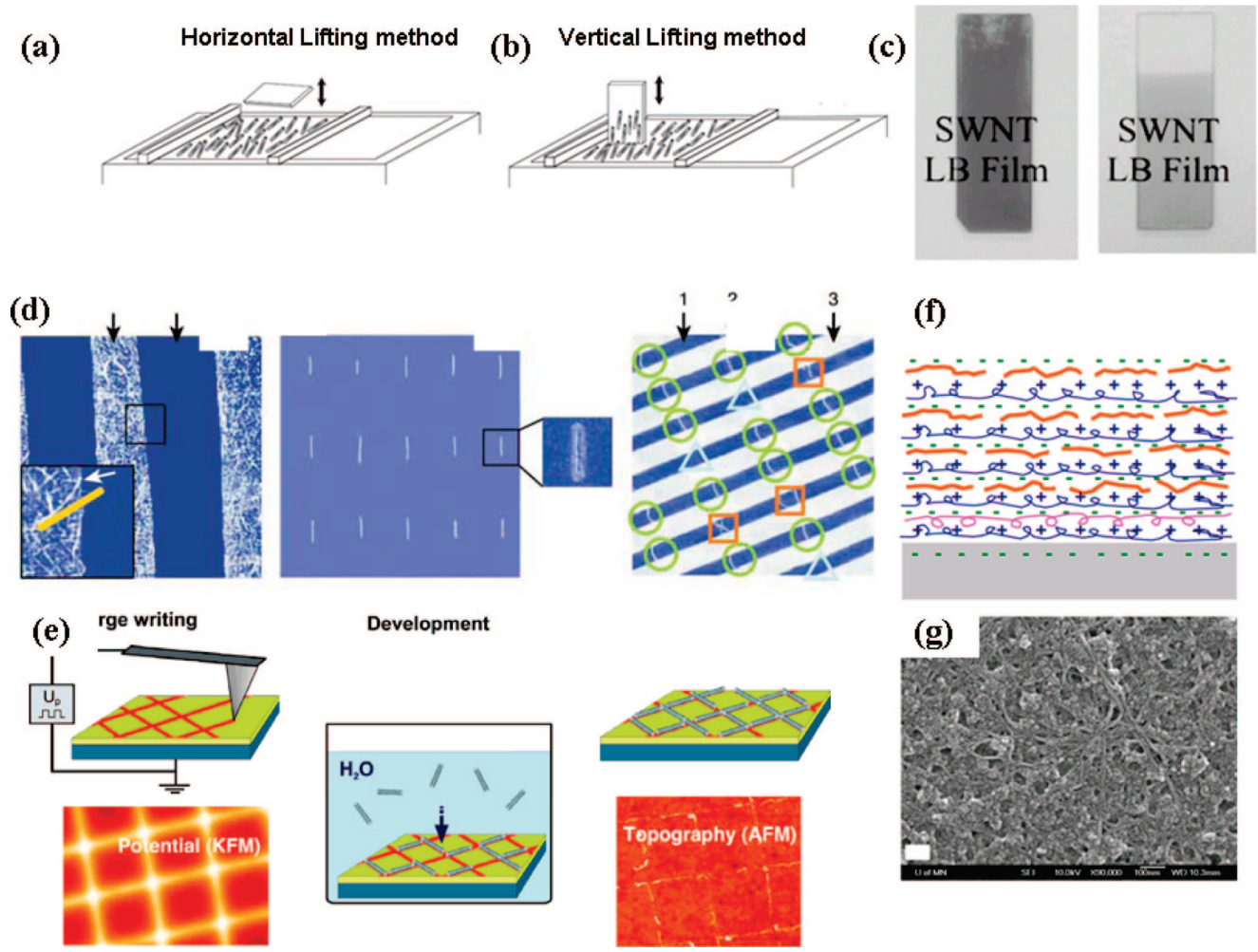

Figure 8. (a,b) Schematic illustration of the mechanism for the in-plane orientation of CNTs with horizontal lifting and vertical dipping. (c) Photographs of CNT film (b) with 140 layers and (c) with 58 layers. (Reprinted with permission from ref 125. Copyright 2004 Institute of Pure and Applied Physics.) (d) (Left) Atomic-force micrographs showing large-scale self-assembly of CNTs. (middle) Topography (30 μm^2) of an array of individual CNTs covering about 1 cm^2 of gold surface. (Right) Topography (20 μm^2) of an array of junctions with no CNTs (triangles), one CNT (circles), or two CNTs (squares). (Reprinted with permission from ref 133. Copyright 2004 Nature Publishing Group.) (e) (Left) Charge patterns are written into an electrets layer on a solid substrate through a conductive AFM tip. (Middle) The sample is immersed into an aqueous suspension to develop the charge patterns. (Right) CNTs are attached to the predefined pattern. (Reprinted with permission from ref 134. Copyright 2004 American Chemical Society.) (f) Structure of self-assembled CNT multilayer thin film on Si substrate. (g) SEM image of assembled CNTs. The sample contains five (PDDA/CNT) bilayers. (Reprinted with permission from ref 137. Copyright 2007 IOP Publishing Ltd.)

aminopropyltriethoxysilane (APTES) as an adhesion promoter. The thickness can be controlled by the concentration of the solution and the time of dip coating. Figure 9a is an SEM image of a CNT film on PET made by dip coating.[138] The immersion time is ~0.5 min, and air drying time is ~5 min. Using a line-patterning method with toner, a patterned film is generated (Figure 9b).[138] The choice of surfactant is critical for drying to avoid "coffee stain" ring patterns during the drying process.[109] One disadvantage of dip coating is that both sides of the substrate are coated, which may not be preferred for certain applications. Other coating methods include spin coating and drop casting where a high shear rate is involved. A small amount of solution is dropped onto a substrate followed by high-speed spinning of the substrate (spin coating), or simply air drying (drop casting). Spin coating is useful for generating submonolayer CNT films due to the low viscosity of CNT solutions. Rogers et al. found that the dual injection of Methanol effectively removes the surfactant during the spin coating process. Bao et al. found that the selective functionalization of a substrate with amine- and phenyl-terminated silanes can lead to selective deposition of either semiconducting or metallic CNTs. In the spin coating deposition process, aromatic molecules like phenyl-terminated silane interact and bind selectively to metallic SWCNTs. The thickness of the amine and phenyl surfaces, measured by ellipsometry, was 0.7 and 0.4 nm.[139] Spin coating is useful for making CNT films for thin film transistors using CNTs as the channel material.[22] However, the nonuniformity of CNT distribution along the radial direction may be a problem for scaling up this process. Lee et al. hasve managed to fabricate transparent and conductive CNT thin films using a spin coating method, with a thickness much greater than a monolayer. Dichloroethane is used, and it was found that good CNT dispersion is essential for making a transparent CNT film.[140] However, it is a multiple spin coating method and will not be easily scaled up. Drop casting followed by air drying is also used to deposit percolating networks for thin film transistor (TFT) applications.[141] The blow drying steps lead to a certain degree of tube alignment. Pan et al. have successfully made CNT electrodes for high power density device applications by controlling the liquid−substrate interface.[45] The choice of solvent is im-

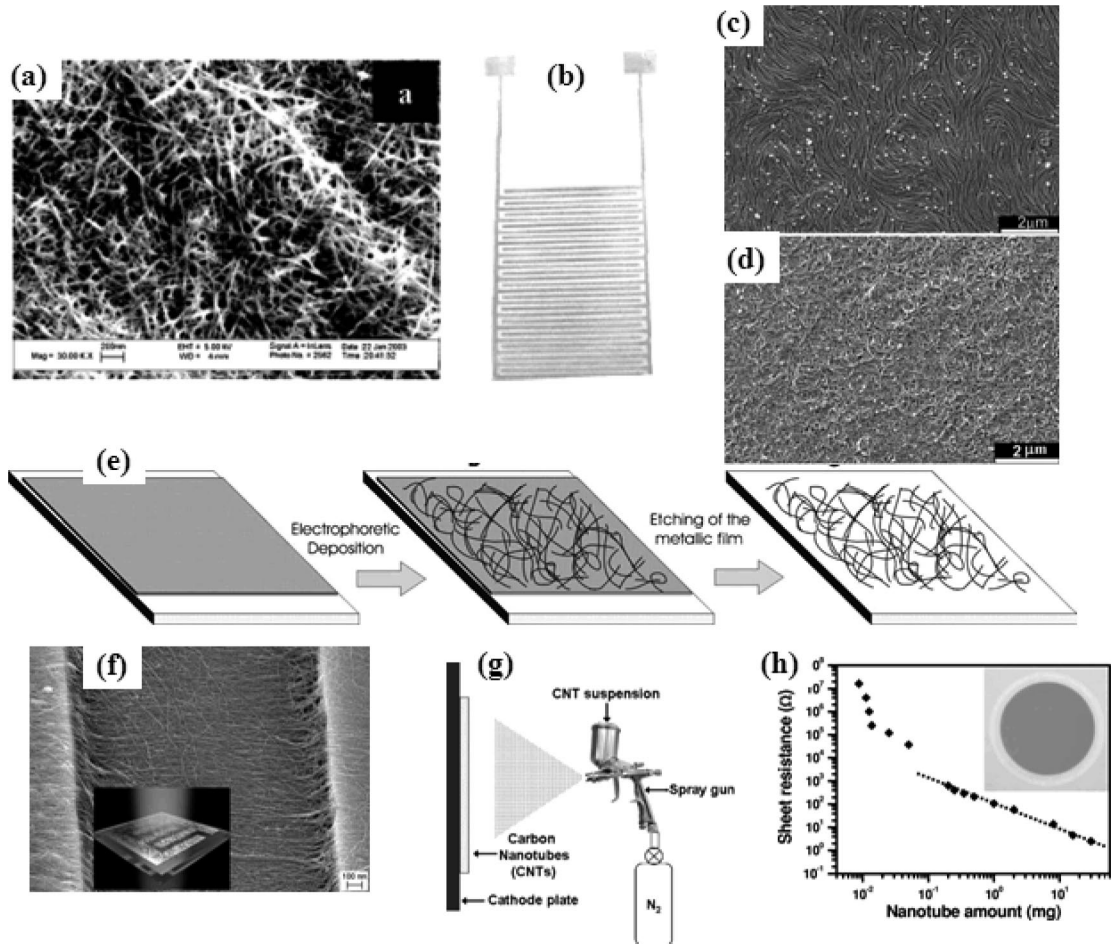

Figure 9. (a) SEM image of CNT film on PET substrate by dip coating method. (b) Patterned CNT lines with line-patterning method. (Reprinted with permission from ref 138. Copyright 2004 American Chemical Society.) SEM images showing the surfaces of CNT films prepared from suspensions using different solvents: (c) distilled water, (d) ethanol. (e) Schematic diagram of the technique: thermal deposition of the metallic layer, electrophoretic deposition of CNTs, and etching of the metallic film, necessary when titanium is used as the metallic coating. (Reprinted with permission from ref 145. Copyright 2008 Royal Society of Chemistry.) (f) SEM of a thin film on a quartz substrate by DEP. (Reprinted with permission from ref 146. Copyright 2006 Wiley-VCH Verlag.) (g) A spray coating setup. (h) The R_s vs CNT mass on a filter. The inset shows a picture of a coated CNT film on a 47 mm diameter alumina filter. (Reprinted with permission from ref 173. Copyright 2006 American Institute of Physics.)

portant for dip coating, and ethanol, water, and DMF have been tried. Figure 9c shows clear local alignment, as opposed to those in (d). It is speculated that the electrostatic repulsion between CNTs and the high concentration of CNT in dispersion are the reasons for forming the ordered structure of the thin film. During the drying process, the self-organization of CNTs in evaporating droplets can be complicated.[35,142,143] The wetting between liquid and substrate, the dynamics of the CNTs in suspension, and the surface tension change with drying time will lead to various types of films. For example, it was suggested that the organization of CNTs during evaporation is controlled by the aggregate hydrophobicity of the substrate. On hydrophobic substrates, the evaporation of SDS-SWCNT sessile drops proceeds through constant contact area. On hydrophilic substrates, nanotube aggregates in SDS-SWCNT dispersion stop the contact line from moving, resulting in the formation of "coffee stains".

Electrophoretic deposition (EPD) has also been used to deposit CNT thin films on conductive substrates.[144] The CNTs are locally charged, and so become polarized under a DC electric field. Recently, Roth et al. used an EPD process to deposit transparent CNT thin films onto an insulating substrate.[145] Figure 9e shows the process. The metallic layer is etched away after the deposition of the CNT thin film layer. This process allows continuous production of transparent CNT thin films for the production of large dimensions. Furthermore, it allows the deposition of patterned films by simply patterning the metallic layer. The CNTs only deposited on the conductive area. The typical deposition time is only a few seconds. The CNTs wrapped with surfactants and the CNTs functionalized with COOH groups acquire a negative charge in water and are attracted to the positive side of the electrode under a DC electric field. Another similar method is called dielectrophoresis (DEP), which uses an AC electric field.[136,146] DEP can allow the deposition and separation of CNTs at the same time. Figure 9f shows a CNT film by the DEP process. DEP relies on the motion of polarizable objects due to an external inhomogeneous electric field. In Figure 9f, the applied voltage is 20 V, the deposition time is 5 min, and the separation of the interdigitated figures is 1.8 μm. The SEM image also shows a good conformal coating of CNTs across the metal electrode. Spray coating is a simple and quick method to deposit CNT film. Several groups have been actively applying this method for making CNT thin films for different applications such as transistors, transparent electrodes, and field emission devices.[23,106,147−152] Figure 9g shows the setup for spray coating. Typically, the

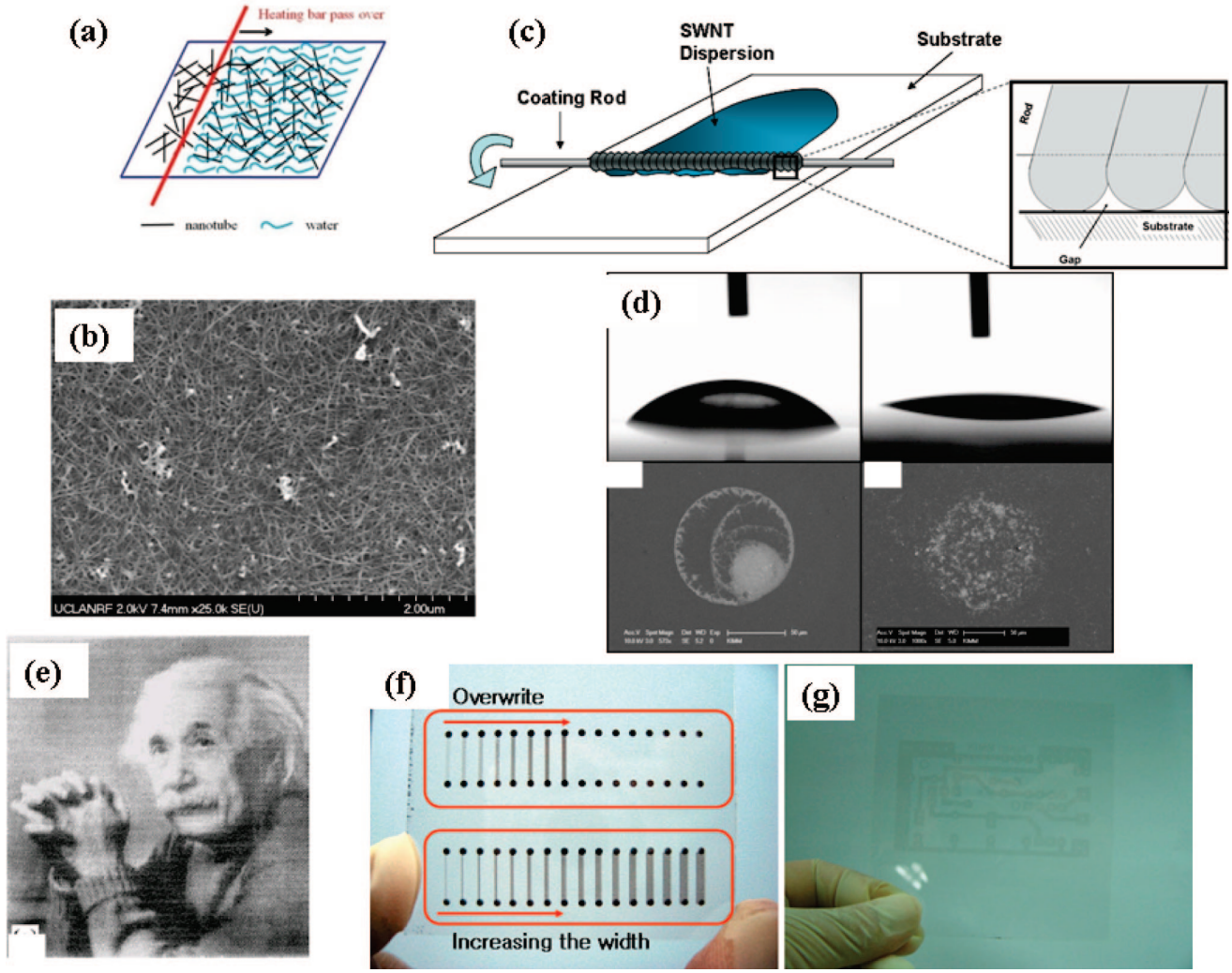

Figure 10. (a) Flash dry deposition scheme. As the heating bar passes the thin CNT liquid, it forces the evaporation of water and leaves the dry CNT and surfactant on the substrate. (b) SEM image of CNT thin film on PET substrate deposited with the flash dry deposition method. (Reprinted with permission from ref 155. Copyright 2009 Royal Society of Chemistry.) (c) Schematic illustration of a drawdown rod coater with a wire-wound Mayer coating rod. (Reprinted with permission from ref 119. Copyright 2009 American Chemical Society.) (d) Contact angle of droplets on (left) bare glass and (right) plasma-treat glass. (e) An SEM of inkjet printed CNTs on Xerox color copier paper. (f) Line images fabricated between Pt electrodes on a glass substrate. (g) The direct printing result of a sample circuit diagram on glass. (Reprinted with permission from ref 166. Copyright 2008 IOP Publishing Ltd.)

CNT ink is sprayed onto a heated substrate. The substrate is heated to 100 °C to facilitate the drying of the liquid. The set temperature for the substrate is adjusted by the choice of solvent. By using diluted solution and multiple spray coating steps, homogeneous films can be obtained. Bundling may happen during the drying process after the sprayed mist of CNT has hit the PET substrate. However, Roth et al. and our group found that there are some intrinsic problems with the spray coating method, especially for making thin CNT films with a small number of spraying steps. SEM images reveal micrometer-size inhomogeneity, which is due to the micrometer size of the CNT mist droplets that exit the spraying nozzle.[153−155] This effect is less dramatic for relatively thicker CNT films. Through multiple spray coating steps, the inhomogeneity of the film is averaged out. However, increasing the number of spraying steps with a less concentrated solution results in increased time and labor when scaled up, especially for transparent CNT film applications. This is not necessarily a problem for making submonolayer film for CNT TFT applications. Another advantage of spray coating is that the requirement for the surface tension of the CNT solution is not as stringent as other direct coating methods. The small amount of solution dries so fast that it does not allow enough time for dewetting. Therefore, some dispersions, for example, SDS-based dispersions, that cannot be dip-coated, can be spray-coated. Also, spray coating can be used for coating extremely rough surfaces. The filtration method involves vacuum filtering a dilute suspension of CNTs in a solvent over a porous filter membrane with pore size of 20−200 nm.[26,32,34] Filtration leads to highly uniform and reproducible films. Therefore, this method can be used as a quick QC method for evaluating CNT material and dispersion quality. Fabrication of CNT films using the filtration method has extremely precise control over density. Figure 9d shows a large range of R_s that can be achieved with a filtration setup by simply varying the solution density and the volume used. This method can be scaled up, with the availability of a large-scale filter. Large-scale filtration of CNT films has been demonstrated.[156] Because of the precise control of density, this method has been used to study physical properties such as percolation behavior, and the temperature- and frequency-dependent transport properties of CNT films. However, the CNT film fabricated by this method is on a filter substrate, which is

not an ideal substrate for device applications. A transfer step after the filtering is normally needed. There have been several methods that will be discussed to transfer the film.

The most widespread deposition method in industry involves depositing solution on a substrate by one of several methods (including Mayer Rod, Slot Die, and Gravure), followed by controlled drying.[57,119,155] In Figure 10a, the CNT dispersion with TX-100 surfactant is laid down on a substrate either by submersion or by Meyer rod, as in Figure 10c. A heating bar is used to control the drying process. The heating bar passes the liquid with a speed that allows the liquid to evaporate fully. As shown in Figure 10b, a uniform film is fabricated on a glass substrate. Figure 10c shows the details of the Mayer rod concept. The amount of liquid is controlled by the wire size that determines the gap spacing. Pasquali et al. have found that NaDDBS solutions do not lead to a uniform CNT film after drying, due possibly to its charging of the particulates in solution. Control over formulation details, such as the surface tension, and the ink/surface interactions, is crucial. This method can be easily scaled up using slot die, forward or reverse gravure, and other roll-to-roll techniques.[5,157] Inkjet printing is an old and popular technology due to its ability to print fine and easily controllable patterns, noncontact injection, solution saving, high repeatability, and scalability. It is very prevalent in printed electronics. Recently, there have been numerous reports about inkjet printing of CNTs.[7,25,86,108,158−165] Because of the promise of CNT networks for TFTs and transparent electrode applications using a solution-based process, there will be further study needed for inkjet printing of CNT films. In a typical ink jet printing process, the droplet size is around ~10 pL and, on the substrate, has a diameter of around 20−50 μm. Printing on paper is much easier than printing on a plastic or glass substrate, due to the high liquid absorption of the paper, which avoids the dewetting of the liquid on substrates. The liquid droplet and substrate interaction is crucial for uniform drying of the liquid. Figure 10d shows the dramatic effect of surface plasma treatment on the contact angle between the droplet and the substrate. Plasma treated substrates lead to much smaller contact angle and uniform drying without the "coffee ring" effect, as seen on the left side of Figure 10d.[166] Figure 10e shows a photograph of an inkjet printed image on paper,[159] and Figure 10f and g represents a circuit diagram composed of lines, curves, and circles, which are directly printed on glass.[166] Here, DMF is used as the solvent for dispersing CNTs. Han et al. also found that 60 °C is the most suitable for producing stable inkjetting and deposition of CNTs on the surface.[165] When the solution slowly dries at room temperature, it produces a "coffee ring" effect. Surfactant-based formulation normally leads to highly conductive films. There has been no effort on developing surfactant-based dispersions for the inkjet printing process yet.

Each of the above methods has its own advantages. The requirements for dispersion, substrate, volume, and ink−substrate interaction are different. For example, Mayer rod coating and dip coating have more stringent requirements for the dispersion rheology, while spray coating and filtration do not. Spin coating is valid for making submonolayer networks on rough surfaces, while filtration, Mayer rod coating, and inkjet printing can generate films with arbitrary thickness. The application of the liquid on substrates is different for different methods, and the drying fate of the liquid on substrate is crucial. The ability to scale up for manufacturing should also be considered for industrial application. Mayer rod coating, dip coating, and inkjet printing can reasonably lead to scaled CNT coatings, while spin coating and spraying are not compatible with existing scale-up processes, especially for large-scale plastic electronics.

2.3. Nanotube Thin Film Transfer

For many applications, the transfer of a CNT film from one substrate to another is required. For example, films made by the filtration method on filters could not be use for device applications. Therefore, it is necessary to transfer them from the filter to the target substrate. In addition, the transfer step can provide additional value such as patterning and alignment. Polydimethylsiloxane (PDMS)-based transfer is widely studied in the John Roger group, with a focus on transferring CVD grown CNT films from rigid substrates.[31,140,167] As shown in Figure 11a, the principle of transfer can be explained by the Dupré equation $E^{AB}{}_A = \gamma_A + \gamma_B - \gamma_{AB}$, where $E^{AB}{}_A$ is the interfacial binding energy between material A and B, $\gamma_{A(B)}$ is the surface free energy, and γ_{AB} is the interfacial free energy. Transfer of material A from B to C requires: $E^{AC}{}_A > E^{AB}{}_A$. Broadly, two materials that both have strong dispersive or polar components are likely to adhere well. Contact for sufficient time at room temperature or slightly elevated temperatures, followed by the removal of the stamp, leaves a metal pattern in the geometry of the relief features on the substrate. The transfer process can be guided either through specific chemical interactions between the metals and the substrates or by general, noncovalent surface forces. On the basis of this, Rogers et al. have successfully transferred CNTs from silicon wafers to PET substrates for flexible and transparent transistor applications (Figure 11b). Rogers et al. also found that a thin layer of Cr/Au metal can assist the transfer of CVD tubes from their growth substrates to plastic substrates.[168] The transfer dynamics is crucial and highly depends on the peeling speed of the elastomeric stamp.[31] More details can be found in a review by Rogers's group.[169] Another category of transfer printing using PDMS is for solution-based CNT thin films, either by filtration or by solution casting.[26,170,171] Floating CNTs on water after etching away the filter and Qausi-LB methods have been developed.[32,37,126,172] However, these methods have little control. The film can be easily broken during the handling process, and it is difficult to get a full film transfer. Gruner et al. have extended Rogers's transfer work for films on filters, but without the need of the metal deposition and etching step.[173] They use a patterned PDMS stamp (Figure 11d). When patterned PDMS is used, patterned CNT films are fabricated (Figure 11c). The choice of filter is critical for this study. They found it difficult to transfer CNTs from a filter to PDMS if polymer filters are used. CNTs tend to adhere to polymers, so an inorganic filter is preferable. During the transfer from PDMS to the receiving substrate, heating and pressure are applied to assist the transfer process.[173]

Film transfer can be done using the assistance of an energy source, such as laser, heat, or microwave.[174−176] In microwave-assisted transfer, the microwave provides local heating of the CNTs such that the CNT−polymer interface exceeds the glass transistor temperature of the polymer. CNTs are transferred from Si substrate to polymer substrate after manually removing the Si substrate. The process results in a rapid transfer of CNTs. Figure 11e shows the steps of the laser transfer method. Laser transfer is widely used in

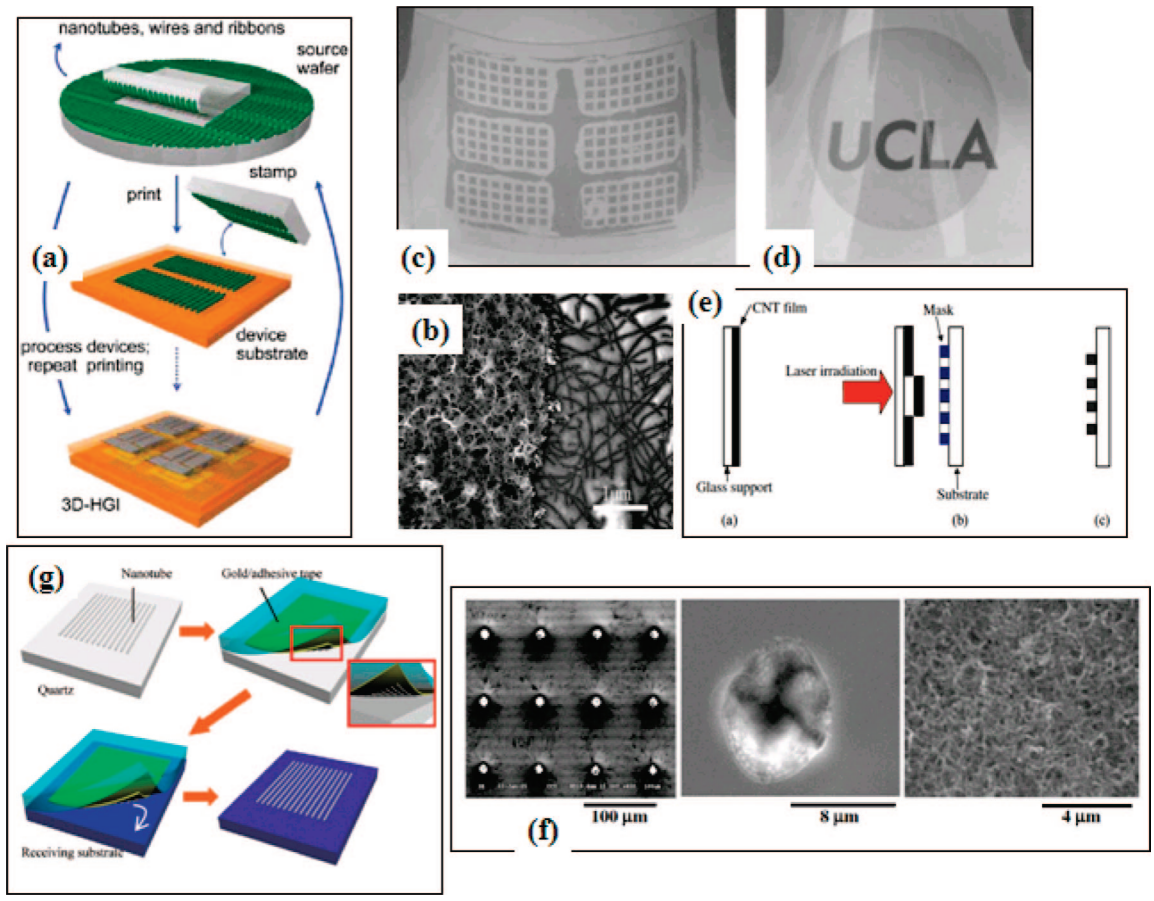

Figure 11. (a) Schematic illustration of a printed semiconductor nanomaterials-based approach to heterogeneous 3D electronics. (b) Transfer printed CNT films as electrode and semiconducting layer for a transistor. (Reprinted with permission from ref 168. Copyright 2004 American Institute of Physics.) (c) A patterned PDMS stamp and carbon nanotube films made by vacuum filtration and PDMS transfer method. The small gray square patterns have a size of 1 mm^2. (d) Photo image of a transparent and homogeneous film with 2 in. diameter on a flexible PET substrate. (Reprinted with permission from ref 173. Copyright 2004 American Institute of Physics.) (e) Schematic diagrams showing the experimental steps for the patterned deposition of a carbon nanotube film by the laser transfer method. (f) SEM images showing the patterned carbon nanotube spots. (Reprinted with permission from ref 175. Copyright 2004 American Institute of Physics.) (g) Temperature-sensitive tape-based transfer method. (Reprinted with permission from ref 80. Copyright 2004 American Chemical Society.)

industry to generate patterned films. A laser pulse with fluence of about 320 mJ cm^{-2} was used to irradiate the support. The CNTs coated on the support adsorbed the laser energy, evaporated and exploded through the hole patterns in the mask, and deposited onto the substrate. Because of the large energy of the laser, a certain degree of damage to the CNTs may happen. Figure 11f shows the results of patterned films by the laser transfer method on specific regions. A tape-based transfer method has also been developed for transferring CNTs.[80] The transfer step from the initial substrate is easy using sticky tape. To transfer CNTs to the receiving substrate, either the tape is dissolved, or the tape loses its stickiness through either increased temperature or pressure. Temperature (Revalpha thermal tape from Nitto Denko)- or pressure-sensitive tape can be peeled off without the CNTs. Figure 11g shows the transfer steps. Etching away the tape may leave large amounts of residue on CNT films.

There are other types of transfer methods for CNT thin films, such as modifying the receiving substrate to enhance the adhesion. Materials such as low temperature solder or conductive composite material can be used to do this modification.[26,149] Adhesive transfer method used for conductive polymers has also been proposed for transfer of CNT thin films.[177] While solution-based coating allows the CNT thin film deposition on a variety of substrates, a transfer method is still needed for certain applications. For example, thermal annealing of CNT thin films to remove surfactant or polymer residue requires higher temperatures than the glass transition temperature for plastic. Therefore, transfer from substrates such as glass to plastic is needed for films where surfactant is to be destroyed through annealing. For films made by direct growth, a transfer step is required for using the films in devices. In addition, a transfer step can also provide patterns when the PDMS stamp is used, and the multiple transfer step allows device fabrication of complicated structures.

3. Modification of Carbon Nanotube Thin Films

3.1. Patterning

Patterning CNT thin films is important for many device applications. For direct CVD growth, patterned films can be generated by first patterning the catalyst, using photolithography, microcontact printing, inkjet printing, or other methods, because CNT film only grows where the catalyst is deposited.[108,178−180] Figure 12a shows an example of patterned films by the direct CVD growth method.[181] Purified and concentrated Co nanoparticle catalyst dispersion is inkjet printed on the substrate. After growth, a patterned array of CNTs was obtained with dot size between 5 and 30 μm. The direct CVD growth technique needs to be combined with

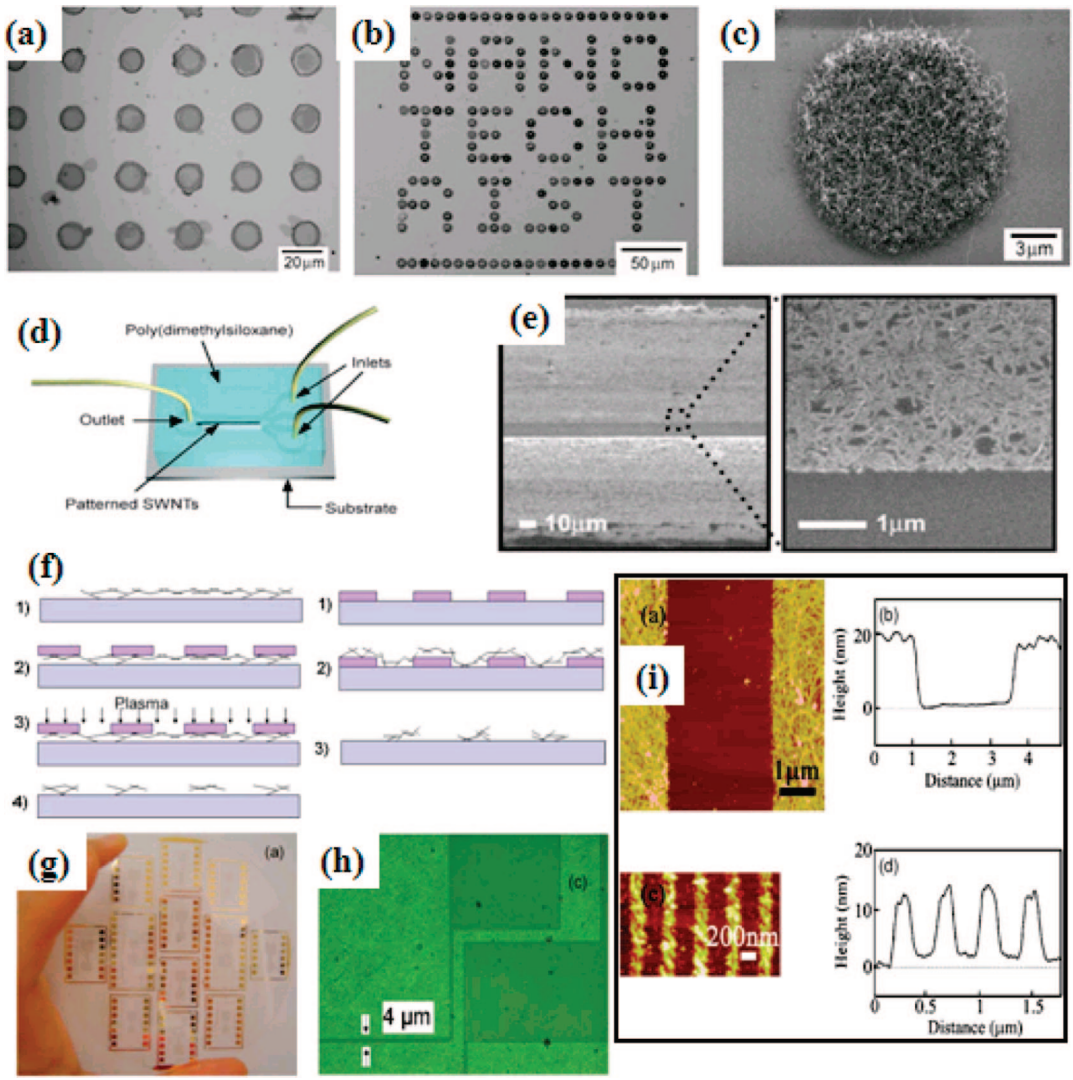

Figure 12. (a) Optical microscope images of catalyst patterns made by an inkjet printing technique. (b) Patterns of letters are demonstrated. (c) SEM image of CNT growth at the patterned area. (Reprinted with permission from ref 181. Copyright 2003 American Institute of Physics.) (d) A microfluidic patterning device built with PDMS. (e) SEM image of patterned films by the patterning device. Three streams were used (center stream, CNT solution; and outside two streams, methanol). (Reprinted with permission from ref 193. Copyright 2006 Wiley-VCH.) (f) Two process sequences used for patterning nanotube films. (g) Patterned nanotube films on 4 in. glass wafer. (h) Enlarged image of the patterned nanotube lines. (Reprinted with permission from ref 154. Copyright 2006 American Institute of Physics.) (i) AFM top view and cross section of a 3 μm line etched in a ~20 nm thick CNT film. (Reprinted with permission from ref. 189. Copyright 2007 American Institute of Physics.)

a transfer method for some device applications, especially for devices on plastic substrates.

For solution-based CNT films, there are two types of patterning methods: additive and subtractive. Additive methods include inkjet printing, patterned filtration, microcontact printing, and microfluidic channel guided coating.[7,86,87,159,160,164,165,182−184] Subtractive methods include PDMS-based patterning, photolithography, or E-beam lithography with plasma etching, laser ablation, or binder-assisted removal of CNTs.[26,57,185−192] Inkjet printing is an ideal additive method for making patterned CNT films, as discussed previously. Lee et al. used a vacuum filtration method to generate a patterned film by blocking certain areas of the filter using photolithography.[183] Rogers et al. developed a simple but powerful method for depositing a patterned SWCNT film in forms ranging from aligned collections of individual tubes to thick network mats (Figure 12d and e).[193] They used a PDMS-based microfluidic channel to flow CNT solution, along with methanol to lower the concentration of surfactant available to interact with CNTs to values below the CMC value. At this point, the CNTs are no longer well suspended, and the interactions with adjacent solid surfaces can cause the CNTs to coat the solid surfaces. Flow velocities, deposition times, channel geometries, multiphase flows, and dynamic control of flow histories can all be exploited to generate complex patterns of SWCNTs that are difficult to construct with other techniques. For subtractive methods, PDMS-based transfer printing using a patterned PDMS stamp has been discussed in detail in a previous section. For the widely used photolithography or e-beam lithography followed by plasma etching, well-defined patterns can be achieved. Figure 12f shows two processes of patterning CNT films. Both processes lead to clear edges of patterned CNT films, as shown in Figure 12g and h.[154] Various types of plasma such as Ar, O_2, CF_4, or CF_6 can effectively etch nanotubes. A gas plasma within a reactive ion etcher (RIE) system (i.e., 100 W rf power and 5 min etching with Ar plasma) removes the nanotubes in the unprotected areas. There are no distinguishable changes in Rs and transmittance in protected areas after five repetitions

of the lithographic patterning process. For transparent CNT thin films with thickness of 10−50 nm, the difference in the etching rate between CNTs and PR is not an issue. It has been found that the etching rate for PR 5214 is 3 times that of CNTs. However, due to the large thickness difference (10−50 nm CNT vs 1−2 μm PR), the difference in etching rates is not an issue here. For even higher patterning resolution, e-beam lithography is needed. Ural et al. used this method to pattern CNT films for widths ranging from 50 μm to 100 nm.[189] They systematically studied the effect of inductively coupled plasma reactive ion etching etch parameters, such as substrate bias power, chamber pressure, and substrate cooling, on the nanotube film etch rate and etch selectivity. They found that the etching rates can be decreased by a factor of 10 by adjusting the parameters. By reducing the substrate bias, the ion energy is reduced, resulting in a substantially slower etch rate.

There are other methods to generate patterned CNT films. Jung et al. developed a combined method of chemical anchoring and photolithography on a patterned substrate.[194] Glatkowski et al. developed a method using a polymer binder to anchor CNTs on selective areas[192] followed by removal of the CNTs where there is no binder. Direct laser writing can pattern CNT films without the need of a mask and can be used roll-to-roll.[195] Instead of removing the CNTs, one can functionalize the CNTs and electrically disrupt them.[196] Zhou et al. developed an ultrathin Si_3N_4 membrane shadow mask, which allows direct deposition of patterned CNT films with high resolution.[26] The choice of the patterning method for specific applications highly depends on the substrates, the required resolution, and the cost. For large-scale device applications such as using patterned transparent CNT films for displays, high speed patterning is needed. Subtractive laser or plasma etching can be performed with high throughput and is widely used in ITO patterning.[197−199] For rigid substrates such as glass that is common in LCD displays, PR with plasma etching is a more feasible subtractive method. For additive methods for generating patterned CNT films, patterned gravure coating or high speed inkjet printing are promising for large area patterning.[200]

3.2. Doping

Similar to semiconductor technology, doping and functionalization of CNT thin films is attractive and essential for further performance improvement and modifications. For example, for complementary circuit applications, n-type doping of semiconducting CNTs is required. For transparent and conductive films, doping CNTs increases the charge carrier number for high electrical conductivity. For thin film transistors with a high on/off ratio, elimination of metallic CNTs can significantly decrease the off current. CNT doping research includes: various methods of doping, doping mechanism studies, charge transfer and the evidence of such, spectral studies of doped CNTs, and device performance before and after doping. There are several outstanding reviews on this topic.[201−203] In practice, CNTs can be doped in various ways, including intercalation of electron donors or acceptors, substitutional doping, encapsulation in the interior spacing, molecular absorption, and covalent sidewall functionalization. Broadly, covalent doping will affect the intrinsic transport properties of CNTs (typically lowering the mobility), but will have good stability, while noncovalent doping has a lower binding energy (so will be less stable) but will have a lower impact on charge carrier mobility. Studies of doped CNTs include electrical measurement of individual CNTs on devices, spectral studies of doped CNTs in solution, and thin film properties such as transport and optical properties. In this section, we will focus on the various aspects of CNT thin film doping for electronic device applications.

For CNT thin films, p-type doping can enhance the conductivity dramatically. The p-type dopants for CNTs include acids such as HNO_3, gases such as O_2, NO_2, and Br_2, molecules such as $SOCl_2$ and F_4TCNQ, polymers, and transition metals.[57,78,204−207] Charge transfer between dopants and CNTs increases the number of charge carriers along the CNTs and improves the conductivity. Such doping is extremely useful for enhancing the performance of a CNT thin film transparent electrode. The doping process is extremely simple and usually consists of dipping the CNT thin films on substrates into the dopant solutions for a certain amount of time. Resistance measurement before and after the chemical treatment reveals a dramatic increase in conductivity (Figure 13a).[78] R_s decreases after initial exposure to 3 M HNO_3 acid, and further decreases after contact with $SOCl_2$. Immersion of the film and complete drying leads to instant improvement in the conductivity by a factor of 5. Longer immersion times did not provide any further change in conductivity. Figure 13b shows the sheet conductance (inverse of R_s) before and after exposure to Br_2 for CNTs with different surface coverage. Br_2 increases the conductivity dramatically by a factor of 8. Smalley et al. have observed that Br_2 and K doping increases the CNT thin film conductivity by a factor of 15.[205] The doping will modify the charge distribution in the band structure and modify the Fermi level position. Accordingly, the optical properties will be modified. Figure 13c shows the spectra of bare and doped CNT thin film in the visible and near IR range. In contrast to sheet conductance, transmittance in the visible range does not change at all upon doping. A separate study by Forro et al. also observed that the K doping modified the dc conductivity but did not change the optical conductivity in the visible range (Figure 13d).[208] On the basis of this transport study, Forro et al. proposed that K doping affects the tube−tube contacts more than the intrinsic on-tube transport. The spectra start to change in the near IR range but not in the visible range. The lack of change in the visible range after doping is extremely important for designing routes for enhance the performance of transparent and conductive CNT thin films through doping. Change in the IR and Raman spectra is evidence of charge transfer between CNTs and dopants. The reason for the change in the near IR spectra is that the CNTs band gap is in the near IR range. Charge transfer can modify the Fermi level, which leads to absorption in this energy range.[92,209−212] Tetrafluorotetracyano-*p*-quinodimethane-(F_4TCNQ), which has a strong electron affinity, is well studied as a p-type dopant for CNTs.[212] Figure 13f−h shows the F_4TCNQ doping results, where CS_2 is used as the solvent. As the number of doping steps increases, the absorption at 0.7 eV decreases and that at 0.4 eV increases. The consecutive enhancement in Drude absorption is associated with the reduction of the S1 transition with the doping steps. This is direct evidence of controllable carrier doping. Based on their results, doping saturates at ~0.01 holes/carbon atom. Smalley et al. used Raman spectroscopy to study the effects of exposing CNT bundles to typical electron-donor (potassium, rubidium) and electron-acceptor (iodine, bromine) dopants. They found that the high-frequency tangential vibrational

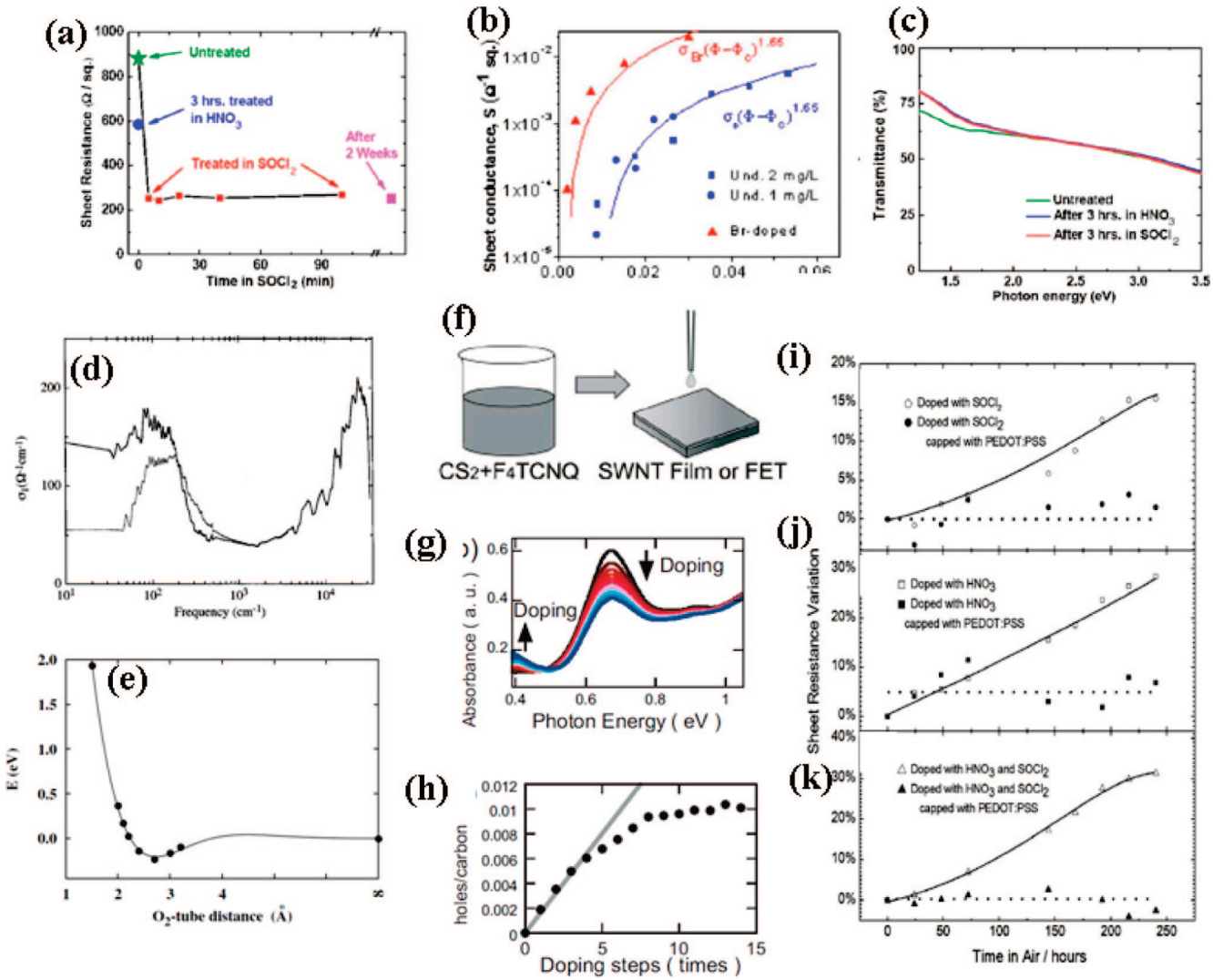

Figure 13. (a) Decrease in resistivity as a function of time for a 40 mL SWCNT thin film after HNO_3 and $SOCl_2$ treatments; (b) sheet conductivity vs the relative CNT fraction. The conductivity of the Br-doped thin films has been substantially improved. (c) Transmittance vs photon energy for untreated, HNO_3-, and $SOCl_2$-treated SWCNT thin films. (Reprinted with permission from refs 78 and 205. Copyright 2007 American Institute of Physics.) (d) Optical conductivity as a function of wavenumber for pristine and potassium-doped SWCNT sample. (Reprinted with permission from refs 78 and 208. Copyright 2007 American Institute of Physics.) (e) Binding energy of O_2 to an (8,0) SWCNT as a function of distance from the tube. (Reprinted with permission from ref 203. Copyright 2000 American Chemical Society.) (f) Experimental procedure for solution-processed continuous chemical doping. (g) Optical absorption spectra of pristine CNTs and F_4TCNQ-doped CNTs. (h) Relationship between carrier density and number of doping steps. (Reprinted with permission from ref 212. Copyright 2005 Wiley-VCH.) (i−k) Relative R_s variation of SWCNT films versus time in air for (i) $SOCl_2$-doped films with and without a PEDOT/PSS layer, (j) HNO_3-doped films with and without a PEDOT/PSS layer, and (k) HNO_3- and $SOCl_2$-doped films with and without a PEDOT/PSS layer. (Reprinted with permission from ref 214. Copyright 2008 Wiley-VCH.)

modes of the carbon atoms in the CNTs shift substantially to lower (for K, Rb) or higher (for Br_2) frequencies. These shifts in Raman spectra are associated with the charge transfer between CNT and dopants.

For gas dopants, the absorption and desorption dynamics depends on the binding energy, temperature, and concentration of the gaseous species and CNTs.[203,213] From first principles, Cohen et al. found the binding energy of O_2 to CNT walls is 0.25 eV with a binding distance of 0.27 nm.[203] A charge transfer of 0.1 electron from CNTs to every oxygen molecule is predicted. This binding energy of 0.25 eV is 10 times the thermal energy at room temperature, so the oxygen molecule should stay bound to the CNT at room temperature.[203] However, at elevated temperatures, the oxygen molecules can desorb from the tube surface. Hertel et al. experimentally studied the physical absorption of oxygen on to CNTs. They estimated that the equilibrium room-temperature oxygen coverage on CNTs at atmospheric condition is on the order of 10^{-5} molecules per carbon atom.[213] This, and the fact that they find no evidence for a chemisorbed species, suggests that the observed p doping must be due to a minority oxygen species. The typically low binding energy of gaseous species to CNTs suggests that gas doping will be inherently unstable. For doping to be useful, the dopants must be stable under normal device conditions. For example, when CNT thin films are used as transparent electrode in OLEDs, touch screens, or OPVs, exposure to elevated temperature may be experienced. To improve the stability of chosen dopants, encapsulation or top coating with another layer of material could help slow and impede the desorption process. Fraham et al. reported the stability of transparent CNT thin films after HNO_3 and $SOCl_2$ after PEDOT top coating (Figure 13i).[214] The resistance of doped CNT films without a top layer increases dramatically after exposure in

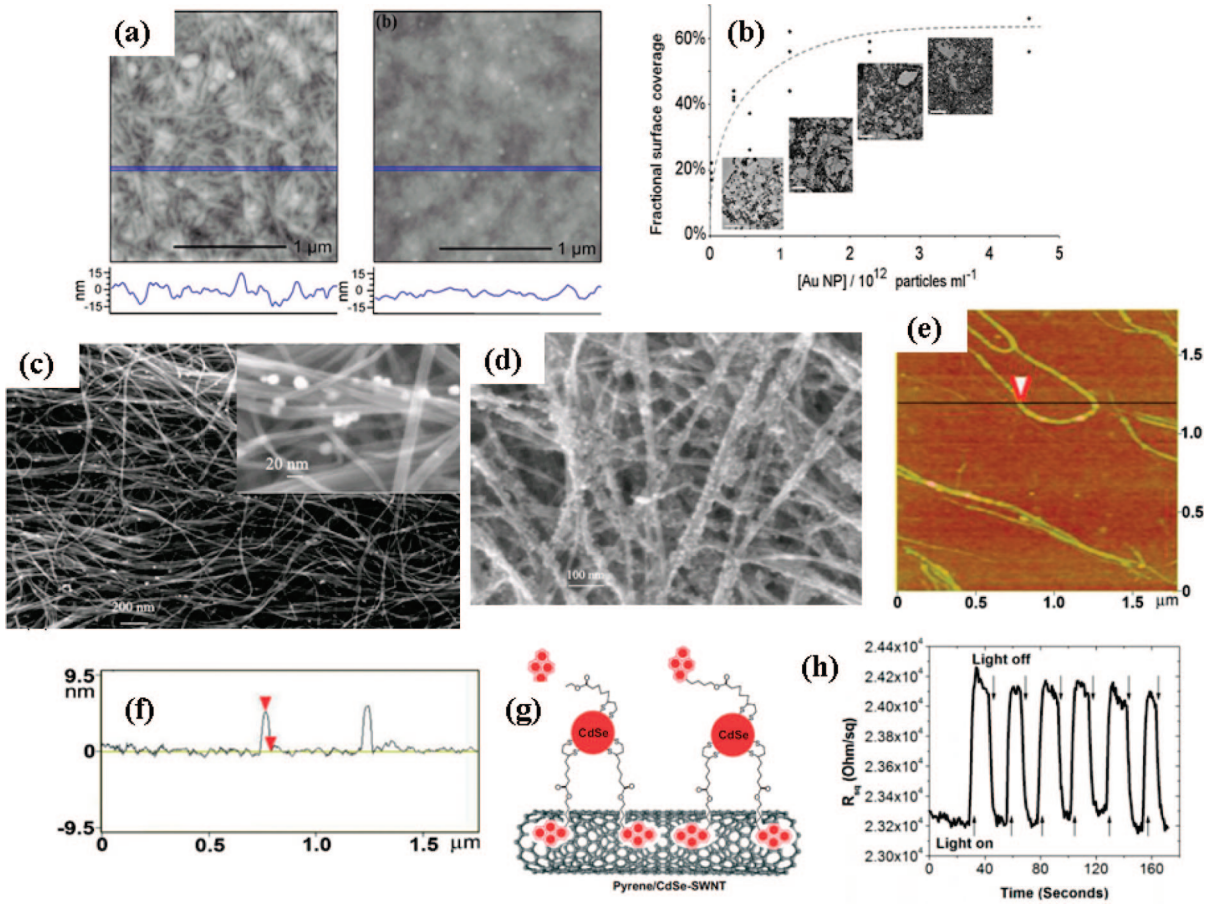

Figure 14. (a) AFM images of CNT network films before (left) and after (right) PEDOT:PSS deposition and annealing at 110 °C for 20 min. The rms roughness is 7 nm before coating and 3.5 nm after coating. (Reprinted with permission from ref 217. Copyright 2006 American Chemical Society.) (b) Plot of the fractional surface coverage of gold nanoparticles, calculated by threshold analysis of TEM images. (Reprinted with permission from ref 220. Copyright 2008 Royal Society of Chemistry.) (c) Oxidized MWCNTs bearing Pd clusters. (d) Thiol-functionalized CNTs with attached Fe clusters. (Reprinted with permission from ref 57. Copyright 2008 American Chemical Society.) (e) An AFM image of self-assembled pyrene/CdSe nanoparticles on CNTs. (f) Cross section analysis of (e). The height of the hybrid is approximately 5.0 nm, indicating the average pyrene/CdSe nanoparticle size is approximately 3.5 nm. (g) Schematic drawing of the noncovalent bonding between surface-functionalized CdSe nanoparticles and a SWCNT. (h) The resistance of a SWCNT-FET device vs time monitored under zero gate voltage, $I = 10$ W m^{-2} and $\lambda = 410$ nm. (Reprinted with permission from ref 222. Copyright 2008 Wiley-VCH.)

air for 80 h, while that with a PEDOT/PSS capping layer significantly increases the stability of the films. Looking for a stable dopant that has high enough binding energy, but will not affect the electronic and transport property of CNTs, will be a challenging task.

3.3. Engineering Nanotube Thin Films

To improve the performance or incorporate more functionality, engineering films based on CNTs is a route. Engineered films discussed here include double or multilayer structures with thin films-based CNT hybrids or/and CNT composites.[165,215,216] The high conductivity, mechanical flexibility, and porosity of a CNT film provide a unique backbone for incorporating other materials to bring in new functionality. Multilayer structures have been widely used for novel electrode applications. A typical area is transparent electrodes based on transparent and conductive oxides (TCO). For example, incorporation of CuO_x on an ITO electrode has been found to lower the operational voltage for electroluminescent devices.[34] Incorporation of In-doped CdO (CIO) on ITO shows significant improvements in the figure of merit as a transparent electrode.[124] Because of their large aspect ratio, CNT thin films have a large surface roughness, in the range of 5−20 nm. Such high roughness can be a problem for OLED and OPV device applications. Spin-coating another layer of PEDOT:PSS material to form a double layer electrode structure is useful in decreasing the intrinsic surface roughness of CNT films.[217] As shown in Figure 14a, the surface roughness is decreased after spin coating of a thin layer of PEDOT:PSS. PEDOT:PSS coating also decreases the R_s by 20% without changing the transmittance in the visible range. A conductive polymer and CNT thin film double layer structure is a valid method to smooth the surface roughness while maintaining the surface electrical conductance. Because of the porous structure of CNT thin films, the polymer coating can penetrate into the pores of the films, leading to better mechanical integrity of CNT thin films. An annealing step after the top coating can improve the mechanical linkage of the two materials to improve the adhesion of the two layers in the double layer structure.

Pristine CNT films do not have enough surface conductance for many applications. For example, CNT-based devices exhibit less than optimum performance versus ITO. However, CNT films have extreme mechanical flexibility. ITO electrodes have high surface conductance but very poor mechanical bending properties, which can be a problem for flexible electronics applications. An ITO/CNT double layer can possibly combine the high electrical conductance of ITO

with the mechanical flexibility of CNTs.[218] This combination is especially attractive considering the ideal work function match. Our group and Futagami's group have done some early work in this area.[57,219] The ITO deposition is carried out by a room temperature ion-assisted deposition process. The rms roughness of these ITO-modified CNT surfaces decreased with increased ITO film thickness. This reflects the marked tendency of IAD-derived ITO to planarize the SWCNT films. Also, the figure of merit after ITO deposition increases. The mechanical flexibility of the ITO/CNT films on PET substrates was investigated in bending tests and found to be much greater than that of ITO-only films of the same thickness on PET. Thirty nanometer ITO-modified CNT films can be bent to a radius of curvature of 4 mm with a 5% increase in R_s, while ITO/PET films show a 600% increase in R_s after bending to a radii of 4 mm, and cracks are obvious in the SEM. This increased ITO/CNT film mechanical flexibility is attributed to the ITO/CNT interpenetrating network microstructure, ITO adhesion to the CNTs, and intrinsic CNT mechanical flexibility. Such a double layer electrode can be used for flexible electronic applications. For solar cell applications, one can incorporate a transparent metal grid on top of CNT thin films to increase the electrical conductivity. This type of double layer structure can be applied generally to any other type of TCOs to form novel flexible electrodes.

Nanoparticles are very attractive tools in biological labeling, solar cells, light emitting diodes, and other applications. However, due to their zero-dimensionality and high percolation threshold, several difficulties need to be overcome for their use. For example, NPs have been incorporated into solar cells as composites with polymers. However, due to the low mobility of the NPs, the composite solar cell has very limited efficiency. Incorporating CNTs with NPs could improve the mobility dramatically, and there is much research in this area.[7,35,99,123] In a review paper, Prato et al. listed the popular methods to assemble CNT−NP hybrids. These methods include: formation of metal NPs directly on the carbon nanotube surface through electrochemical deposition, covalent linkage between NP and CNTs, hydrophobic interactions and hydrogen bonds, π-stacking, electrostatic interactions, and others. The NPs are assembled onto CNTs through thiol-mediated binding and van der Waals force.[220] Figure 14b demonstrates that the number of particles included in the film, measured as fractional surface coverage by threshold analysis of TEM data, can vary from sparse to dense, while maintaining a 2D morphology. The number of nanoparticles incorporated into the films increases significantly as the concentration of components increases in the aqueous phase. Metal clusters have also been incorporated into CNT thin films, which is useful for electrochemical energy storage applications. Kreupl et al. have studied the formation of metal clusters onto CNTs. The metals include Pd, Au, Fe, Co, and Ni.[221] For example, for formation of Pd cluster onto CNTs, CNTs in ethanol−water mixtures with Pd were stirred for 24 h. A bucky paper was obtained with 10 nm size Pd clusters attached to the CNT walls. For Au clusters, the control experiment without thiol groups revealed that no Au clusters had been bonded to the CNT surface. This indicates that the Au NPs have been covalently attached at the thiol groups along the side walls of CNTs. Figure 14c shows the SEM image of CNT papers with Pd and Au clusters attached. We have shown an example of light-sensitive NPs on CNTs, which could be used for composite solar cell application due to the high carrier mobility along the CNTs.[57] Gruner et al. have successfully assembled CdSe nanoparticles onto CVD grown CNTs on silicon wafers through pyrene interaction, as shown in Figure 14e−g.[222] The NP size from AFM images is 3.5 nm in this study. The resistance of such hybrid films responds quickly and selectively to light with wavelength centered at 410 nm (Figure 14h), which is the absorption wavelength of CdSe NPs. Such a hybrid structure can be thought of as light harvesting centers (CdSe NPs) along a conductive, high mobility backbone (CNTs). Metal NPs can be used to dope CNTs to improve the performance of transparent and conductive electrodes based on CNT thin films.[223] Jung et al. have found that the conductivity change of CNT thin films largely depends on the duration of the immersion time of CNT thin film in gold ion solutions. The soaking of CNT thin films in gold solution leads to up to 150% conductivity increase, with a small percent change of transmittance at 550 nm. This method is very promising to make transparent stable CNT films due to the large weight of the gold NPs. It is suggested that the increase of conductivity is due to the doping effect from NPs to CNTs. However, the stability of such transparent hybrid films still needs further investigation.

4. Properties of Nanotube Thin Films

CNT thin films are a novel 2D structure with a mixture of semiconducting and metallic tubes. The electronic, transport, optical, and mechanical properties of individual CNTs have been extensively studied and well documented. CNT thin films will have the collective behavior of the individual tubes with additional properties arising from the tube−tube interactions. This section will be devoted to the properties of CNT thin films, covering the electronic properties such as work function and the contact resistance with metals, the transport properties with different geometries and energy scales, optical properties, chemical properties, and mechanical properties. The extensive Review here will guide the applications of CNT thin films in devices, especially electronic device applications.

4.1. Electronic Properties

The band structure of individual CNTs has been extensively explored.[26,224−226] The electronic structure of both metallic and semiconducting CNTs sensitively depends on the wrapping angle of the graphene sheet. For semiconducting CNTs, the band gap varies with diameter as $E_g \approx 1/R \sim 0.6$ eV/d (nm).[227] For metallic CNTs with $n \neq m$, a secondary band gap exists and varies with diameter as $\sim 1/R^2$.[21] Because of oxygen doping in air, semiconducting CNTs show p-type behavior. For device integration, one crucial issue is the contact resistance between CNTs and metal electrodes. Different metals have disparate work functions, Fermi levels, and wetting behavior with CNTs, and therefore can have dramatically different contact resistance. This has been confirmed in research, which focuses on transistors using individual semiconducting CNTs as the active channel. For example, Ti and Pd contact electrodes lead to p-type conducting behavior, while Mg contact electrodes show ambipolar characteristics, and most devices with Ca contact electrodes show n-type conduction behavior.[228] Theoretical calculations based on first principles show that Ti leads to the lowest contact resistance with CNTs, followed by Pd, Pt, Cu, and Au. This correlates well with the predicted

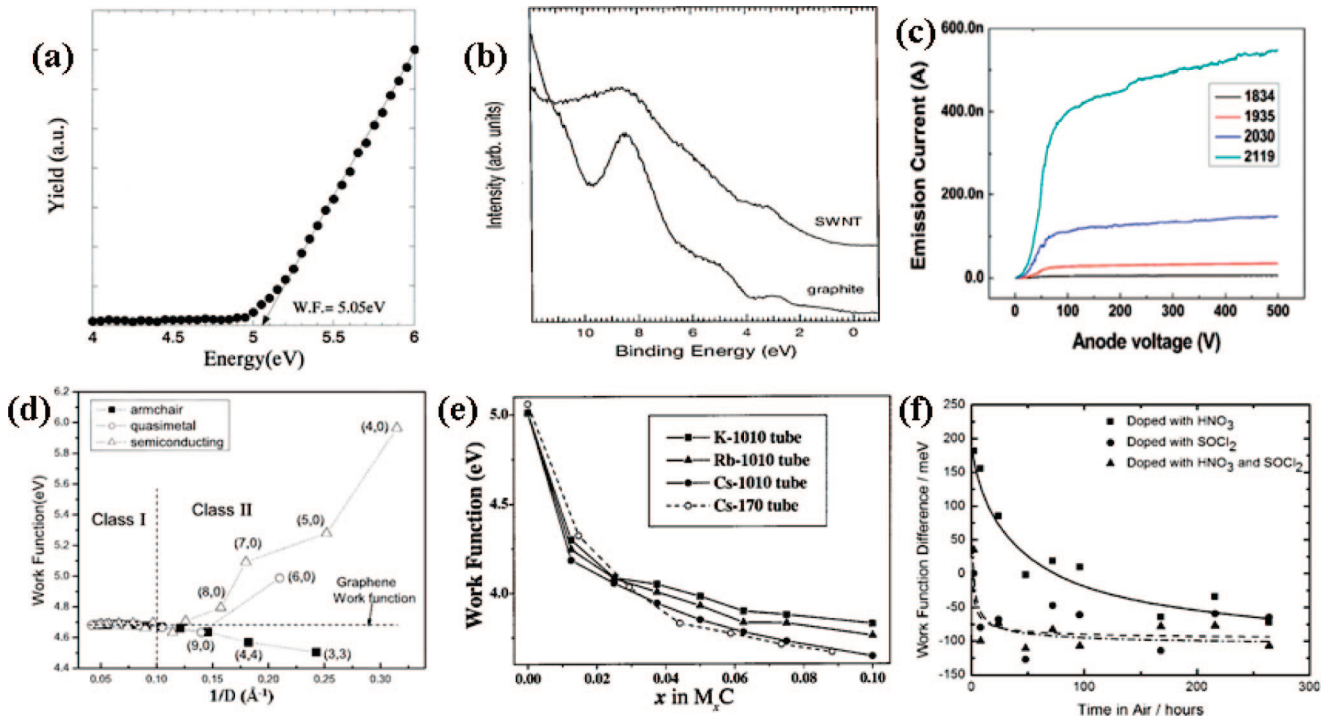

Figure 15. (a) PEE spectrum of SWCNTs. (Reprinted with permission from ref 239. Copyright Elsevier.) (b) Valence band photoemission spectra of the pristine CNT bundles and graphite. (Reprinted with permission from ref 240. Copyright American Institute of Physics.) (c) Thermionic $I-V$ curves of SWCNT bundles at different temperature. (Reprinted with permission from ref 57. Copyright 2008 American Chemical Society.) (d) Work function (eV) of individual CNTs vs tube diameter. The work function for graphene is shown for comparison. (e) Work function (eV) of alkali−metal intercalated CNT bundles vs the intercalation density. (Reprinted with permission from ref 243. Copyright 2002 American Institute of Physics.) (f) Work function difference between doped and undoped CNT samples as a function of air exposure for various doping processes. (Reprinted with permission from ref 10. Copyright 20087 Wiley-VCH.)

cohesive strength of the electrode−carbon interface.[229] In a separate study, Forro et al. found the contact resistance between Au and CNT lies in a narrow range of 0.35−2.6 kΩ at room temperature.[230] Reifenberger et al. also found that the contact resistance depends on the contact length between CNT and metal. They estimated that the optimal contact length lies in the range of 1−3 μm, depending on the ratio between contact resistance and the CNT resistance. At this optimal contact length, the contact resistance is 10% higher than the contact resistance with infinite overlap length.[231] Graham et al. studies the specific contact resistance between CNT and deposited silver electrode to be 20 mΩ cm^2.[232] The contact resistance between CNTs and metal can of course be modified by annealing or chemical doping.[233,234] Annealing will improve the physical wetting between CNTs and metal, while chemical doping will shift the Fermi level of CNTs and adjust the Schottky barrier (SB) in the junction to modify the contact resistance. Mizutani et al. found that chemical doping by F_4TCNQ is effective in reducing the contact resistance between CNTs and Au metal, as well as the CNT channel resistance, 4−59% and 73−94%, respectively.[235,236] The change of energy-level alignment at the nanotube/metal contact was given as the reason for causing the reduction of R_C. Another important aspect for the interface between CNTs and metal contacts is Fermi level pinning. Tersoff et al. found that when a semiconducting CNT is end contacted to a metal, the behavior is radically different as compared to the metal−semiconductor interface.[237] The interface between CNTs and metal also depends sensitively on temperature, electric field, and the evaporation details with different wetting behavior. Studies show that the contact resistance between CNT thin films and metal is not an issue.[34] The low contact resistance between CNT films and metal may be due to the large quantity of CNTs at the interface in parallel, which leads to minimal contact resistance. CNT work function is important for applications in field emission devices and as anodes in OLED and OPV devices. There are several methods to measure the work function of CNT thin films, including Kelvin probe, ultraviolet photoelectron spectroscopy (UPS), transmission electron microscopy (TEM), photoelectron emission (PEE), and thermionic methods.[28,123,218,238−241] Some theoretical studies based on first principles have been carried out. The PEE method allows easy and precise measurements of work function.[239] Figure 15a shows a PEE spectrum of SWCNTs. The extracted work function based on the plot is 5.05 eV. Ata et al. found that the work function of CNTs is 0.1−0.2 eV larger than that of highly oriented pyrolytic graphite (HOPG), which they attribute to the formation of $\sigma-\pi$ mixed valence states in CNTs. In the TEM method, a static charge Q_0 exists at the tip of the NT to balance the potential difference due to the work function difference between CNTs and Au. The measurement relies on the mechanical resonance of the CNT induced by an externally applied oscillating voltage with tunable frequency. The resonant frequency will lead to information on the work function of CNT films. With this method, Wang et al. found a work function of 4.6−4.8 eV, 0.2−0.4 eV lower than that of carbon. In the UPS method, a He discharge lamp and an angle-integrated-type electro energy analyzer are used. Figure 15b shows spectra of UPS measurement for pristine CNT and graphite. The calculated work function based on the spectra is about 4.8 eV for CNT and 4.6−4.8 eV for graphite, respectively.[241] Estimation of the work function based on the Fowler−Nordheim model suffers from the uncertainty of the local geometry of the CNT surface. In the thermionic method, the

work function is calculated according to Richardson's formula, $j_0 = AT^2 \exp(-(\phi)/(kT))$, where j_0 is the zero field thermionic emission current density, A is the emission constant, T is the absolute temperature, and Φ is the work function of the CNT film as cathode in the setup. On the basis of the emission current of CNT sidewalls (Figure 15c), Fan et al. found that the sidewall work function is around 4.7−4.9 eV.[57] The diameter and the number of walls have no obvious influence on the work function.

While experiments measure the collective work function of CNT thin films, theoretical calculation can take into account individual CNT chirality, length and diameter, the tube−tube distance and interaction, and the bundle size. Theoretical calculation can provide insight for further improvement or modification of the work function for desired usage. Chan et al. takes into account the tube length, tube−tube separation, and tube type for work function calculation.[242] They found that the work function can exhibit significant variations depending on the length of the tubes and the way they are arranged, changing the sign of the dipoles formed at the tips of the tubes. The dipole layer can be positive or negative, and the density of the dipole layer will affect the work function. Lu et al. found that the work function for metallic CNTs is independent of the chirality and increases slightly with tube diameter.[243] The work function for semiconducting CNT decreases significantly with tube diameter (Figure 15d). The work functions for metallic CNTs are all around 5 eV in bundles, higher than that of individual CNTs.

Work function modification is important for device applications. For field emission devices, lowering the work function will decrease the field emission threshold voltage. For anode applications in solar cell and OELD devices, higher work functions will facilitate charge separation. Several methods have been tested to modify the work function such as chemical doping, intercalation of alkali metal into CNT films, and plasma treatment.[243] Figure 15e shows the work function change versus the loading of alkali metal.[243] Upon alkali−metal intercalation, the work function of tube bundles decreases dramatically, and the electronic states near the Fermi level are significantly modified. Silva et al. found that Li-salt functionalized CNTs have lower work function as compared to pristine CNTs as well. The Li-salt is simply coated on CNTs. In the work of Zhou et al., CNT work function is lowered to 2.4 eV by Cs intercalation into CNT bundles, which is low enough to be used as a cathode in OLED and OPV devices.[241] Friend et al. studied the work function of CNTs with different functional groups.[244] The treatments include air and oxygen plasma, and acid oxidation. They found the oxidations all lead to an increase of the work function, as confirmed by XPS. Plasma treatment destroys the π-conjugation and forms an amorphous carbon phase, while acid-oxidation introduces carboxylic acid group on the surface and produces the highest work function. The stability of the work function modification is critical. The alkali metal treatment retains the lower work function value for hours, but the long-term stability still needs to be investigated for practical device usage. Graham et al. studied the work function stability of chemically doped CNTs in air (Figure 15f).[9] As shown in the figure, the work function measured by the Kelvin probe is close to that of undoped CNT film within only 2 h. It is suggested that the anticipated shift is effectively mitigated on the surface of the films rapidly after exposure to the moisture in air. Comprehensive studies of the work function will be important, especially for stable cathode replacement using CNT film electrodes. There are other aspects of the electronic properties of CNT thin films such as the Hall effect. Hall effect measurement confirms that CNT thin films are a p-type material, in contrast to most electrodes, which are n-type. Forro et al. found that the carrier density at low temperature is $1.6 \times 10^{19}/\text{cm}^3$, while Biris et al. found the carrier density is around 3.1×10^{15} to $4.6 \times 10^{17}/\text{cm}^2$.[206,245] Overall, the ability to tune work function and contact resistance will have tremendous applications in electronic devices.

4.2. Transport Properties

There is extensive study of the transport properties of individual CNTs. SWCNTs have extremely high mobility (>100 000 $\text{cm}^2/(\text{V s})$) and current carrying capacity. Statistically, 1/3 of SWCNTs are metallic and 2/3 are semiconducting. The transport along metallic and semiconducting nanotubes is dramatically different. For example, semiconducting CNTs show p-type modulation behavior upon gate voltage, while metallic CNTs show weak dependence on gate voltage. Semiconducting CNTs also show much stronger temperature dependence in the conductivity due to the thermal excitation of the transport carriers. MWCNTs have similar transport properties; however, some differences arise due to the transport coupling between the walls of the tube.[73] Similarly, for CNT bundles, the coupling between tubes needs to be considered.[246,247] Figure 16a lists examples of transport properties of individual CNTs. For CNTs, the resistance of tubes shorter than 500 nm has a minimum resistance of 6−7 kΩ and scales with length at about 6 kΩ/μm.[248] The sum of the total resistance when measuring an individual CNT with metal contact is $R = h/4e^2 + R_c + R_t$, $R_t = hL/4e^2l$, where L is the tube length and l is the mean free path from backscattering, R_t is the phonon scattering contribution, and R_c is the contribution from imperfect contacts to the additional contact resistance.[249] Gomez-Herrero et al. found that the scaling of the resistance depends on the bias voltage, the defect density, and the tube length.[250] For high frequency transport, coupling between CNTs and the substrate should be considered. However, Burke et al. found that the CNT dynamic impedance is equal to its dc resistance (R_{dc}) for frequencies less than $1/2\pi R_{dc}C_{total}$, where C_{total} is the total capacitance including quantum and electrostatic components. Also, the transport in long CNTs or CNT bundles will have stronger temperature dependence than in individual CNTs, because the on-tube resistance dominates the contact resistance. The modulation of a metallic CNT in the measured temperature range is much weaker than that of semiconducting CNTs. Here, all of the data are for the on-tube transport properties, which exclude the contact resistance between CNT and metal contacts. CNT films are a mixture of metallic and semiconducting objects (Figure 16c). For such a novel 2D material, the transport can be extremely complicated. A simplified picture is that transport occurs along the tube to its end, and then crosses a tube−tube junction. Understanding the transport along each individual CNT will help in understanding the collective transport in such a mixture. The contact resistance between tubes will be the largest contribution to the film resistance. Almost all of the junctions will be heterojunctions, because crossing tubes are likely different chiralities. It was found that, at room temperature, the contact resistance for metal−metal or semiconducting−semiconducting junctions is approximately 20 kΩ and the metal−semiconduc-

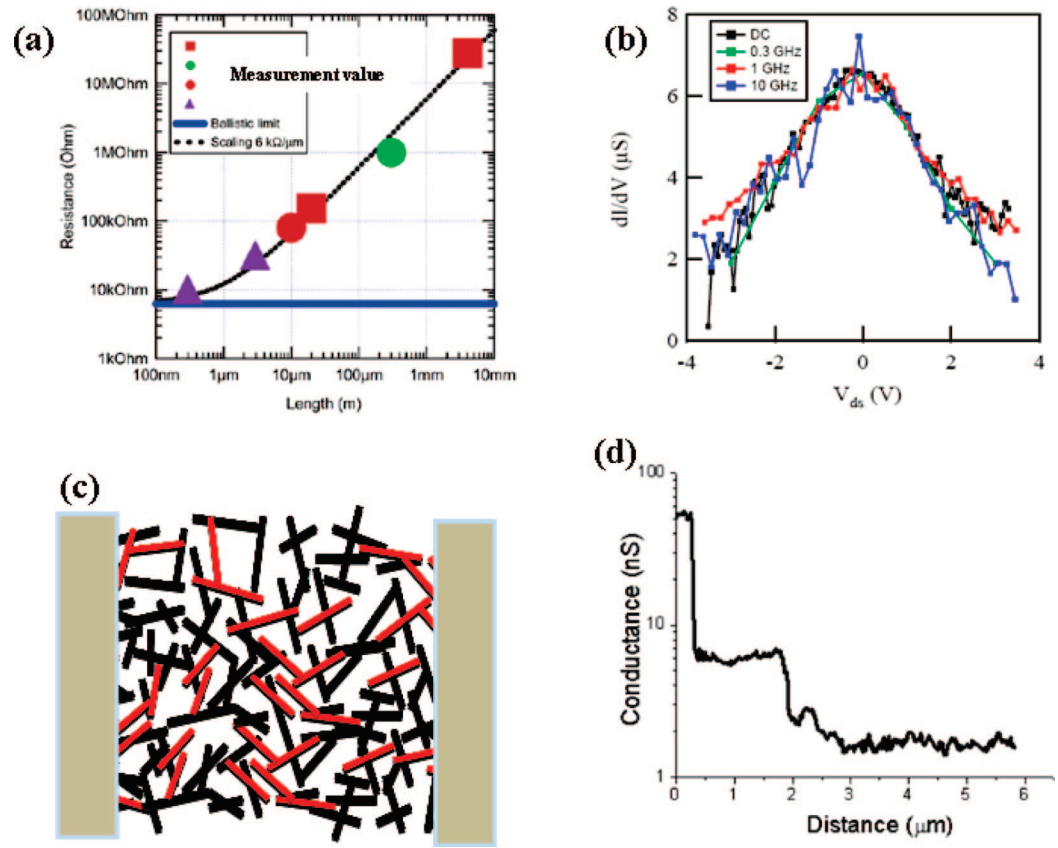

Figure 16. (a) Transport properties of individual CNTs. (a) Length dependence scaling of resistance. (Reprinted with permission from ref 248. Copyright 2004 American Chemical Society.) (b) Differential resistance of CNT at DC, 0.3, 1, and 10 GHz. (c) Scheme of CNT network, where 2/3 are semiconducting (black) and 1/3 are metallic (red). (d) The conductance drop at junctions in a CNT network. (Reprinted with permission from ref 253. Copyright 2004 American Institute of Physics.)

ting contact resistance is ~1 MΩ.[251,252] Figure 16d shows a conducting AFM scan. The AFM tip scans along the CNT network, and the large jump at the tube−tube junction indicates a 100 MΩ resistance.[253] The tube−tube junctions are much larger than the on-tube resistance. Therefore, the junction resistance dominates the overall transport behavior of CNT films. Because of the heterojunctions, the transport properties of CNT films will have strong dependence on frequency, voltage, and temperature. For example, increasing the field frequency will increase the capacitive coupling between tubes, thus increasing the total conduction of CNT films. It is obvious that the electric field and temperature will affect the transport through the heterojunctions between CNTs. From a geometrical point of view, CNTs have an extremely high aspect ratio. The current flows along the tubes as far as it can before it is forced to couple to another tube. For films with CNT bundles, the current will flow on the outside tubes before coupling into the inner CNTs. Therefore, the transport property of CNTs will depend on the tube length and diameter, as well as the bundling. Because of their large aspect ratio, a CNT network will have an extremely low percolation threshold. As the film thickness increases, the number of paths for carrying the current will increase more than linearly with the tube layers due to the coupling between different layers. Such a crossover from 2D to 3D will lead to a thickness dependence of the DC conductivity for CNT films. A similar phenomenon occurs when narrowing the film width, as it becomes close to the length of CNTs. In this case, the conducting path for tubes on the edge will be blocked and the conductivity will show a dependence on the film width. In the next section, we will discuss the geometric effects on the transport properties first, followed by the transport scaling with energy including temperature, frequency, and electric field.

4.2.1. Geometric Scaling

Percolation in CNT−polymer composite systems has been widely studied, where CNTs provide the conduction path in the system. The system shows a 3D percolation behavior, and the electrical conductivity varies several orders of magnitude over a small range of CNT loading.[254] For a thin film (network) of CNTs on a flat substrate, the problem becomes a 2D percolation system. There are many experimental studies about the percolation behavior in 2D systems with conducting objects of various shapes and geometries.[254−258] Because of the large aspect ratio of CNTs, the surface coverage needed to form a conducting path is extremely low. Figure 17a shows our calculation of the percolating surface coverage for objects with two different shapes, where D and L are the width and the length of the object. For CNTs with $D/L \approx 1/1000$, the surface coverage for percolation is ~0.57%, much smaller than that of conducting disks ~68%. We have tested this percolation behavior using[259−261] the filtration method to make films of controlled density (Figure 17b). The experimental data fit well to the percolation formula. The exponent coefficient is 1.31, close to the theoretical prediction of 4/3. The two basic formulas for percolation are:

$$\sigma \sim (N - N_c)^{\alpha} \quad (1)$$

$$l(\pi N_c)^{0.5} = 4.236 \quad (2)$$

where σ refers to the DC conductivity, N is the CS density, N_c is the critical density corresponding to the percolation threshold, and l is the length of the CNT. For CNTs with a typical length of 2 μm, the percolation threshold is 1.43 CNTs/μm^2. Obrzut et a. and Haddon et al. have also studied the percolation behavior for CNT networks by varying the density of the tubes and found similar results.[23,262] Chhowalla et al. found two distinct percolation thresholds: the metallic tube percolation threshold, $\Phi \approx 5.5 \times 10^{-3}$, is much higher than the overall threshold, $\Phi = 1.8 \times 10^{-3}$.[32] Percolation issues are extremely important for CNT thin film transistor applications, where the density of the CNT film needs to be above but close to the percolation threshold. Ideally, the surface coverage of CNTs for thin film transistors needs to be between the two percolation thresholds, to provide full conduction pathways but to avoid a shorting metallic pathway. Winey et al. studied the dependence of the electrical conduction and the percolation threshold on the alignment of the CNTs.[263] Figure 17c shows the simulation result where θ_μ is the cutoff angle. They found that at fixed loading, slightly anisotropic networks form more percolated pathways than isotropic networks. As shown in Figure 17d, the cutoff angle, an indication of the alignment level, shows strong dependence on the loading of the sticks for a 2D percolation system. At low loadings, even slight anisotropy significantly increases the number of percolation clusters relative to the isotropic case. Ural et al. studies the 1/*f* noise of transport measurement in percolating CNT networks, and they propose that the 1/*f* noise is a more sensitive measure of percolation than resistivity.[49] Therefore, 1/*f* noise measurement can help improve the performance of these nanomaterials in potential device applications where noise is an important figure of merit. They studied the noise of percolating networks versus film length and width. As shown in Figure 17e, the noise amplitude (A) decreases with the width, which is due to the

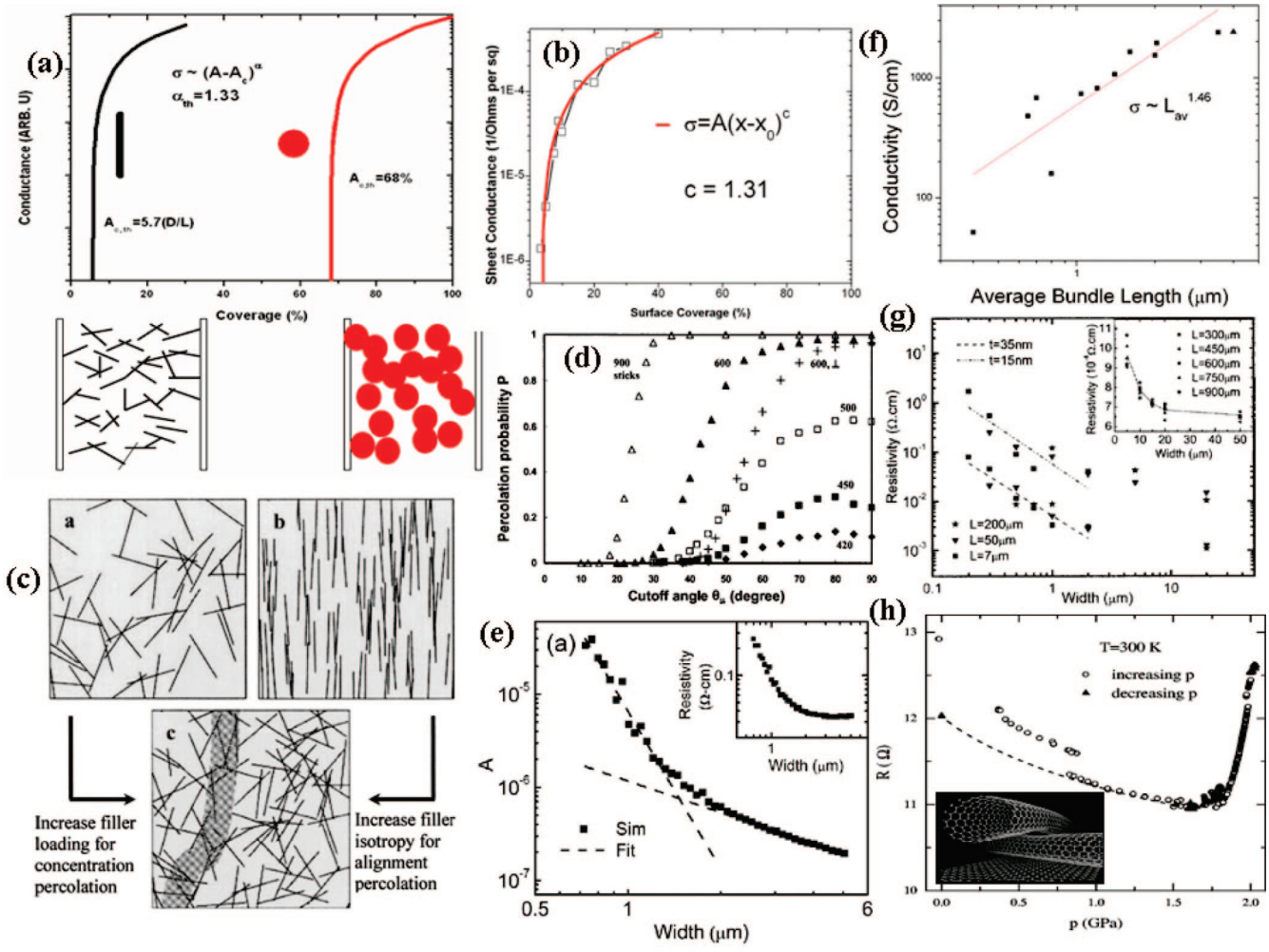

Figure 17. (a) Comparison of conductance vs surface coverage for sticks and circular objects based on calculation. (b) Experimental data for sheet conductance vs surface coverage for films with filtration method. (Reprinted with permission from ref 260. Copyright 2004 American Chemical Society.) (c) 2D stick-in-unit square simulation. (a) 50 sticks with $\theta_\mu = 90°$ (random). (b) 100 sticks with $\theta_\mu = 5°$ (highly aligned). (c) 100 sticks with $\theta_\mu = 90°$ exhibit percolation. All of the sticks have $L = 0.255$ relative to the unit square. (d) Percolation probability, P, along the stick alignment direction from simulation results. The cutoff angles from the left to right are 11°, 21°, 31°, 33°, 37°. (Reprinted with permission from ref 263. Copyright 2005 American Institute of Physics.) (e) Log−log plot of calculated noise amplitude (A) vs width for a device with $L = 5$ μm and $t = 16$ nm. There are two regions divided for large width and small width. (f) DC conductivity of CNT film vs average bundle length in the film. (Reprinted with permission from ref 49. Copyright 2008 American Institute of Physics.) (g) Log−log plot of resistivity vs width for CNT film with thickness of 15 and 35 nm and $L = 7$, 50, and 200 μm. For width <2 μm, the resistivity vs width can be fitted to power law. (Reprinted with permission from ref 37. Copyright 2006 American Institute of Physics.) (h) Pressure dependence of the room temperature resistivity. The inset shows the molecular mechanics calculation on the radial deformation of the CNTs. (Reprinted with permission from ref 208. Copyright 2000 American Institute of Physics.)

fact that A scales inversely with the number of carriers (N), which increases linearly with device width.

Because CNT film resistance is dominated by the junctions between tubes, it is favorable to have longer tubes in the film. We have experimentally proven this idea.[264] CNTs with different lengths (made by various sonication times) were used to make films, and the conductivity of the films was measured, as well as the CNT bundle length and diameter. In this study, CNT bundles rather than individual CNTs exist. However, because the current mostly flows along the outside of CNTs before coupling to the inside tubes, this is a still a valid study, which is applicable to CNT networks with well separated tubes. We found that the conductivity scales with length as $\sigma \approx L_{av}^{1.46}$ (Figure 17f). There are several assumptions made before using the power law fitting: (1) the coupling from outside tubes to inside tubes is small; (b) the contact between CNT bundles is rigid and point-like; and (c) the resistance of the network is dominated by the junctions. We also predicted that the conductivity scales with the bundle size as $\sigma \approx D_{av}^{-\beta}$, where β is between 0 and 2. This length-dependent study is important for predicting the CNT film performance with the tube length and can be a guide for further improvement of CNT conductivity.

Another geometrical dependence is the film width dependence. Ural et al. studied the resistivity scaling of CNT films patterned to submicrometer dimensions with e-beam lithography.[37] Figure 17g shows the resistance scaling with film width for widths less than 2 μm. The data fit well to a power law, as $\rho \approx W^{-1.53}$ for a thickness of 15 nm and $\rho \approx W^{-1.43}$ for a thickness of 35 nm. They did not observe such dramatic resistance scaling for widths larger than 2 μm. The reason for such a power law decrease of resistivity with film width is related to percolation. The nanotube film consists of many parallel conducting paths, each path consisting of multiple nanotubes in series. Because the in-plane orientation of individual nanotubes in the film is random, conduction paths are not perfectly aligned with the direction of current flow. As a result, reducing the device width W eliminates not only those conducting paths that lie entirely in the etched area, but also those that partially lie in that area. Consequently, reducing W increases the resistance at a rate faster than $1/W$. Molecular mechanics-based calculation shows that CNTs will deform under extreme pressure. Forro et al. and Fischer et al. have done some work on the pressure dependence of CNT film transport.[55,208] In both studies, they found that the resistance decreases first with pressure due to improvement in CNT−CNT contact leading to a lower transport barrier (Figure 17h). As the pressure increases to a large value (1.8 GPa in the Forro study), the resistance starts to increase dramatically. This increase is due to hexagonal deformation of the tubes, which is evidenced by Raman experiments.[265]

4.2.2. Energy Scaling

This section will focus on the transport properties of CNT films with respect to temperature, frequency, and electric field. These three energy scales (kT for temperature, hv for frequency, and eV for electric field), will affect the transport properties, which are typical and well studied for percolating networks.[261] Because of the mixture of metallic and semiconducting CNTs in a thin film, the junction resistance dominates the overall transport. These junctions increase the transport dependence on temperature, frequency, and voltage for percolating CNT films. Overall, the transport is governed by transport through the metallic regions and hopping or tunneling between metallic regions. The transport also shows thickness dependence, because the metallic path number increases as the CNT film thickness increases.[266] Temperature-dependent transport properties of SWCNT films have been widely studied, usually for thin nanotube films (on the order of 10 nm thick).[267,268] The resistance of such films includes two parts, which follows eq 3:

$$\rho(T) = A \exp\left(\frac{-T_m}{T}\right) + B \exp\left(\frac{T_b}{T + T_s}\right) \quad (3)$$

The first term accounts for the quasi-1D metallic conduction with a characteristic energy $k_b T_m$ to account for backscattering of the charge carriers, and the second term corresponds to fluctuation-assisted tunneling between nanotube boundaries. T_b and T_s characterize the barriers' height and width, respectively. For many cases, the first term is dropped because the junction resistance dominates the overall resistance of the films. Another model, as shown in eq 4, sometimes is employed as well:

$$\rho(T) = AT + B \exp\left(\frac{T_b}{T + T_s}\right) \quad (4)$$

Here, the metal-like term replaces the first term in eq 3 (i.e., the transport on nanotubes can be views as in pure metals). On the other hand, for submonolayer networks close to the percolation threshold, transport along the nanotubes is essentially eliminated, and the transport in such a network follows the variable range hopping (VRH) model:

$$\rho(T) = \rho_0 \exp\left(\frac{T_0}{T}\right)^{1/1+d} \quad d = 2 \text{ for 2D and 3 for 3D films} \quad (5)$$

One would expect that, as the film thickness decreases, one would see a crossover from 3D VRH to 2D VRH behavior.

Kaiser et al. did extensive research on the temperature dependence of transport properties of CNT thin films with varying film thickness (Figure 18a).[266] For a thick CNT buckypaper, they used eq 3 to explain the transport and suggested that the main contribution to the metallic behavior arises from the zone boundary in-plane phonon scattering. As the CNT film thickness increases, the transport transitions from semiconducting to metallic behavior. Such a transition is indicated by a change in sign of the slope of the resistivity versus temperature curve. Haddon et al. used this sign change to study bolometric infrared photoresponse of suspended CNT films.[269] The temperature coefficient of resistance (TCR) sign change is due to competition between transport in the highly conductive metallic-like regions (negative TCR) and the hopping or tunneling between the metallic clusters (positive TCR). As CNT film thickness decreases, the metallic characteristics are essentially eliminated, with the conductivity extrapolating to almost zero in the zero temperature limits (Figure 18a). Kaiser et al. also studied the temperature-dependent resistance of chemically treated CNT films (Figure 18b). After a treatment with $SOCl_2$, the conductivity increases by a larger fraction at low temperatures than at high temperatures, but the sign change of the TCR is retained. They suggested that fluctuation-assist tunneling between the metallic clusters is the transport mechanism for $SOCl_2$-doped films.[24] They concluded that the main effect of exposure to different chemicals is a change

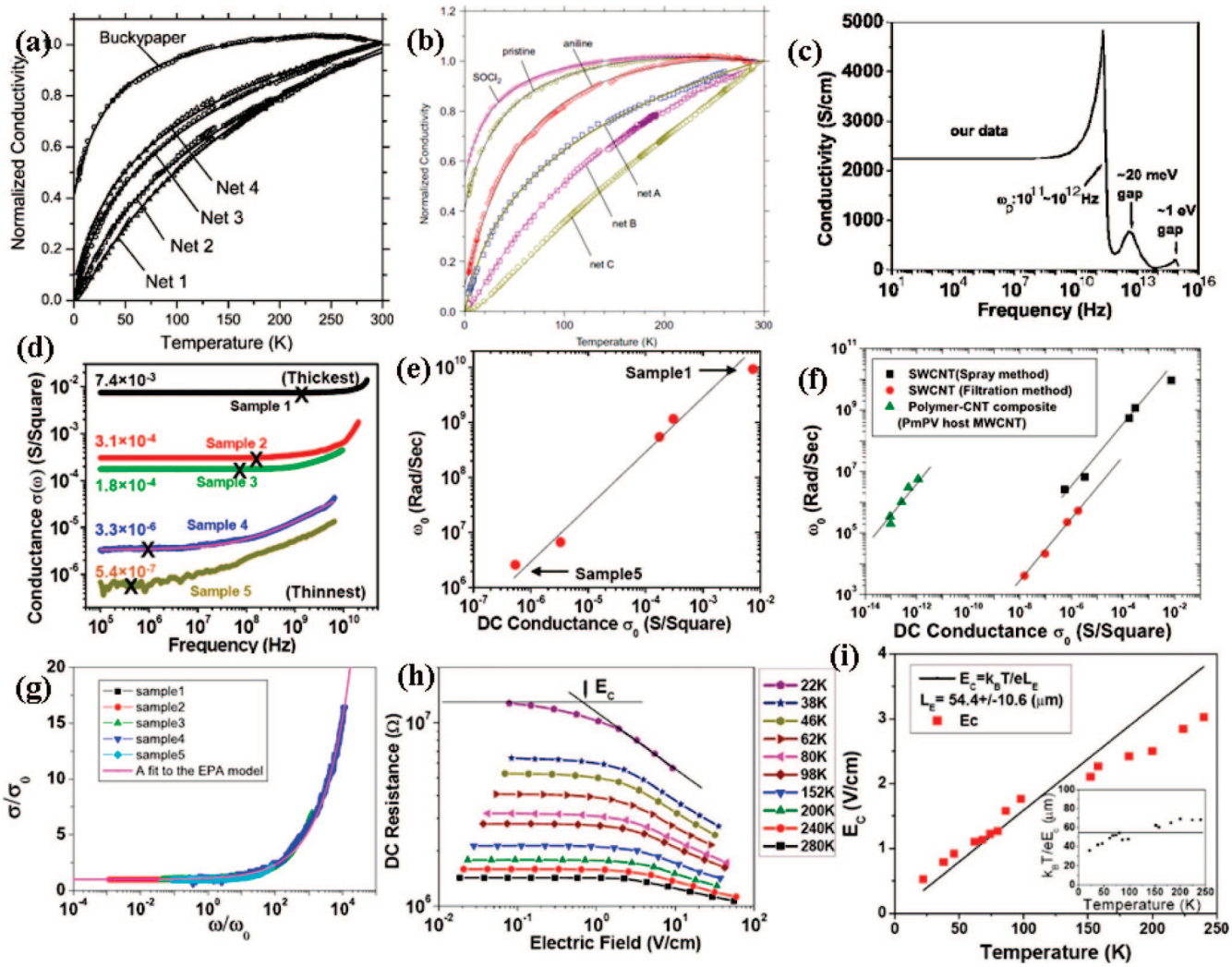

Figure 18. (a) Temperature-dependent resistance of CNT bucky paper (free-standing) and thin CNT films. The resistance is normalized to their room temperature values. Film thickness increases from net 1 to net 4.[266] (b) As (a) for doped CNT films. From A to C, the film thickness is reduced. (Reprinted with permission from ref 266. Copyright 2006 American Institute of Physics.) (c) Conductivity of SWCNT films in a broad frequency range: from DC to visible.[280] (Reprinted with permission from ref 280. Copyright 2007 American Institute of Physics.) (d) Real part of ac conductance for samples with different thickness at room temperature. (Reprinted with permission from ref 280. Copyright 2007 American Institute of Physics.) (e) The onset frequencies vs dc conductance of CNT films. The solid line has a slope of 1. (f) The onset frequency vs dc conductance for different CNT film thickness at room temperature. (g) Master scaling curve showing the ac conductance for CNT films with different density from (b). (h) Resistance vs current and (i) E_c vs temperature for monolayer nanotube film. The inset shows the localization length at different temperatures.[170] (Reprinted with permission from ref 170. Copyright 2008 American Institute of Physics.)

in the density of charge carriers that leads to increased or decreased conductivity, while the overall nature of conductance is retained. Wang et al. studied the transport properties of MWCNT films over a much higher temperature range, 328−958 K.[270] However, they found that in such a high temperature range, they observed that the dense MWCNT films show exclusively nonmetallic temperature dependence of electrical conductivity due to the absence of metallic conduction mechanism in such a highly disordered system. The weak dependence of resistance on temperature (only 35% change of resistance over a range from 328−958 K) is explained by variable range hopping and fluctuation-assist tunneling.

Frequency-dependent conductance in a percolating system with randomly distributed objects is a universal phenomenon.[261] At low frequencies, the conductivity increases with increasing frequency as the coupling due to capacitance or inductance starts to increase. This increase in conductance typically follows a power law.[271] The conductivity continues to increase through microwave frequencies. At higher frequencies in the THz range, the plasma frequency is reached and the carriers can no longer follow the electric field; a sharp decrease of the conductivity is observed. Above the THz range, optical absorption dominates the conductivity. The optical conductivities will be dominated by the optical properties of the material. Detailed studies of the frequency dependence of the conduction along CNT films will greatly benefit applications. From the radio frequency to the microwave frequency range, understanding the transport will benefit applications in high speed CNT thin film transistors, interconnects use in high speed circuits using CNT electrodes, and microwave shielding.[272−275] For higher frequency ranges in the THz and optical frequencies, applications as optoelectronic materials for devices such as infrared modulators and infrared electrode applications emerge.[276] Conductivity of SWCNT films has been measured in various frequency ranges. The AC conductance of percolating SWCNT networks up to 100 MHz has shown that there is a

universal power law in such CNT systems with randomly distributed barriers.[277] The frequency-dependent conductivity follows the plasma behavior similar to that in metals in the frequencies from 0.1 to 1 THz.[278] At higher frequencies, Ugawa et al. and Ruzicka et al. found that the conductivity has two peaks: one is near 20 meV, corresponding to the secondary band gap; the other one is the optical band gap around 1 eV.[208,279] The optical band gap does not depend on chemical doping or SWCNT purity, whereas the secondary band gap largely depends on these factors. Combined with our measurements, a plot of the conductivity over a broad frequency range (DC to 10^{16} Hz) is shown in Figure 18c.[170] For different SWCNT sources, purities, and chemical doping levels, the position and height of the peak corresponding to the 20 meV gap, as well as the plasma frequency, will change. However, the peak at the optical band gap will be unchanged for various SWCNT sources, purities, and doping. A Corbino reflectometry setup was used to investigate the conductivity of SWCNT networks over a broad frequency range.[280] To measure the conductivity in as broad a frequency range as possible, two different network analyzers covering different frequency ranges were used. The Agilent E8364B network analyzer covers between 10 MHz and 50 GHz and the Agilent 4396B network analyzer covers between 100 kHz and 1.8 GHz, giving five and a half decades of frequency coverage. For all of the films, the real parts of the conductance keep their dc value up to a characteristic frequency and start to increase at higher frequency (Figure 18d). This behavior has been widely observed for disordered systems. Similar behavior has been observed in CNT−polymer composite systems.[277,281] The data were fitted using the model of the extended pair approximation model, which is described in eq 6.

$$\sigma = \sigma_0(1 + k(\omega/\omega_0)^s) \quad (6)$$

Here, σ_0 is the dc conductance, $s \leq 1$, k is a constant, and ω_0 is the onset frequency. The fitted onset frequency increases with film thickness and scales well with the film conductance (Figure 18e). Films with higher density require higher frequency to see the contribution from ac coupling to the overall conductance, due to the larger contribution from the metallic background. The data from DC to 1 MHz, together with the microwave frequency range data and the CNT−polymer composite data, are shown in Figure 18f. Although the intercepts are very different due to the varying dc conductance, the slopes of the three different samples are essentially the same. The linear relationship shown in both Figure 18e and f is one of the characteristic features of the ac conductance of disordered solids. Taking the DC conductivity and onset frequency, we observed that all of the data scales to a universal curve, as shown in Figure 18g.[170]

Tunneling is the transport mechanism for nanotube films with nonmetallic barriers between nanotube bundles, which leads to electric field-dependent nonlinearity. Such nonlinearity was observed previously by M. Fuhrer et al. and A. B. Kaiser et al.[128,170,282,283] Their studies were for relatively thick films with low R_s, and one of the main conclusions was that the temperature-independent localization radius is approximately 330 nm. Together with the microwave frequency independence of the resistance, they suggested that the disorder of the system is due to the imperfections in the individual CNTs. In a separate study, Grüner et al. observed clear frequency-dependent conductivity up to microwave frequencies. Figure 18h shows the resistance versus electric field for films at different densities at 4.4 K and at room temperature, respectively. At 4.4 K, nonlinear behavior is observed for all of the samples. As the electric field increases, the resistance starts to decrease above a certain value of the electrical field, a typical semiconductor-like behavior. This behavior can be understood given the fact that the nanotube networks are comprised of nanotube−nanotube junctions. As the electric field increases, the carriers gain enough energy to tunnel through the SB, and therefore the resistance decreases. At room temperature, nonlinear behavior is not observed in the measurement voltage range. Fuhrer et al. also observed a temperature-quenching effect of the nonlinear behavior.[283] As in the SB, the resistance follows the trend as $R \propto \exp(-eV/kT)$. The critical electric field is defined as the intersection of the extension from the constant resistance and the deep decrease. The critical electric field depends on the R_s and the temperature. As the film thickness decreases, the nonlinear behavior is more pronounced, and the critical electric field decreases. For thinner films (submonolayer films), there is no full path of metallic nanotubes, and the network is a purely SB system. As the films get thicker, there are more metallic paths with weak electrical field-dependent conductance. Figure 18i shows the dependence of the critical electric field on the R_s, that is, on the film thickness. The fitting leads to $E_c \approx \ln(R)$. The critical field increases linearly with the temperature, leading to a localization length of approximately 50 μm. Although the localization behavior may be affected by the properties of individual nanotubes, the result shows that the observed behavior is more likely a consequence of poor electric conduction through interbundle junctions. As the thickness and density increase, there are more connections, which decreases the length scale. A thinner film has a larger correlation length, so it has a smaller onset frequency. An approximate empirical formula relating the onset frequency and nonlinear transport length scale establishes contact between the frequency and electric field-dependent conductivity, which helps us to understand the electric transport properties of the nanotube films.

In summary, scaling of resistance with nanotube bundle length and diameter networks varied as a power law in the average bundle length, with an exponent of 1.46, and the conductivity should vary as $D_{av}^{-\beta}$, where β is between 0 and 2; these facts can provide a guideline for improving nanotube film conductivity, using longer nanotubes and smaller bundles. 2D density-dependent percolation behavior was observed, in which the percolation threshold density depends on the nanotube length, which can benefit nanotube transistor design, where the nanotube network is needed to be slightly threshold density. The frequency-dependent power law conductivity follows the universal phenomenon observed for systems with randomly distributed barriers. The study of the network transport properties at high frequencies will be useful for high speed nanotube thin film FET designs. The frequency-dependent conductivity ranging from DC to visible frequency is plotted, which can be useful for electronic and optoelectronic device design. Temperature and electrical field nonlinearities are observed for nanotube films with different densities. For submonolayer films, 3D VRH hopping is the transport mechanism, while for thicker films, fluctuation-assisted tunneling is the mechanism. The electric field nonlinearity leads to a thickness and temperature-dependent onset in the electric field. The temperature- and electric field-

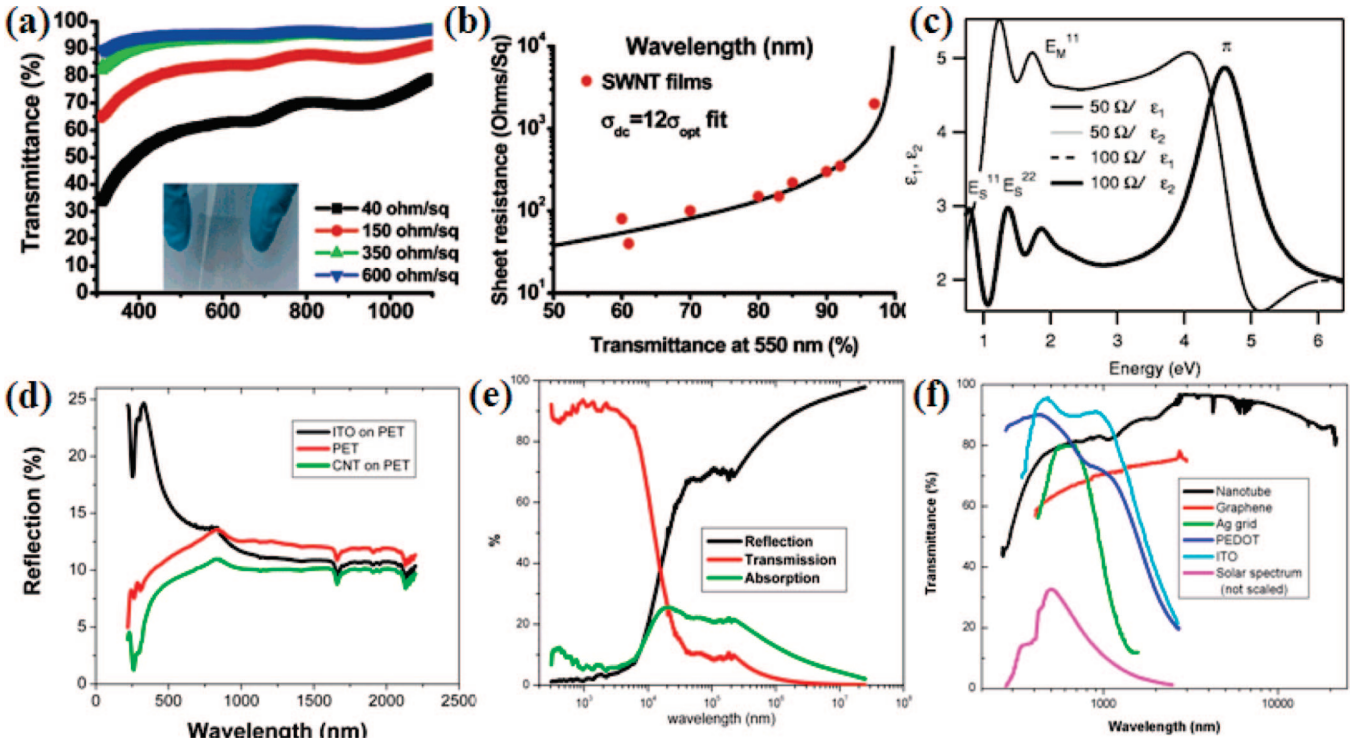

Figure 19. (a) Transmittance vs wavelength for CNT films with different film thickness. The inset shows a photograph of a CNT films on a flexible PET substrate. (b) DC R_s vs transmittance of CNT films at 550 nm for different film thickness. The solid line is the fitting using equation. (Reprinted with permission from ref 35. Copyright 2006 American Chemical Society.) (c) Real and imaginary dielectric constants as a function of energy for 50 and 100 Ω/□ films. (Reprinted with permission from ref 286. Copyright 2007 American Institute of Physics.) (d) Reflection comparison between CNT and ITO films. (e) Calculated reflection, transmission, and absorption of CNT thin films in a broad wavelength range from 400 nm to 2 cm. (f) Comparison of spectra for various transparent and electrically conductive materials including nanotube thin film, graphene thin film, Ag nanowire thin film, PEDOT, and ITO to demonstrate the advantages of using nanotube and graphene thin films in the longer wavelength range. (Reprinted with permission from ref 276. Copyright 2009 American Institute of Physics.)

dependent resistance studies can benefit applications using nanotubes for macroelectronics.

4.3. Optoelectronic Properties

Thin films of CNTs with thicknesses between ~10−100 nm have high electrical conductivity and optical transmittance in the visible range due to the sparse structure of such a network.[7,28,35,38,57,119,242,284] As the film thickness increases, the film loses transmittance through absorption. Figure 19a shows the transmittance of CNT films in the visible range. The inset shows a bent CNT film on a PET substrate with high optical transparency.[35] The performance of transparent and conductive films highly depends on the tube purity, doping level, tube length, and dispersion quality. The material quality and the process details determine the film performance. DC conductivity can be used as a gauge to evaluate film performance, and is calculated from the R_s and thickness of the films, $\sigma_{dc} = 1/R_s d$. The thickness of CNT films is normally measured by an AFM image taken at the film edge. Another method was developed to quantify and compare conductive and transparent CNT films using the following formula:[259]

$$T = \left(1 + \frac{1}{2R_s}\sqrt{\frac{\mu_0}{\varepsilon_0}}\frac{\sigma_{op}}{\sigma_{dc}}\right)^{-2} = \left(1 + \frac{188(\Omega)}{R_s}\frac{\sigma_{op}}{\sigma_{dc}}\right)^{-2} \quad (7)$$

This formula characterizes thin metal films where the absorption of the material is much smaller than the reflectance, and the thickness of the film is much less than the wavelength of interest. One needs to be careful when applying this formula, especially for CNT thin films meet these two conditions. Degiorgi et al. have measured the optical conductivity for their CNT films at 550 nm to be 200 S/cm, and it is this number that is typically used.[208] Because the optical conductivity is independent of the doping level, this value of ac conductivity is assumed to be constant across different films. By fitting our data into this formula, we obtain a dc conductivity of 2400 S/cm, which agrees well with the dc conductivity obtained from the calculation of $1/R_s d$. Care should be used when applying this formula. The optical conductivity depends on the tube wall number and diameter. This method is valid to compare the relative performance of transparent and conductive films with the end parameter being the dc conductivity. Another commonly used method for characterizing the performance of transparent conductors is using the figure of merit, defined as T^{10}/R.[285]

There are two methods for obtaining the optical constants for CNT films. One method is to measure the reflection of films over a large frequency range and used a Kramers−Kronig transformation to extrapolate the other parameters.[208] Alternatively, one can use a technique known as spectroscopic ellipsometry that measures the s and p components of the incident light before and after the CNT films.[286] The optical constants can be fitted on the basis of the two parameter measurements. Figure 19c shows the dielectric constants based on the ellipsometry measurement.[286] The optical constant values were based on the fittings to spectroscopic ellipsometry. The reflection constants (n, k)

Table 2. Comparison of Various Types of Transparent Electrodes[a]

	thickness (um)	R_s (OPS)	T at 550 nm (%)	figure of merit 550 nm T^{10}/R_s	conductivity (S/cm)	n (550 nm)	k (550 nm)	carrier density/cm^{-3}	cutoff wavelength (μm)
carbon nanotube	25	200	80	0.54	2000	1.03−1.5	0.24	10^{17}	10−20
graphene	10	1800	70	0.02	555	1.57	0.25	10^{18}	4
metal nanowire or thin film (i.e., Ag or Au)	average 10	22	88	12.66	45 454			5.9×10^{22}	0.33
PEDOT	50	200	85	0.98	1000	1.5	0.04−0.2		~1
ITO	50−120	10−300	88	0.93−27.85	~1000 on plastic	2.0	0	$\sim 10^{20}$	~1

[a] Reprinted with permission from ref 276. Copyright 2009 American Institute of Physics.

in the visible range can be calculated on the basis of a standard optics formula. For the THz range, Shimano et al. measured the THz time-domain spectroscopy of CNTs from 0.2 to 20 THz. The complex dielectric constants were obtained without the use of the Kramers−Kronig analysis. The real part of the dielectric constant shows very large and positive values at frequencies below 2 THz.[7,287,288]

The complete optical characterization of CNT films allows the calculation of optical performance such as transmittance, reflection, and absorption for any given wavelength and film thickness using the standard optics formula. Figure 19c shows the reflection comparisons between CNT film and ITO electrodes.[195] The CNT film is coated on a flexible PET substrate. Because of the good index matching between CNTs and polymers, CNT coating on PET does not significantly change the reflection of PET. This is different from ITO, which can add substantially to the reflection from a PET surface. The loss of transmittance for CNT films is largely due to the absorption of the CNT films. For ITO, the loss of transmittance is mainly due to the high reflection. The optical properties depend on the band gap, which can be tuned by an applied voltage. Rinzler et al. have reported the voltage-dependent transmittance of CNT films.[284] Because of the intrinsic 2D properties of nanotubes, CNT films also show an interesting angle-dependent transmittance. Chhowalla et al. reported on the optical anisotropy in CNT thin films by combining transmission measurements at a few incident angles with spectroscopic ellipsometry measurements. They found that the resulting solar cell using transparent CNT electrodes shows angle-dependent efficiency.[289]

The optical properties over a broader wavelength range have been studied by several groups. The reflection, absorption, and transmittance were calculated on the basis of the optical constants (Figure 19e).[276] Grüner et al. have also measured the CNT film transmittance in the IR range by using an IR transparent ZnSe substrate. The data, together with other transparent films, were compared in Figure 19f. They also summarized the electrical performance, the cutoff wavelength, the free carrier density, and the figure of merit for various transparent electrodes including CNT thin films, graphene, Ag grids, conductive polymers such as PEDOT, and ITO.[92,161,290−292] It is clear that graphene and CNT films outperform other transparent electrodes in the far-infrared range. CNT films are transparent all of the way up to 22 μm, which make them attractive for infrared applications such as IR imaging and IR solar cells. For applications, PEDOT, CNT, and graphene thin films have high work functions, so that they can be used as anodes in optoelectronic devices. Second, due to their low charge carrier density, CNTs and graphene have high cutoff wavelengths, which make them appropriate for applications requiring IR transparent electrodes. CNT thin films have the highest cutoff wavelength and are the best candidate for longer wave IR applications. Last, CNT thin films have the lowest reflection among the transparent films discussed here. Metal nanowires, graphene, and ITO all have reflection larger than 10% in the visible range, such that an antireflection coating is preferred for these electrodes. Table 2 lists the comparison of various transparent electrodes.[276]

4.4. Mechanical Properties

Because of the large aspect ratio and strong bonds, individual CNTs have superior mechanical flexibility and elastic properties under large strain and load.[293] The mechanical properties of individual CNTs have been widely studied through simulation and experiments.[294] CNTs maintain their structure up to large strain, and their response depends on CNT chirality. Several classes of behavior of CNTs under a tensile loading have been proposed through molecular dynamic simulations. Under large deformation such as large strain and bending, different types of defects are formed, which greatly affects the electrical transport properties.[295] On the other hand, individual CNTs have strong binding energy with substrates. Avouris et al. found that the can der Waals interactions between CNTs and a substrate lead to a substantial axial and radial deformation of adsorbed CNTs, destroying their idealized shape.[296,297] The strain energy caused by the CNT−substrate interaction varies with tube diameter as d^4, while the adhesion energy varies as d. Thus, a substrate with surface curvature higher than the critical surface curvature c_c will lead to the kind of elastic deformation seen in Figure 17. Because of the superior mechanical properties of individual CNTs and their strong substrate interactions, thin films made of randomly distributed CNTs show unprecedented mechanical performance such as mechanical flexibility, stretchability, and foldability, which are essentially useful for flexible displays. Figure 20a shows a large piece of transparent and flexible CNT film on a PET substrate as a product from Unidym Inc. The mechanical flexibility of CNT and ITO electrodes is measured by wrapping the film along a cylinder of known radius and measuring the resistance before and after the bending. As shown in Figure 20b, CNT films can be bent down to a radius of 2 mm without any electrical failure, while ITO on PET begins to fail at a bending radius of 13 mm.[197] ITO failure is typically due to the internal stresses built up due to its thickness and the solid packing of the material; CNTs, however, have outstanding bending ability, strong interactions with substrates, and a large portion of void volume to relieve stress built up during the bending test. Figure 20c shows an SEM image of ITO on a PET substrate after bending. Clear cracks were developed across the bending direction, which explains the large resistance change.

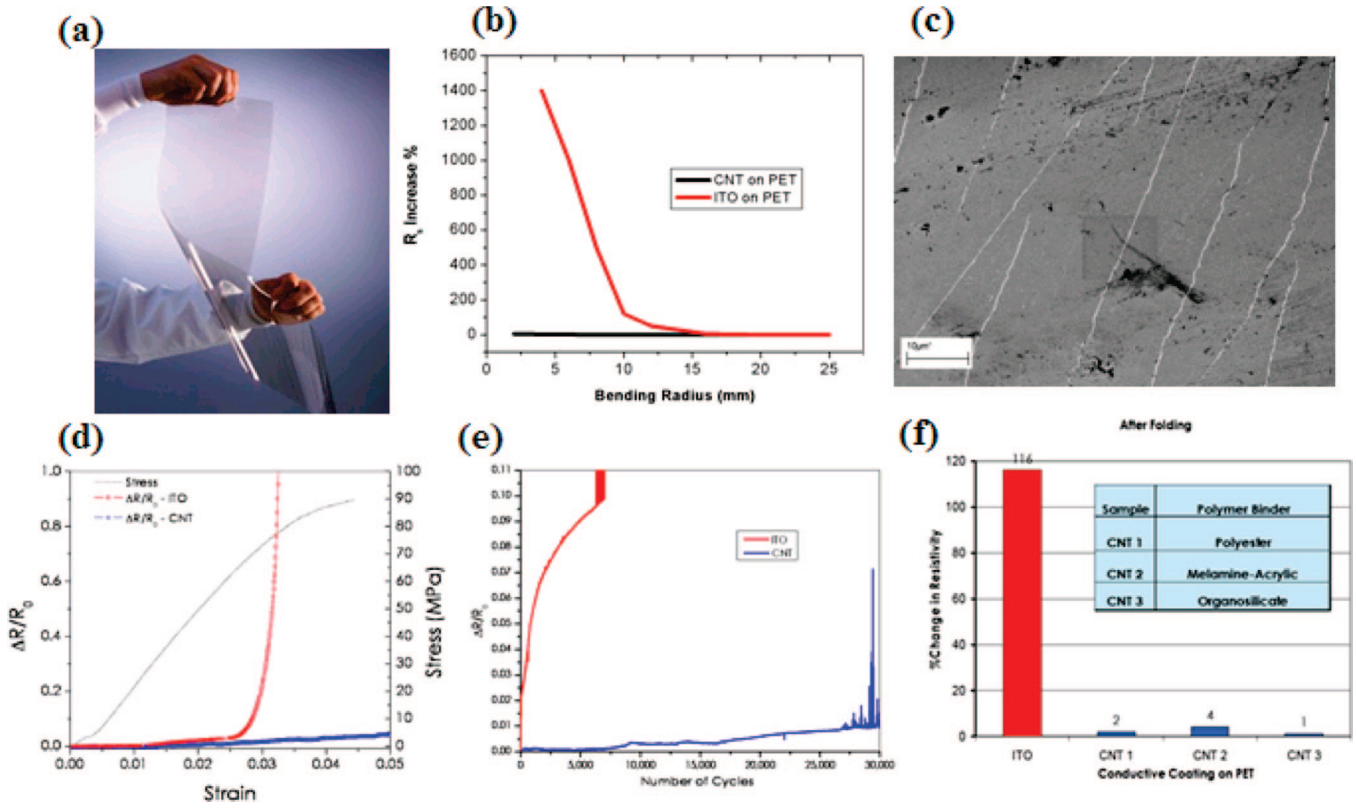

Figure 20. (a) A small sample of a carbon-nanotube-coated plastic film that could be used as the transparent electrode in touch screens, roll-up displays, and thin-film solar cells. (Copyright Unidym Inc.) (b) Bending test result comparison for CNT thin film and ITO on PET substrates. (c) SEM of SWCNT network on PET after bending on 2 mm curvature. (d) Minimat tensile testing machine at 0.1 mm/min strain rate, in uniaxial tension comparing CNT and ITO-coated PET. (e) Cyclic testing of Invisicon CNT coating on 175 μm PET as compared to ITO on PET. (f) The abrasion resistance comparison between CNT and ITO. CNT are with a different polymer. (Reprinted with permission from ref 106. Copyright The Society of Information Display.)

Tensile testing of CNT thin films on plastic substrates has been studied by several groups.[106,298] Figure 20d shows the results from Luo et al.[106] In their study, CNT films on heat-stabilized PET substrates were fabricated with a spray coating method, followed by a binder coating of melamine/acrylic with dip-coating. The films were air-dried and cured at 135 °C for 5 min. The film thickness is around 75 nm, and the R_s is around 650 Ω/□. The resistance was measured in situ using a digital multimeter. As shown in Figure 20d, the CNT film behaves elastically between 1−5% tensile strains. Above 5% strain, there appears to be plastic deformation in the PET substrate, which dominates the electrical-resistance response. However, even after 18% tensile strain, only a 14% change in resistance was observed. The onset of cracks in the ITO film occurs at ∼2% tensile strain, with ITO failing catastrophically before 3% tensile strain is reached. For certain device applications such as touch screen devices with transparent electrodes, the abrasion resistance, the single point touch resistance, and the cycling loading are important.[299] Figure 20e shows data by Luo et al. The sample condition is the same as for the tensile test. For the abrasion test, a 1 lb weight cotton cloth moves back and forth over transparent CNT films. One cycle includes two passes across the surface, and the R_s was measured before and after the abrasion. Figure 20f shows comparison data between CNT and ITO. Clearly, ITO film on a PET substrate shows a much larger change than CNT film on PET. For the flex cycling test, 0.7% strain amplitude and 1.25 Hz were used, and the resistance was measured continuously throughout the experiment. As shown in Figure 20f, the CNT coating shows <0.5% change in the resistance after 2500 cycles, whereas ITO on PET shows >2% increase after only 1000 cycles. The degradation in ITO resistance during flex testing is attributed to cracking of the ITO film. As flex cycling continues, these cracks continue to grow, ultimately leading to catastrophic failure (open circuit). At these strain levels, this failure mechanism is not observed for CNT coating on PET substrate. Gruner et al. recently reported CNT thin films on 3 M VHB 4905 substrates maintain electrical conductive up to 700% strain.[300] This substrate stretches uniformly without local cracks, which truly supports the CNT film during the stretching test. The failure of CNT films from other studies may be due to cracking of the substrate, and not due to the CNT films. The conductance of CNT films under large strain is extremely useful for flexible and stretchable electronic device applications. Although CNT thin films have superior mechanical properties, the interaction of CNTs without binder is poor, and the integrity of CNTs is not strong enough to maintain the mechanical properties.[301] Therefore, for device applications, normally another layer of polymer is deposited into CNT to form interpenetrated CNT/polymer networks.[302,303] Dokmeci et al. incorporated parylene-C into CNT films. The encapsulated CNT film is a mechanically robust, flexible, and conductive nanomaterial. The superior mechanical properties of CNT thin films on plastic substrates have enabled flexible or stretchable device applications. Rogers et al. have shown that the thin film transistor with CNT electrodes maintains device performance after repeated bending or 2.2% strain.[31,185,186,302]

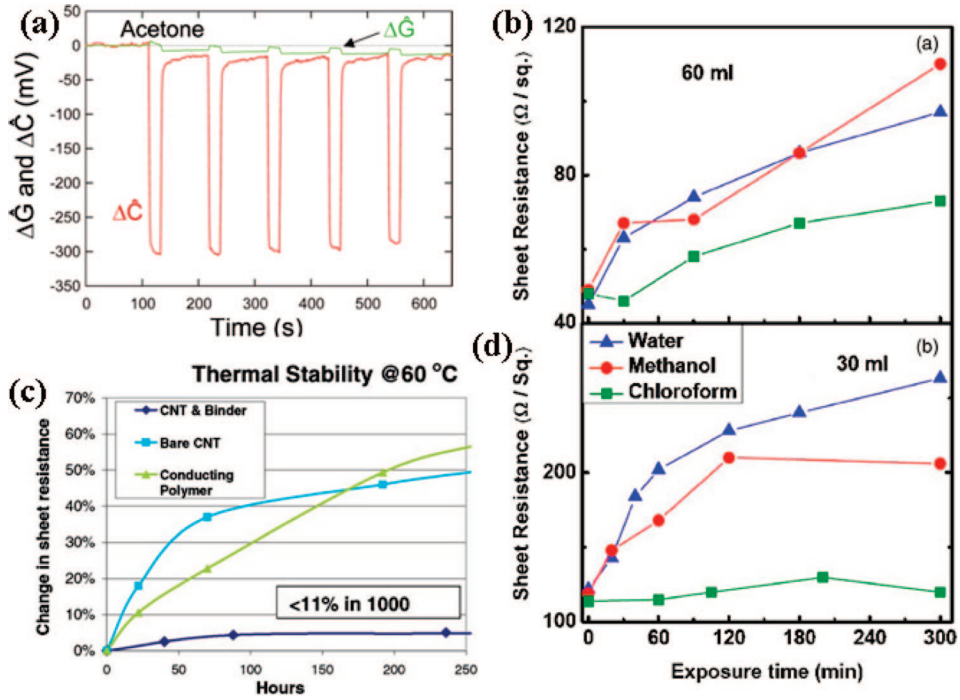

Figure 21. (a) Real time monitoring of normalized capacitance and conductance response to 20 s doses of acetone.[305] (Reprinted with permission from ref 305. Copyright 2005 American Chemical Society.) (b) Stability of bare CNT, CNT with binder, and conductive polymer under 60 °C for 250 h. (c,d) Resistance as a function of exposure time in solvents for a 60 and 30 mL of $SoCl_2$ treated. (Reprinted with permission from ref 78. Copyright 2007 American Institute of Physics.)

4.5. Chemical, UV, and Heat Stability

Because of the strong C−C bonds in CNTs, CNTs are relatively more robust as compared to conductive polymers. Because each carbon atom is on the surface, CNTs have been thoroughly studied for chemical and biological sensing applications.[96,207,304] For example, CNT-based sensors exhibit high sensitivity to NO_2 at concentrations as low as 10 ppb.[96] The absorption of chemicals and biological species has two possible effects: there could be a charge transfer to change the carrier number (commonly referred to as doping), or it could create a potential energy barrier for mobility along the CNTs. For example, exposure of CNTs to HNO_3 greatly improves the conductivity due to charge transfer (hole doping of CNT) between CNTs and HNO_3. There are two situations for film stability. One is the real time change in conductance as the film is being exposed to chemicals, and the other one is the conductance change after being exposed to chemicals. Perkins et al. used interdigitated electrodes to monitor the capacitance and conductance in real time as the CNT network is being exposed to various chemical vapors.[305] They found that for most vapors, the dielectric effect for the molecular adsorbate dominates the capacitance, and the charge transfer controls the conductance response. Figure 21a shows the capacitance and conductance response observed for CNT network exposed to acetone. The response is quick due to acetone vapor weakly physisorbed on the CNT surface, allowing it to quickly desorb once the ambient vapor is removed. The conductance of CNT films decreases dramatically after being exposed to acetone and also recovers quickly. Liu et al. studied the responses of CNT networks to different surfactants.[306] They found that adsorption of ionic surfactants on the surface in liquid significantly modulates the conductance of CNT network. Unmodified CNT devices were sensitive to the presence of cationic surfactants, while PEI-modified devices were sensitive to anionic surfactants. Because the optoelectronic devices such as OLED and touch screens where CNT thin films are to be used are well sealed, the sensitivity of CNT films will not affect their applications.

For electronic device applications, the CNT films need to be stable after exposure to chemicals, UV, heat, and moisture. For example, transparent electrode applications using CNT thin films must have a limited change of resistance after exposure to chemicals. The chemicals include acetone, isopropanol, acid, base, and toluene among others, as these are commonly used in the device fabrication process.[307] Changes in conductivity upon chemical exposure may be due to changes in film morphology, or doping effects.[195] Figure 21b and d shows the stability of $SOCl_2$-treated CNT films.[78] HiPCO CNTs were used, and films were exposed to water, methanol, and chloroform. The films were stable in chloroform, which is significant because chloroform is widely used for spin-coating polythiophene−-fullerene blends used in organic photovoltaic devices. The R_s change after exposure to methanol and water is rather significant. Also, we found that the films have poor resistance to base solvents. After the exposure of CNT films to base such as NaOH, CNT films peel off the substrates easily, and the electrical conductance decreases significantly. Binders or encapsulation incorporating polymers into the CNT network can significantly improve the stability.[106,308] Note that, unlike conducting polymers, the optical transmittance of the films does not change after exposure to solvents. Figure 21c shows the heat stability of CNT films as compared to conductive polymers. The binder significantly improves the heat stability of CNT films, and the overall stability of the CNT films is much better than conductive polymers. The change of resistance under 60 °C for 250 h is less than 10%, which meets the requirement for transparent electrodes in optoelectronic device applications. For certain optoelectronic devices such as solar cells and touch screen panels for GPS navigators, the UV stability of CNT films is critical. CNTs are doped with oxygen through physisorption, and the binding energy is low, ∼10 kJ/mol,

comparable with UV radiation energy.[213] In a separate study, Cohen et al. found the adsorption energy of carbon and oxygen is 0.25 eV.[203] Directly exposing CNT films to UV will remove the oxygen dopants from the CNT surface and may cause defects.[309,310] The removal of oxygen is reversible, while damage to the surface is permanent. In real device applications, CNT thin film electrodes are under the protection of substrates and not directly exposed to UV energy. Baxendale et al. have compared the transport properties of bare and UV treated CNT films, and they found that the UV energy desorbs most of the dopants from CNT surfaces.[310] The UV stability of CNT films highly depends on the CNT source. We found that CNTs starting with more defects are much more vulnerable to UV irradiation. For device applications where UV exposure is unavoidable, higher quality and more robust CNTs are needed.[195]

5. Applications of Nanotube Thin Films

5.1. Overview

CNT thin films have found a large range of applications. The physical properties of CNT thin films with three different density ranges will guide specific applications. As outlined in the Introduction, we will discuss mainly three major applications in this Review. The first one is CNT thin film transistors, using a percolating network as the semiconductor active layer.[3,7,22,26,27,87,190,311−315] We will review the design criteria for various aspects of CNT FETs such as mobility, on/off ratio, and hysteresis. Transistor applications in flexible electronics and chemical and biological sensors will also be discussed. The second application for CNT thin films will be as optical transparent electrodes.[7,28,30,35,57,91,119,316,317] We will review the applications for transparent CNT electrodes in solar cells, displays, artificial actuators, and microwave shielding. In this part, novel applications such as transparent speakers and heaters will also be discussed. The third application for CNT thin films will be as nanoporous electrodes for energy storage application including batteries, fuel cells, and supercapacitors.[34,40,45,50,52,92,309,318−320] There are many applications for CNT thin films beyond these three major categories such as interconnects in microelectronics and field emission display; however, these will not be discussed in detail due to the limit and the focus of this Review.

5.2. Thin Film Transistor

5.2.1. TFTs with Carbon Nanotube Conductive Channel

Solution-based electronics have advantages over single-crystalline inorganic semiconductors such as Si and Ge in several aspects such as variety of substrate choice, low temperature fabrication processes, and no need for high vacuum deposition. Organic-based conjugated polymers have been envisioned as a viable alternative to mainstream thin film TFTs based on inorganic materials. However, solution-based TFTs cannot rival the performance of inorganic-based TFTs. Because of the nature of CNT networks as a mixture of semiconducting and metallic tubes, the heterojunctions dominate the overall conductance. CNT networks have been extensively explored as a semiconducting material used for thin film field effect transistors. Because of the high mobility of each individual CNT, thin film TFTs with CNTs have shown high mobility, which is essential for high speed electronics applications. Figure 22a shows the yearly improvement of mobility in thin film TFTs.[321] Widely used organic semiconductors such as polythiophenes and pentacene seem to have reached maturity as far as their performance is concerned. Device mobility based on CNT networks shows higher mobility than that demonstrated by the best organic materials. "Pick-up stick" transistors use a subpercolation network incorporated into organic materials to form a CNT−organic material hybrid transistor; these FETs have a high on/off ratio (dominated by the organic material), while having a large mobility thanks to the CNTs.[322] This section is devoted to pure CNT network-based thin film FETs. The key parameters of such thin film transistors such as mobility, on/off ratio, network capacitance, sub threshold swing, hysteresis, and high frequency response will be discussed in detail. Device configuration, p- and n-type devices, circuits based on CNT thin film TFTs, and electrolyte gating will also be discussed. In the end, CNT network enabled plastic transistors with outstanding mechanical flexibility and stretchability will be discussed.

CNT network-based field effect transistors have device structure similar to that of organic thin film FETs. In silicon-based transistors, the channel width between source (S) and drain (D) is modulated by the application of gate voltage, and the charge carriers are depleted, thus modulating the conductance (Figure 22b). The basic operating principle is that the transport properties of the CNT network between S/D can be modulated by applying a gate voltage. The CNT network and heavily doped Si separated by SiO_2 forms a capacitor structure. The application of voltage between the gate and S/D input can modulate the charge carrier number along the CNT film. This is often referred to as the "bottom gating" architecture. A polymer electrolyte can also be used as a "top gate", and this has a larger gating effect due to the strong coupling between the gate and the conductive channel.[171,323,324] The choice of metals is normally chosen to have the minimum contact resistance with CNTs. Different metals have different contact resistance with CNTs, and Pd is believed to have the smallest contact resistance.[230,232,235,325] Thanks to development work for organic TFTs, there is rich documentation for the study of various dielectric layers, device fabrication processes, patterning, and device physics, which can be applied to CNT network-based TFTs. To achieve superior device properties, using a high percentage of semiconducting CNTs is critical. The density of CNT networks is an extremely important parameter for achieving good performance due to the presence of possibly shorting metallic CNTs. The conduction path due to a metallic CNT channel significantly increases the off current, which lowers the on/off ratio of TFTs. For films made of CNT bundles, the metallic tubes in a bundle dominate the overall conduction of the bundle and will have no dependence on the gate voltage. Therefore, CNTs need to be as individualized as possible when a solution-based process is used to make TFTs. As detailed in the percolation study in the transport section, the percolating density for CNTs is around $1.4/\mu m^2$. Because 1/3 of CNTs are metallic, the design rule for CNT network TFTs is to avoid densities above the percolation density of metallic CNT paths, which is 3 times the CNT network percolation threshold, or $4.2/\mu m^2$.[273] Therefore, CNT TFTs with high on/off ratio should be in the range of $1.4-4.2\ \mu m^2$. For solution-based thin films with CNT bundles, the density of the CNT network should be slightly above $1.4\ \mu m^2$.

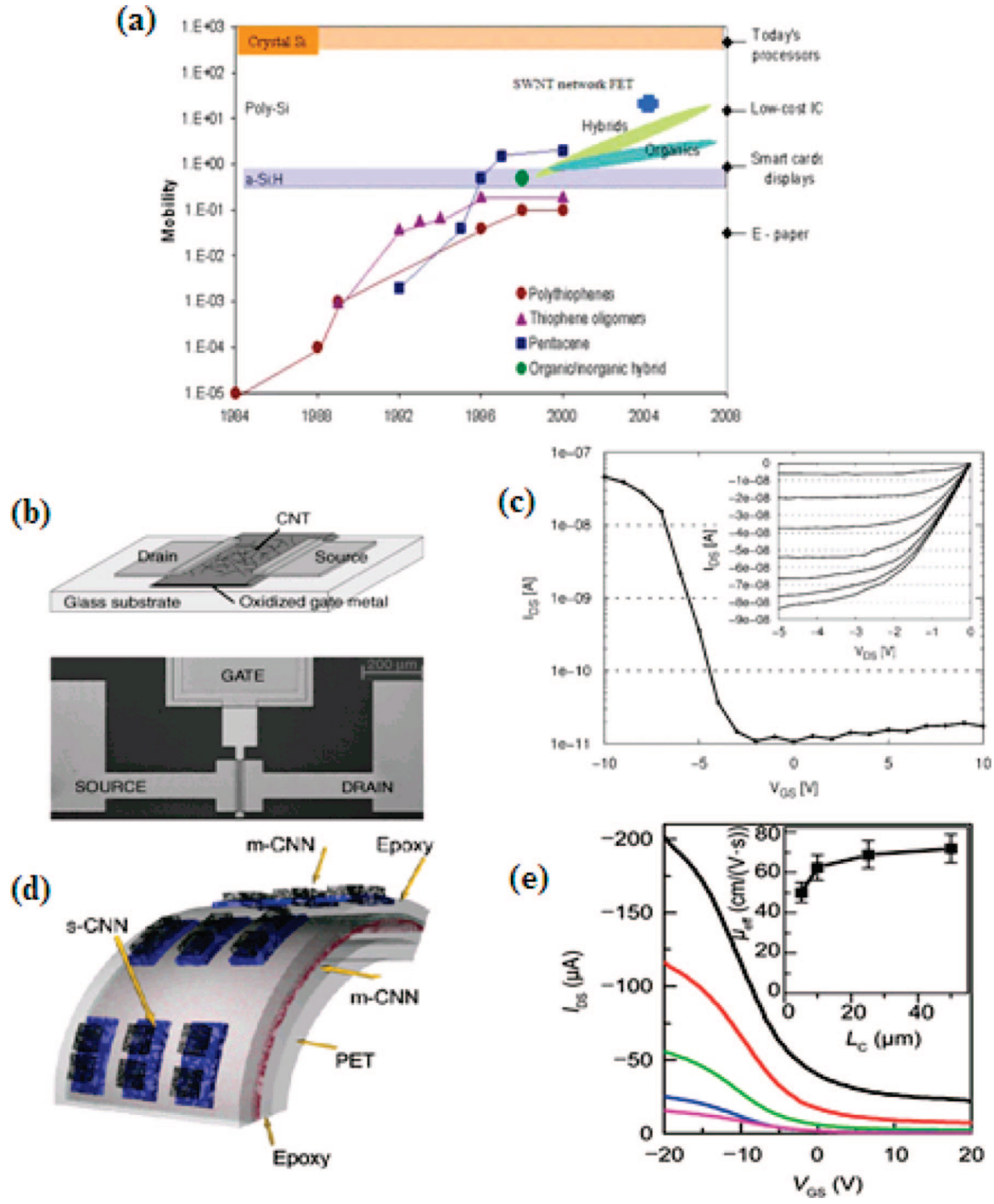

Figure 22. (a) Yearly performance progress improvement in the thin film transistors with organic materials, together with the performance of SWCNT network transistors. After ref 321. (b) Schematic of the device geometry. The CNT network is deposited either through direct growth or through a solution-based process on top of the dielectric. The source and drain metal contacts were evaporated on top of CNT network to ensure good contact. The gate electrode is heavily doped Si or metals. (c) Transfer and output characteristics of a CNT network TFT device. (Reprinted with permission from ref 329. Copyright 2008 The Society of Information Display.) (d) TFTs using single walled CNT random networks as the semiconductor. Metallic CNT networks are used as the S/D/G contacts. (e) Transfer curves for devices for L_c are 5, 10, 25, and 100 μm, respectively, from the top to the bottom. Inset is the effective device mobility μ_{eff} as a function of L_c. (Reprinted with permission from ref 31. Copyright 2006 Wiley-VCH.)

However, the reproducibility of devices with density close to the percolation threshold is extremely poor.[32,326]

The device characteristics of CNT transistors have been measured by several groups, and substantial variation has been observed. This is in part due to the variables in the process, such as CNT source/purity, electrode composition, dielectric material, and device geometry. To date, CNT TFTs cannot be made reproducibly and cost effectively, while achieving high mobility, high on/off ratio, small hysteresis, and stability. CNT TFTs are still in their early stage, while the investigation of individual CNT FET has a history of well over a decade. The knowledge of individual CNT-based FETs can be transferred to CNT TFTs such as the choice of metal contact to minimize the contact resistance and the method of doping. Other TFT related studies, especially scaling laws, warrant further study. Although some theories

have been advanced,[229,327,328] the measured device characteristics are typically compared to standard formulas that have proven to be useful for CMOS architectures.[309] Figure 22c shows typical performance data including the transfer and output characteristics of CNT TFTs.[329] The souce-drain current (I_{sd}) versus gate voltage (V_{gs}) at constant source−drain voltage (V_{sd}) is the transfer curve, and the I_{sd} versus source−drain voltage (V_{sd}) at constant gate voltage is the output characteristic. These curves can be used to calculate important TFT parameters such as on/off ratio, mobility, and subthreshold voltage. Because the device characteristics for CNT TFTs are normally analyzed with CMOS architectures, it is necessary to list the basic equations for the transfer and output characteristics. Equations 8 and 9 describe the output curves in the low V_{SD} (linear) and high V_{SD} (saturation) regions, respectively. Here, μ is the mobility, L is the channel length, W is the channel width, C_g is the gate capacitance per unit area, and V_T is the threshold voltage. The mobility can be calculated from the linear or saturation region. Note the calculated mobility is the TFT device mobility, which is different from the inherent charge transport mobility. The device mobility will include the effect from the source/drain and nanotube network contact resistance, which will be minimized for large channel TFT devices where the channel resistance dominates the overall resistance. These four formulas are typically used in CMOS transistor analysis. Using these equations for data in Figure 22c, Yaniv et al. obtained $V_T = -4.7$ V, on/off $= 10^5$, $\mu \approx 1$ cm^2/(V s), and a slope of 1.1 V/decade.[329]

$$I_D = \frac{WC_G}{L}\mu\left(V_G - V_T - \frac{V_D}{2}\right)V_D \quad V_D < (V_G - V_T) \tag{8}$$

$$I_D = \frac{WC_G}{2L}\mu(V_G - V_T)^2 \quad V_D > (V_G - V_T) \tag{9}$$

There is an ongoing debate regarding the modulation mechanism, with one side arguing that it is fundamentally a SB modulation at the CNT/metal contact, while the other side claims that the active channel is the source of the conductance modulation. The CNT−metal contact undoubtedly plays a significant role in CNT FETs. For TFTs based on individual CNTs, the choice of contact metal can dramatically change the transistor performance. For example, most metals lead to p-type CNT transistors, while some metals such as Ca lead to n-type CNT FETs. The SB at the contact for short channel devices is more dramatic than longer channel devices, especially when the channel length is smaller than the CNT mean free path. However, for CNT TFTs, the contact resistance may not play as significant a role as in FETs based on individual CNTs. The channel length is typically 50 μm or longer for microelectronic device applications, several times longer than the tube length and mean free path. For CNT thin films, due to the large CNT−CNT contact resistance, the overall resistivity of the network is normally at least 100 times larger than that of individual CNTs. Therefore, the CNT network resistance dominates the overall resistance, and the modulation for transistor applications occurs in the network itself rather than at the CNT/metal contacts. A systematic study of the scaling of the device performance with device geometry will be necessary for further optimization.

One advantage of CNT TFTs is their potential for high mobility due to the high conductivity of individual CNTs. As shown in eqs 8 and 9, the mobility can be calculated either from the linear region or from the saturation region. There are two important scalings for the device mobility: the density scaling and the device geometry scaling. For the density scaling, notice that the source−drain conductance and the gate capacitance depend on the network density. For densities above the percolation threshold, CNT films can be modeled as a percolation system composed of a one-dimensional tube on a 2D flat surface. As discussed in the transport section, the channel conductance scales with density as $G_D \approx (N - N_c)^{1.33}$, where N is the CNT density and N_c is the critical percolation density. The gate capacitance also depends on the network density as $C_G \approx N$ when the CNT coverage is less than a full monolayer of CNTs. Therefore, the mobility scales with density as $\mu \approx ((N - N_c)^{1.33})/(N)$. Mobility also scales with device geometry. Rogers et al. have extensively studied this scaling. As shown in Figure 22d, Rogers et al. have made all CNT TFTs, using CNT networks as source/drain/gate electrodes as well as the semiconducting channel. The density of CNTs for electrodes is much larger than that for the semiconducting channel. The contact resistance between the source/drain and the semiconducting channel was measured to be low.[31,186] They extracted the effective mobility from the transfer curves in the linear response regime is in the range of 40−80 cm^2/(V s). The mobility is significantly higher than materials such as organic semiconductors for flexible electronic device applications. Because of the negligible role of contact resistance for channel lengths greater than 10 μm, the mobility shows weak dependence on the channel length in this regime (Figure 22e). However, the mobility decreases significantly when the channel length is less than 10 μm due to contact resistance contributions.

Individual semiconducting single-walled CNT FETs have on/off ratios greater than 10^5 even at room temperature,[330,331] while CNT network-based TFTs have a large range of on/off ratios from approximately 1 to 10^5. High on/off ratios can be achieved for networks with density close to the percolation threshold. As the density increases, conduction through metallic CNT channels increases and the off current increases dramatically; therefore, the on/off ratio decreases as the density increases. So, CNT films with a target density slightly above the percolation threshold should be used. There are experimental data that show the dramatic density dependence of the on/off ratio for CNT network transistors. Figure 23a shows the on/off ratio versus the density of tubes (ρ). The unit for ρ is tube number per μm^2 area.[184] For the CVD grown CNTs in this study, the on/off ratio dramatically depends on the tube density. For tube densities approaching the percolation threshold, the on/off ratio increases dramatically. However, the reproducibility for making percolating CNT networks at slightly above the threshold is poor from a manufacturing point of view. The reported on/off ratio from the literature is typically between 100 and 1000, which is lower than required for many device applications. One obvious route to increase the on/off ratio is to remove metallic CNTs. This can be done in the CNT dispersion using solution-based chemistry, during the deposition, or post deposition.[47,68,82,139,332−336] One common chemical functionalization scheme is using diazonium functionalization, which is based on the difference in available states in metallic CNTs and semiconducting CNTs, which leads to the selective reaction of diazonium with metallic CNTs in solution. This has been confirmed through optical studies of the dispersion

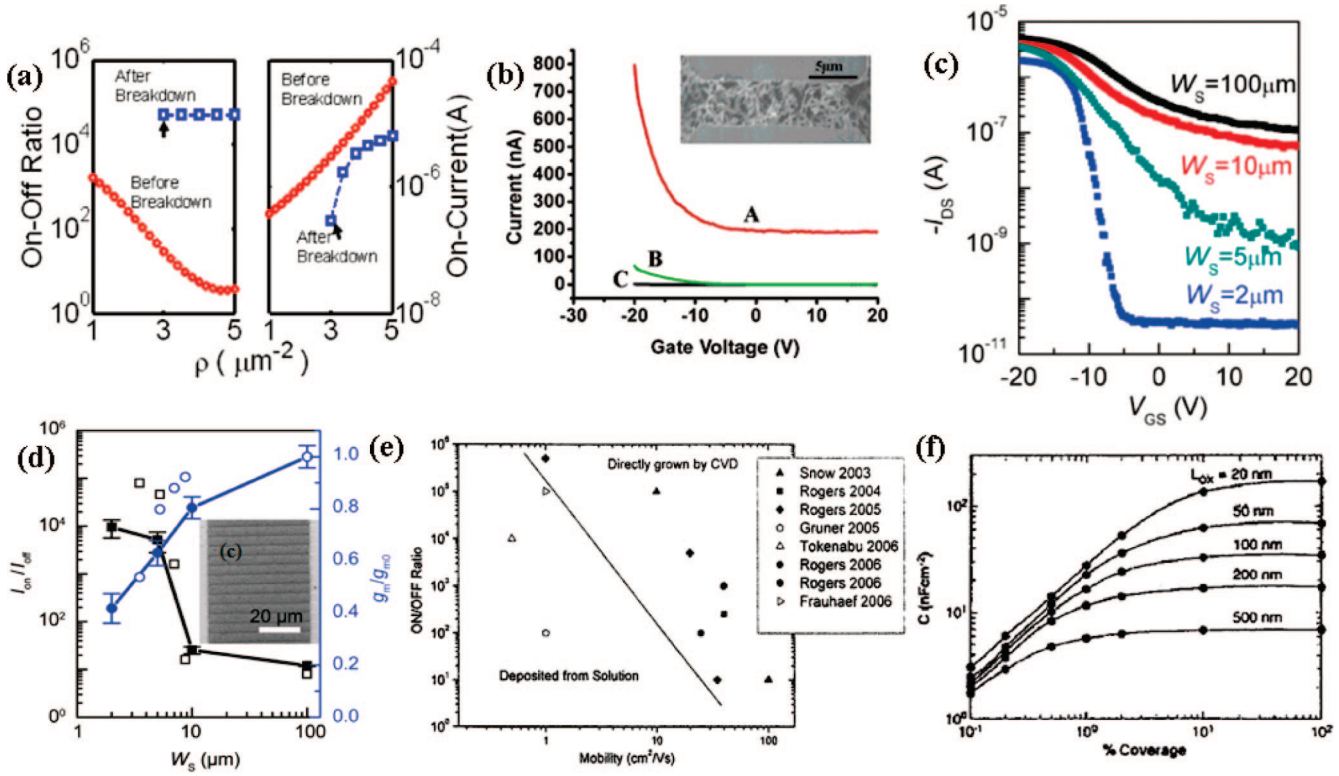

Figure 23. (a) Dependence of on/off and on-current on the nanotube density before and after electrical breakdown. (Reprinted with permission from ref 184. Copyright 2006 American Institute of Physics.) (b) Gate dependence curves of the device. (A) Before the diazonium reaction. (B) After the reaction with the diazonium reagent (3.7 mM). (C) After further reactions (3.7 mM). The inset is an SEM image of a typical SWCNT network device. The bias was 100 mV. The doped Si substrate was used as a back gate in all measurements. (Reprinted with permission from ref 334. Copyright 2004 American Chemical Society.) (c) Transfer characteristics of TFTs with L_C of 100 μm, channel width (W) of 100 μm, and strip widths (W_S) of 100, 10, 5, 2 μm, from top to bottom, plotted on a semilogarithmic scale (V_{DS}: 0.2 V). (d) Measured (filled) and simulated (open) on/off ratio (I_{on}/I_{off}) and normalized transconductance (g_m/g_{m0}, where "0" represents the state without strips) as a function of W_S for SWCNT devices shown in (b). Inset: SEM image of the channel region of such a device. (Reprinted with permission from ref 185. Copyright 2009 Wiley-VCH.) (e) Plot of on/off ratio vs device mobility for CNT TFT made by various groups. The diagonal line coarsely separates the solution deposited device (open points) from the CVD grown device (filled point).[337] (f) Capacitance of a CNT film on dielectric as a function of the density through modeling. (Reprinted with permission from ref 339. Copyright 2005 American Institute of Physics.)

before and after the reaction. Bao et al. reported a method to functionalize the substrate surface selectively with phenol groups or amine groups.[139] During the spin coating process, the selective deposition of metallic or semiconducting CNTs is achieved due to the binding force difference. They claim that TFTs with an average on/off ratio of over 10^5 have been achieved through this deposition method. This one step solution processed CNT network TFT without the need of additional processing makes a large step toward commercialization. Post deposition treatments to selective remove metallic CNTs have also been developed, methods such as electric breakdown, on-film cycloaddition reactions, and selective UV light irradiation.[336] As shown in Figure 23a, the on/off ratio is independent of the tube density after electric breakdown of the metallic tubes, and the on current decreases after the electric breakdown. The independence of the on/off ratio with tube density after the electrical burn is favorable for the large-scale manufacturing of CNT-based FETs. Liu et al. demonstrated the in situ fabrication of high performance semiconducting CNT network transistors (Figure 23b) by selectively eliminating metallic nanotubes in the devices. After diazonium functionalization, the transistor performance gets much better due to the elimination of metallic nanotubes in the network.

Another scaling behavior for CNT TFTs is its dependence on the device channel width and length. The logic is similar to the density dependence for device mobility. When the device channel length L_C is much larger than the tube length, the possibility of forming a conductive path through all metallic tubes is less; therefore, the off current decreases, which is beneficial for the device on/off ratio. The same logic applies for the case when the device width is on the order of the tube length. Figure 23c shows the transfer curve of CNT network transistors with varying device widths. The CNT network width is controlled through phase-shift lithography and reactive-ion etching. It is clear that the on/off ratio dramatically increases as the width decreases, along with an increase of the transconductance (Figure 23d). As compared to chemical methods to remove metallic CNTs, this method is to diminish the metallic conducting path through geometry engineering, which is more feasible from a production and reproducibility standpoint. Figure 23e summarizes the on/off ratio versus device mobility for both solution-based and CVD grown CNT TFTs by various groups.[337] Although there are different details regarding their device configuration, dielectric choice, and the device dimensions, the plot shows the general trends. High mobility corresponds to large tube densities, which leads to a small on/off ratio. The solid line is a rough guide separating solution-based and CVD grown CNT network TFTs. The solution-based TFTs have lower mobility at the same on/off ratio, likely due to the poor contact in CNTs due to surfactant residue. The on/off ratio is also lower for solution-based CNT TFTs because of the larger bundle sizes, which contain shorting metallic tubes.[186]

The gate coupling capacitance of transistors is crucial for device operation, and the right characterization of the device capacitance is important for the correct evaluation of the device parameters. A higher capacitance leads to a lower operating voltage range. At higher network density such that the average tube−tube distance, d, is comparable to the dielectric thickness, L_{OX}, the device capacitance approaches a standard parallel plate capacitor. The capacitance per unit area is $C_G = (\varepsilon_0\varepsilon_r)/(L_{OX})$, where ε_r is the dielectric capacitance. Below this density, detailed calculation shows that the percolating network capacitance is approximately the same as the sum of individual CNTs coupled with the gate through the dielectric. The capacitance for each tube can be treated as a cylinder embedded in a dielectric above an infinite conductive plate. Therefore, the total capacitance is $C_G = (2\pi\varepsilon_0 L_T \varepsilon_r N)/(\ln((2L_{OX})/(r)))$. The capacitance is a function of the dielectric thickness and the CNT surface coverage, as plotted in Figure 23f.[338] As shows in the formula, there are two major routes to increasing the capacitance, either through high-k gate dielectrics such as hafnium oxide (HfO_2) or through decreased dielectric thickness such as self-assembled nanoscale dielectrics.[339] Ideally, a dielectric forms a pinhole free surface upon deposition to avoid leakage current. For correct device parameter extraction, the CNT density needs to be measured. The experimental determination of the capacitance through capacitance−voltage ($C-V$) curves reveals that characteristics of the network closely resemble results based on individual tubes, with symmetric $C-V$ curves in the depletion region and accumulation region.

Hysteresis in not desired in FET curves and should be minimized. It is thought that large hysteresis is due to trapped mobile ions or water residue at the dielectric interface, either on the CNT film or on the dielectric layer.[340,341] Coating a polymer electrolyte layer on the CNTs leads to a larger hysteresis. The hysteresis decreases with increasing gate voltage sweep frequency, as the surface ions can no longer follow the field. There are several methods to decrease the hysteresis in CNT transistors. Such methods include using a thin hydrophobic layer over the dielectric layer, and UV or heat treatment during the device deposition to remove surfactant.[342] Operation voltage and threshold voltage are also important parameters for TFT applications. The required voltage range to turn the device from the off to the on state is called the operation voltage. Most CNT TFTs on silicon have an operation voltage of −10 to 10 V, while devices on flexible substrates may require a larger operation voltage, as much as −100 to 100 V.[343] Major routes to decrease the operation voltage include increasing the coupling between the gate and CNT network through increasing the capacitance, such as using nanometer thick dielectric.[339] The threshold voltage is the voltage at which the device begins to switch from an off to an on state. The threshold voltage for CNT network-based transistors can be modified through chemical n- or p-type doping. For practical applications, the stability of CNT TFTs is crucial. Because CNTs are p-doped in air and the binding energy of oxygen to CNTs is 0.25 eV, the operation of CNT-based TFTs will be sensitive to vacuum, heat, and light. Also, due to the high surface area and sensitivity of CNTs, the stability of CNT TFTs could be a potential problem. To solve this, a stable dopant with large enough binding energy will be needed, or an encapsulation layer to protect the CNT network from the environment will be necessary. For example, tetrafluoro-tetracyanoquinodimethane-doped CNTs have shown stable performance for 60 h in vacuum.[344] Another important parameter is the high frequency response of the transistor. Because of the high conductivity at high frequencies even in the microwave range, CNT network-based TFTs will not have an issue to operate at high frequencies (up to GHz range).[280] CNTs in air are doped by oxygen to behave as a p-type material. Because of the small band gap of CNTs, n-type doping can be achieved using electron-rich materials. Certain polymers, when noncovalently bound to CNTs, act as electron -donating materials. A PEI layer is widely used to achieve n-type CNT TFTs.[26] There are many other n-type doping materials studied for CNTs.[323] Rogers et al. fabricated CNT network transistors followed by electric breakdown. The device turns from p-type to n-type after PEI spin coating (Figure 24a−c).[171] They selectively exposed one-half of the devices to PEI and the other to PMMA. The resulting p−n junction exhibits diode-type behavior with series resistance. Using p-type and n-type CNT transistors, complicated logic circuits could be fabricated. TFTs on plastic substrates are a key component for flexible electronic. CNT TFTs on plastic have several advantages as compared to organic-based devices such as their mechanical flexibility and stretchability, which are essential for flexible electronics. Grüner et al. have demonstrated that the channel conductance decreases by 12% during 60° bending with a 0.5 mm radius of curvature. The change of the conductance is reversible when unbent.[7,345] Rogers et al. studied the transistor properties under different strains. Relatively small changes were observed in the transfer characteristics and normalized transconductance up to 2% strain with complete recovery after relaxing (Figure 24d). The data in Figure 24e show the transconductance for devices with epoxy (solid line) and PDMS (dashed line) dielectric layers. Because of the excellent optical transparency, CNT networks also enable transparent TFTs, which enables transparent electronics for innovative consumer electronics.[30,186] CNT networks have potential for plastic integrated circuits. Rogers et al. recently demonstrated medium scale CNT TFTs on plastic substrates with nearly 100 transistors. The transistors show excellent properties such as high mobility (80 cm^2/Cs), low subthreshold slopes (40 mV dec^{-1}), small operating voltage (<5 V), and large on/off ratio ($\sim 10^2-10^5$) (Figure 24f).[186]

Although tremendous progress has been made and medium scale integrated circuits have been demonstrated, several challenges remain before commercialization. The major challenge is the typically low and inconsistent on/off ratio, especially for solution deposited CNT networks. Although several methods have been demonstrated to selective remove the contribution of metallic CNT paths to diminish the off current, all of the methods are difficult to control and sensitive to process conditions. Roger's patterning method leads to improved performance; however, 2 μm patterning resolution is difficult for traditional lithography. More recent reports by Bao's group rely on the self-sorting, aligned nanotube network through surface functionalization that leads to a high on/off ratio, up to 9×10^5.[139] However, scalable device fabrication with aligned nanotubes will have poor reproducibility. Solution-based CNT devices also face large challenges. For example, removal of the metallic paths can be difficult. Also, relying on tight density control is not realistic for large-scale fabrication, so the reproducibility will be extremely poor. Selective deposition of CNTs by spin coating CNTs on pretreated surfaces with phenol or amine

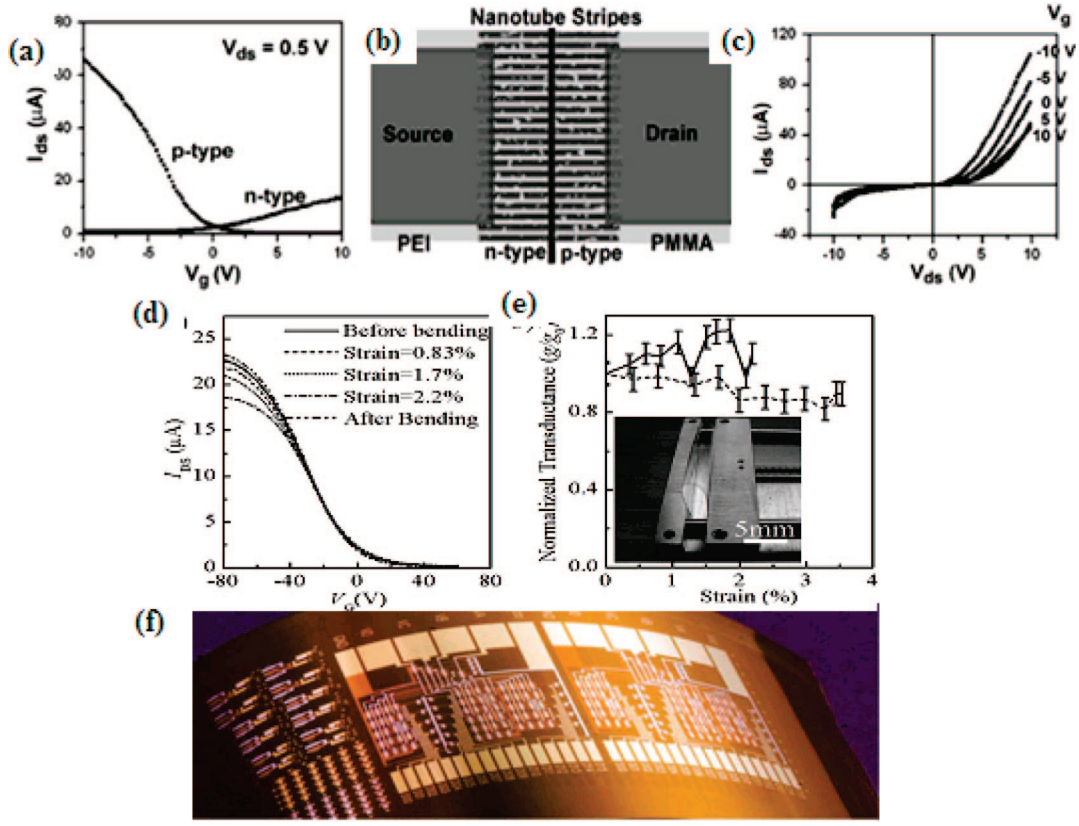

Figure 24. (a) Transfer characteristic of a CNT TFT measure before and after PEIT coating. (b) Schematic illustration of a p−n diode formed by patterning PEI onto one-half of the channel region. (c) Output characteristics of the p−n at different gate voltages. (Reprinted with permission from ref 171. Copyright 2004 American Chemical Society.) (d) Transfer characteristics of a CNT TFT whose channel length is 225 μm and width is 750 μm at different bending. (e) The change of normalized transconductance for transistors with different strain. The inset shows a transistor with extreme level of bending. (Reprinted with permission from ref 31. Copyright 2006 Wiley-VCH.) (f) Optical image of a flexible SWCNT integrated circuit chip bonded to a curved surface. (Reprinted with permission from ref 186. Copyright 2008 Nature Publishing Group.)

groups can be difficult to control and will have a radial distribution of density along the spin coating direction. More chemistry including the control growth of only semiconducting CNTs or CNT separation after growth will be crucial, albeit extremely challenging.

5.2.2. Sensing

There is tremendous interest in sensing using nanoscale materials, especially individual CNTs and nanowires in light, gas vapor, chemical, and biological sensing applications. The major advantages of nanomaterial-based sensors lie in their size compatibility, high sensitivity due to the large surface area, and use of electronic sensing instead of optical sensing, which eases the signal processing. For example, the diameter of CNTs is typically close to 1 nm, similar to the diameter of DNA, and 10 times smaller than an average protein (Figure 25a).[314] Size compatibility between a sensing target and the detector is critical to get adequate sensitivity. SWCNTs are particularly sensitive because all of the carbon atoms are at the surface and can act as sensor sites. Also, most processes, especially biological processes, involve electrostatic interactions and charge transfer, which can be directly and quickly monitored by electronic methods using CNTs. This dramatically simplifies the complicated polymerase chain reaction (PCR) data processing for optical basing sensing. With the nanoelectronics developments based on CNTs, an integrated sensor system platform suitable for sensing with high accuracy and high selectivity level could be achieved.[151,207,275,304,346−348] Startups such as Nanomix Inc. and research groups such as Star's group at the University of Pittsburgh have been devoted to the fundamental study and development work on CNT-based sensing applications. For sensors based on individual CNTs, the sensing mechanism is either due to a change in the CNT−metal interface (SB change) or due to the conductance change along the CNT itself; this argument is ongoing. The device structure for sensing applications can be a simple two-terminal resistor with the CNT surface exposed to the environment, or a three-terminal transistor. The resistance signal can be monitored in real time to probe the dynamics of the sensing process, and the transistor signal can be used to calculate the charge transfer amount between the sensing species and the CNT detector. If a charge transfer occurs, the threshold voltage will shift due to electron withdrawal (positive voltage shift) or electron donation (negative voltage shift). The adsorption of sensing species will cause an overall drop in conductance due to scattering of the charge carrier. While these devices have extreme high sensitivity and can sense species down to the ppb level, they have found little commercialization success. The major challenge is device reproducibility and manufacturability. The variations in CNTs and CNT−metal contacts are among many variations in sensors based on individual CNTs. Sensors with randomly oriented CNT networks can statistically average out the variations in individual CNTs, leading to device performance with excellent reproducibility, and adequate sensitivity. The signal can be detected by monitoring the resistance change of the CNT thin film, the capacitance change of a capacitor having a CNT

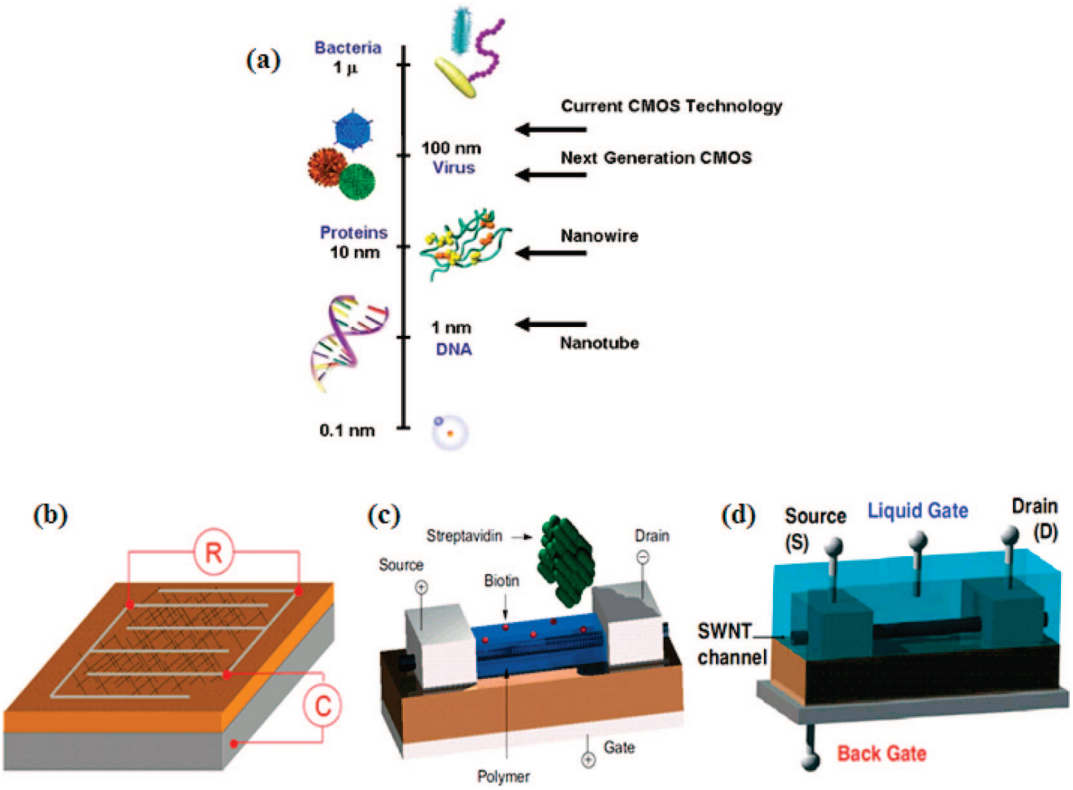

Figure 25. (a) The dimension comparison of CNT, nanowire, biological species, and COMS technology dimensions.[314] (b) Network-based capacitance monitoring. Transistors-based sensing using bottom gated TFT (c) and liquid gated TFT in buffer (d). (Reprinted with permission from ref 314. Copyright 2006 Elsevier.)

film as a component, or the transistor behavior of top, bottom, or liquid gated TFTs with CNT active channels. Some of the sensor structures are shown in Figure 25b−d. Snow et al. report the real time monitoring of capacitance along with resistance leads to high-performance chemical sensors by thinly coating the CNTs with chemically selective materials that provide a large, class-specific gain to the capacitance response.[349,350] There are two major CNT-based TFT configurations, either in air or in liquid. Liquid gating is more suitable for real time monitoring of bioreactions in a real environment. There are excellent reviews on CNT network-based sensors, especially for biological sensing, vapor sensing, and chemical sensing.[7,99,351,352] The sensing mechanisms were discussed in detail, and the comparison between CNT-based sensors and other types of sensors, MOSFET sensors in particular, was discussed. Gruner et al. investigated the interaction between biotin-streptavidin using CNT FETs. They were able to successfully detect such binding events and further found that a biotinylated polymer layer of PEI successfully prevents the nonspecific binding between biotin and streptavidin. Application of CNT network-based TFTs in the detection of glucose, carbohydrates, and their enzymatic degradation, and DNA hybridization, have been successfully demonstrated. Star et al. also reviewed extensively gas and vapor detection using CNT networks.[99] Gases included NH_3, NO_2, CH_4, N_2, CO, O_2, SO_2, H_2S, HCl, organic vapor, and defense related explosives such as TNT, DNT. CNT networks can also be functionalized for additional sensitivity. For example, a porphyrin-sensitized CNT network transistor can detect certain wavelengths of light. We will use this example to discuss some sensor related calculations using a CNT FET.[264]

Porphyrin plays a central role in photosynthesis, and the uniqueness of porphyrins is their long-lived intermediate electronic states upon irradiation by visible light. Hecht et al. have used CNT transistors to monitor the charge transfer between CNTs and porphyrin and found that the charge transfer is a function of visible light intensity and wavelength.[264] Figure 26a shows the zinc metalloporphyrin molecular structure used in the study. CNT networks with density of 1.6 tubes/μm^2 (close to the percolation threshold) were used to maximize the on/off ratio of the TFT device. Bottom gating is used with 500 nm of SiO_2 as the dielectric. The device dimension is in the range of 500 μm, much larger than the tube length. Therefore, the CNT network resistance dominates the overall resistance, and the change upon light irradiation is mainly from the CNTs, not the CNT-S/D contacts. The transfer curves of the CNT FET before and after the porphyrin deposition are shown in Figure 26b. There are two distinct changes noticeable. First is the suppression of the SD current, which is due to the addition of charged scattering sites by porphyrin molecules distributed along CNTs. Another change is the shift of the threshold voltage toward negative gate voltages. Such a shift of threshold voltage could be due to charge transfer from porphyrin to CNTs. The photoresponse of porphyrin coated CNT transistors was studied by illumination using LEDs with wavelength of 420 nm. The transfer curve was shifted to the right when the light is on; this effect is reversible when the light is turned off. Using CNT transistors rather than resistors allows one to distinguish between charge transfer and changes in mobility. For a thin film, the conductivity σ is equal to $ne\mu$, where n is the carrier density and μ is the carrier mobility. On the basis of the transfer curve, changes in carrier density and mobility can be detected in real time, as shown in the Figure 26e−g. Furthermore, one can calculate the quantity of charge transfer per porphyrin upon the illumination. The following assumptions are used: (1) full coverage of por-

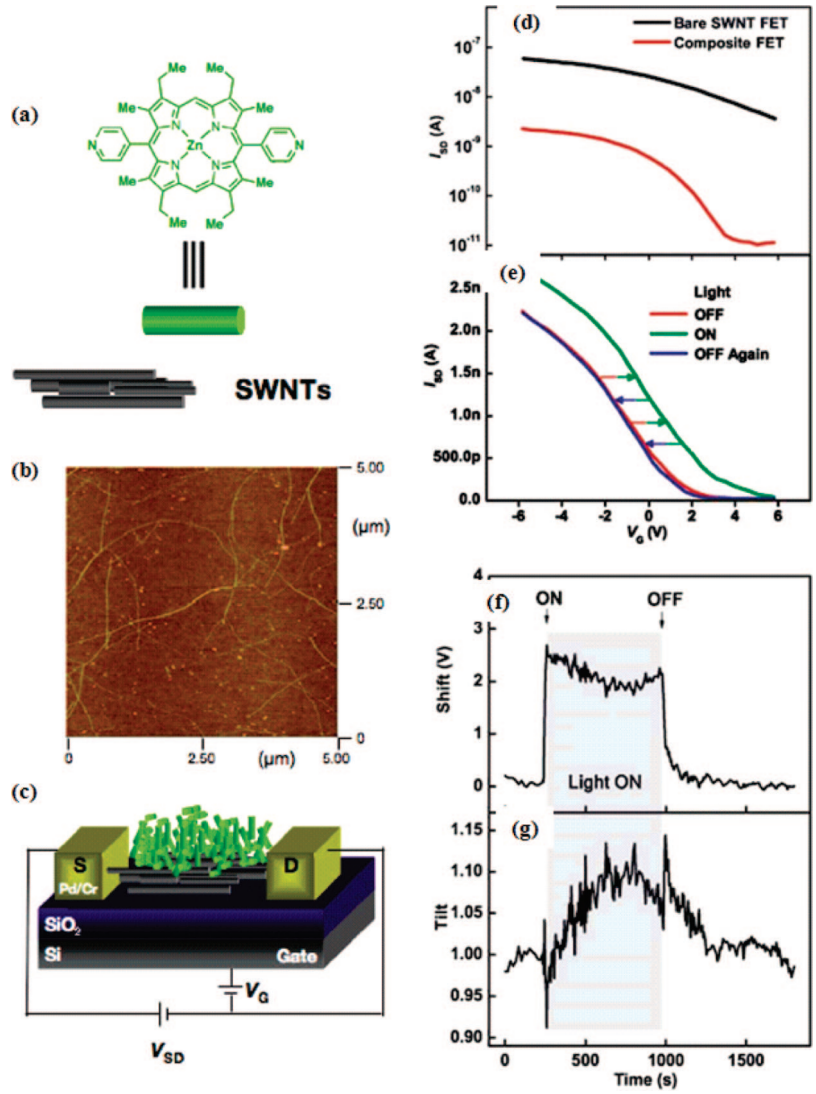

Figure 26. (a) Structure of zinc metalloporphyrin; (b) AFM image of CNT network for conductive channel in transistor; (c) schematic of device for light sensing; (d) transfer curve of CNT FET (250 mHz gate sweep rate, 15 mV gate sweep amplitude), before (black) and after (red) addition of 1 μL of 1.2 μM porphyrin in DMF; (e) transfer curve of device before (red) and after (green) illumination by 100 W/m^2 (420 nm peak at 15 fwhm) light supplied by an LED. (f,g) Fits to the data obtained in (e) show the shift and the tilt of the transfer curve as a function of time. Light is on during times indicated by the shaded box. (Reprinted with permission from ref 264. Copyright 2006 American Chemical Society.)

phyrin onto the CNT surface and (2) only porphyrins in contact with CNTs will contribute to the charge transfer. The formula $Q = C\Delta V$ allows the calculation of the charge transfer per area. On the basis of the density of CNTs from AFM images, we have calculated the charge transfer as 0.37 electrons per porphyrin molecule. Besides various advantages of using CNTs in sensing as discussed in detail in the previous reviews,[7,99,351] CNT transistor-based sensors can lead to additional information regarding changes in conductivity. For example, Grüner et al. have studied the charge transfer between CdSe nanoparticles and CNTs using network transistor and found the charge transfer strongly depends on the light intensity and wavelength and reaches a maximum of 2.2 electrons per pyrene/CdSe nanoparticle.[222]

Transistors with percolating CNT networks as the conductive channel are ideal for sensing applications, because they have high sensitivity and manufacturing potential. Future work for integrating CNT TFT sensors into real applications will include continuing in vivo study of sensing in real biological systems such as serum, increasing the selectivity of the sensor to avoid false positives, and improving the stability.[349,351,353,354] System integration includes a "lab on a chip" sensor, and incorporation of sensors with microfluidic delivery systems, which is possible using existing MEMS technology. Advances in the semiconductor industry will help to decrease the cost of producing such sensors. Because of the flexibility and the compatibility of CNTs with plastic substrates, cheap and disposable CNT TFT sensors could also be developed.[7,284,355,356]

5.3. Transparent Electrodes

Transparent and conducting electrodes are the essential elements of many optoelectronic devices applications, including solar cells, flat panel displays, touch panels, organic light emitting diodes, electroluminescent lighting, and many others.[307,357−360] Remarkable research has been carried out on various types of transparent and conducting oxides (TCOs) to perfect the materials for achieving highly conducting and transparent electrodes. Among them, indium tin oxide (ITO) is one of the dominant materials used in the market. Intrinsic TCOs are semiconductors with large band

gaps (~3 eV). The electrical conductivity is introduced by dopants; p- and n-type conductors are achieved depending on the dopant choice. The carrier concentration introduced by dopants will increase the optical conductivity as well as the plasma frequency. Above the plasma frequency, the carriers cannot follow the field and the TCOs become transparent. Below the plasma frequency, TCOs are highly reflective. As the carrier concentrations increase, the wavelength window for TCOs is narrowed. Wide band gaps are needed to avoid optical absorption through direct band gap transitions, which will reduce the optical transparency of the materials. Therefore, the main aim of new research on TCOs should be to search for wide band gap materials with high mobility. Effective transparent and conducting electrodes should have high electrical conductivity σ and low absorption α of visible light. The appropriate quantitative measure of the performance of TCOs is the ratio of the two parameters $(\sigma)/(\alpha) = -(1)/(R_s \ln(R + T))$, where R_s is the sheet resistance, and R and T are the reflectance and transmittance, respectively.[307,357−359] The overall figure of merit is defined as $\Phi = T^{10}/R_s$. For example, commercial ITO on glass having R_s of 18 Ω/□ and 95% transmittance at 550 nm has an overall figure of merit of 33.6. The higher is the figure of merit, the better is the performance of the TCO. For real applications, other properties of TCOs are important, including work function, thermal stability, chemical stability, etching methods, mechanical properties, etc. For industrial applications, the cost, including the materials and the manufacturing, should be taken into account. The price of indium, a rare earth element that is a byproduct of mining, fluctuated dramatically over the last several years; therefore, alternatives to indium-based products are actively being sought. Also, high vacuum is needed for the deposition for highly conductive ITO, which can be costly. Conducting polymers, sometimes referred to as synthetic metals, have progressed much in the past decade. Transparent and conducting electrodes can be fabricated on the basis of thin films of conducting polymers. One of the most successful materials is poly(3,4-ethylenedioxythiophene) poly(styrenesulfonate) (PEDOT). A conductivity of several hundred S/cm, and R_s of 200 Ω/□ with 80% optical transmittance, have been demonstrated. Various types of devices including OLEDs, OFETs, photovoltaics, and electrochromic devices have been fabricated using PEDOT as the electrodes.[361−363] PEDOT solutions in water (Baytron P HC) are available from Bayer. The solutions-based deposition process makes this material attractive for use as future TCs. However, the intrinsic instability, chemically and thermally, together with its relatively low conductivity, currently prevent the application of PEDOT in industry. CNTs are highly conducting objects with conductivity up to 10^5 S/cm. Thin films with randomly distributed CNTs have been shown to possess high transmittance in the visible range and high conductivity, as discussed in the optoelectronic property section. Transparent and conducing CNT thin films with thicknesses of approximately 30 nm are emerging as a new type of electrode, which show promise as a replacement for the traditionally used ITO. With robust mechanical properties and ease of patterning, nanotube electrodes have been incorporated into devices such as flexible transistors on plastic and field emitters.[31,61,230,364,365] Theoretical and experimental studies have also established the work function of CNT networks to be in the range of 4.7−5.2 eV.[28,123,218,239,242,244] Such high work functions meet the requirement for anodes in several types of photonic devices, such as organic light-emitting diodes and organic solar cells. These characteristics and the simple room temperature fabrication avenues indicate that this novel anode is a promising candidate for next-generation photonic device applications. In this section, we will review extensively the device applications of transparent and conducting nanotube electrodes. Current device performance will be described below, and routes for future development will be discussed.

5.3.1. Thin Film Solar Cells

Transparent electrodes are the essential components for PV device applications, and there is an increasing need for alternative materials for use as transparent electrodes. Currently ITO is the most widely used material for this application; however, replacement ITO materials are actively being studied. The deposition of TCOs needs high vacuum and high temperature and is significantly slower as a roll-to-roll process than solution-based methods. The R/T performance, the work function, and the cutoff wavelength highly depend on the doping level. Zinc oxide-doped indium oxide (IZO) has a low work function but is one of the most promising alternative TCOs to replace ITO for transparent electrode applications due to its high conductivity. Typically R_s of <20 Ω/□ is needed for solar cell applications, although the R_s requirement depends on the cell dimensions. Because of the large need for transparent electrodes, there are several active emerging forms of materials, which have potential to replace TCOs for solar cell applications. These materials are conductive silver nanowire films, thin metal films, microscale metal grids, nanotubes, or graphene thin films.[155,291,366−369] In particular, solution-based materials are more favorable from a large-scale manufacturing point of view and recently caught much attention. ITO nanoparticles, silver nanowires, CNTs, and graphene can all be deposited from solution using roll-to-roll coating methods, followed by some thermal treatment.[78,92,161,291,366,370−374]

There are two major methods to incorporate CNTs into solar cells. The first method is to mix CNTs into the active layer of the semiconductor. Because of the high aspect ratio and high conductivity, the incorporation of CNTs into the active layer will help separate the electrons and holes after the excitations in the semiconductor materials before a recombination event occurs.[92,217,257,375−377] For this application, the volume concentration needs to be somewhat above the percolation threshold, but cannot cause shorting of the device.[375,376] The second method of incorporating CNTs into solar cells is to use CNT thin films as a transparent electrode. The other incorporation methods of CNT into solar cell device include growth of CNT on top of ITO electrode to improve the surface area for charge collection or using CNT as the p-type material directly deposited on top of n-type silicon to form a p−n junction for light harvesting.[158,218,219,378] Zakhidov et al. deposited CNTs on top of transparent ITO electrodes to use the hybrid as a 3D anode for OPV devices. They found that the incorporation of CNTs on top of ITO increases the overall efficiency to ~2%, and increases the short circuit current by a factor of 2. This effect is due to the combined effect of enhanced hole collecting by the 3D transparent CNT layer and improved transport through the planar ITO contribution.[149]

Because of their high work function, CNT thin films can be used as a transparent anode in OPV devices.[217,379−382] In addition to the advantages of solution-based processing, transparent CNT anodes will have the advantage of (1)

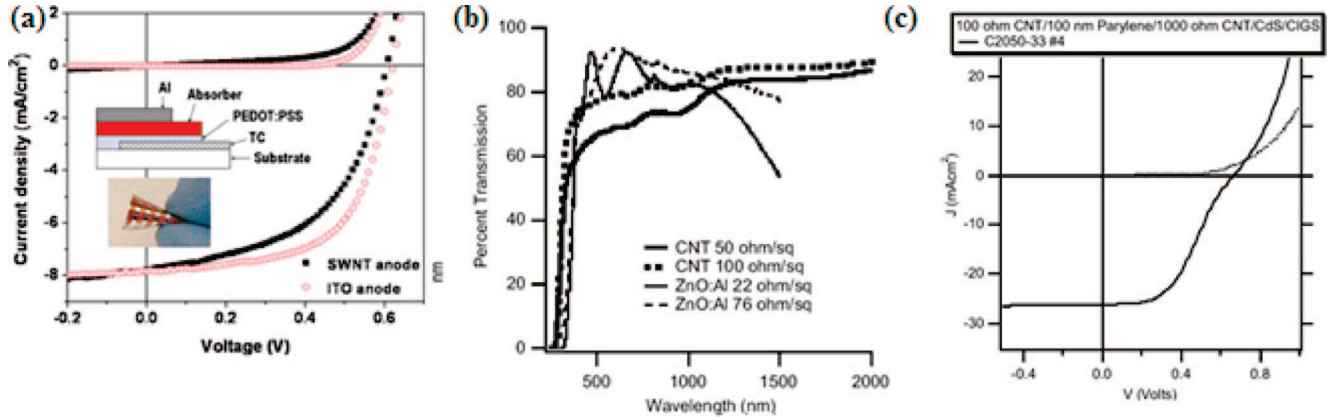

Figure 27. (a) Current density−voltage characteristics of P3HT:PCBM devices under AG1.5G condictions using ITO on glass (○) and flexible CNT on PET (■) as the anodes, respectively. Inset shows the schematic of device and the photograph of the highly flexible cell using CNTs on PET. (Reprinted with permission from ref 217. Copyright 2006 American Institute of Physics.) (b) Optical transmission of CNT and n-ZnO layer used in CIGS solar cell. (c) $J-V$ characteristics of solar cell test structure incorporating Parylene-N.[383] (Reprinted with permission from ref 383. Copyright 2007American Chemical Society.)

mechanical flexibility and (2) the porous structure of the surface allows better charge separation and higher fill factor in OPV devices. The concept of incorporating transparent electrodes in OPV devices has been demonstrated by several groups.[380,382] The active layers include MDMO-PPV:PCBM and P3HT:PCBM, and the substrates are glass or PET. Figure 27a shows the device performance. Laser ablated CNTs were used, and the CNT thin films were fabricated using the filtration and transfer printing method on PET substrate. The R_s is 200 Ω/□, and the transmittance for the CNT thin films only, not including the PET substrate, is 80% in the visible range. The transmittance spectra for CNTs in the visible range are fairly flat as compared to ITO electrodes in this range. The PET substrate thickness is 120 μm, enough for handling and flexibility demonstration. Prior to the deposition of P3HT: PCBM, a layer of PEDOT:PSS was spin coated as in standard ITO-based devices. PEDOT is used here as the transport layer to improve the OPV device performance. For improved penetration of PEDOT into the 3D surface of CNT films, the films were coated with PEDOT several minutes before spin coating. The PEDOT layer decreases the R_s by 20%, which may be due to additional conduction paths from the PEDOT layer or from the doping effect of PEDOT to CNTs. Note that the PEDOT itself on a substrate with the same deposition method has much higher R_s, around 15 kΩ/□. The standard reference device here in this study is an ITO electrode with 15 Ω/□ R_s. Note the cell dimension is 1 × 4 mm. The CNT network device operates almost identically to those for ITO coated glass. The fill factor is only slightly lower than that of ITO-based devices, likely due to the relatively high R_s, which increases the series resistance in the device. The high R_s effect on the performance of OPV devices is evaluated with the established formula as $P_{loss} = (jlw)^2/R_{eff}$. The power conversion efficiency of the CNT network-based device is around 12%, in broad agreement with calculations based on this formula. One method to solve the high R_s problem for OPV applications is to use a metal grid to decrease the cell size to compensate the power loss from the series resistance due to the high R_s. Note that the PEDOT spin coating on the CNT layer greatly decreases the surface roughness of the CNT electrode, from 7 to 3.5 nm. The flexibility of OPV device was also demonstrated. The stability of the OPV device based on CNT electrode is much greater than that of ITO-based devices. This is not surprising due to the fact that ITO has inferior bending properties as compared to CNT electrodes. CNT devices can be folded down to 5 mm with no degradation in power efficiency and a radii of 1 mm with a 20−25% loss in efficiency. They found that annealing at 130 °C for 5 min completely restores the device performance, which may be due to the reorganization of the active materials during the annealing. Glatkowski et al. also reported OPV devices with flexible CNT anodes using a P3HT:PCBM system.[289] The maximum efficiency they achieved is 1.5% with PEDOT as the hole transport layer. They also made PEDOT-free OPV devices with an efficiency of 0.47%. Both types of devices show strongly rectifying behavior, proving that CNTs are selective for holes and not efficient recombination sites.

Another type of solution-based solar cell using transparent CNT electrodes is a CIGS thin film solar cell. This type of solar cell, as compared to OPV devices, has shown high power efficiency up to 20% and good stability for application. NREL and Eikos together have demonstrated a proof of concept device for this application.[383] The device structure they incorporated is ZnO/i-ZnO/CdS/CIGS/Mo. The optical spectra of CNT films with different R_s are shown together with AZO in Figure 27b. The device was fabricated on top of a Mo substrate. ZnO is the transparent electrode, and intrinsic ZnO is used as the carrier blocking layer to improve device efficiency. They have used CNT electrodes to replace ZnO with or without i-ZnO layer. The overall device performance with CNT electrodes was poorer as compared to ZnO due to lack of optimization and a high R_s. For example, they found the device performance depends on the CdSe layer thickness. They also found that the CNT films have better transmittance performance in the IR range as compared to ZnO, specially above a wavelength of 1.5 μm. This high transmittance in the IR range is beneficial for solar cell applications because much of the solar energy is in the IR range.[276] Furthermore, they managed to make CIGS solar cells with efficiency larger than 12% using the structure: CNT/Parylene-N/CNT-CdSe/CIGS/Mo, as shown in Figure 27c. Parylene-N is used for the same purpose as i-ZnO and is capped by two CNT layers. As shown in the figure, the device performance shows clearly rectifying behavior. They argue that the replacement of multiple layers of ZnO/i-ZnO/CdS with a CNT coating could greatly reduce the overall module cost.

The initial results suggest that transparent CNT electrodes are promising for solar cell applications, although further

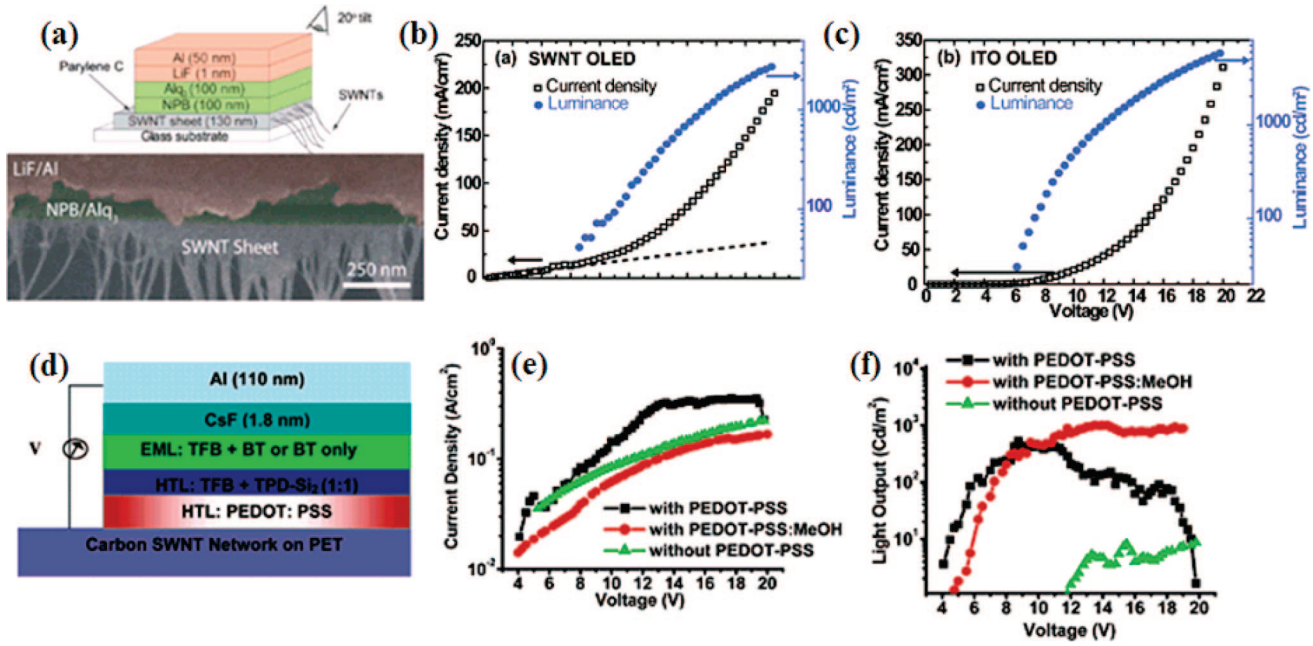

Figure 28. (a) Schematic of CNT OLED device with small molecule Alq_3. The bottom SEM image shows the cross-sectional view of the devices. (b and c) Current density and luminance as a function of applied voltage for OLEDs fabricated on CNT anode and ITO anode respectively. (Reprinted with permission from ref 386. Copyright 2006 American Institute of Physics.) (d) Polymer device structure. (e,f) Responses of OLED devices: current density vs voltage and luminance vs voltage. (Reprinted with permission from ref 35. Copyright 2006 American Chemical Society.)

optimization is needed. They offer a direct alternative to ITO and other TCOs, particularly in situations where flexibility is required. PEDOT and ITO free OPV devices with roll-to-roll compatible CNT anodes would be a large step toward an all printable OPV device. CNT electrodes are extremely promising for flexible and rollable solar cells due to their mechanical flexibility. Chhowalla et al. found an anisotropy in the light transmittance through CNT thin films due to the large aspect ratio of CNTs causing a large in plane carrier response, much different from that with ITO electrodes.[289] The film stability under UV light is critical for solar cell applications. CNTs are doped materials, and the dopants can be removed by UV light. Good sealing of the films in solar cell devices as well as UV protection under the encapsulation layer will be useful to solve this problem. CNT films have a reflection index similar to that of PET substrates, but an antireflection coating may still be useful for improved solar cell efficiency. The high sheet (~200 Ω/□) resistance could be the major barrier for the application of transparent CNTs in solar cell devices. The route for solving this problem is to incorporate CNT films with metal grids, or to mix CNTs with highly conductive metal nanowires for enhanced conductivity.[217] Although CNT separation could lead to films with all metallic CNTs, this task could be extremely challenging.[108]

5.3.2. Current-Driven Displays

Another unique application for transparent and conductive CNT films is flexible electronics, especially flexible displays due to their mechanical flexibility and outstanding optical properties.[7,35,38,44,218,329,384−386] There are two types of displays: current-driven display and voltage-driven. Current-driven display includes p−n diodes, resistive touch screens, and organic light emitting diodes.[387−391] Voltage-driven displays include electrochromic, elecrophoretic, electrowetting, and liquid crystal displays.[154,392] Generally the R_s requirement for current-driven displays is stricter than that for voltage-driven displays. We have estimated that the R_s for voltage-driven displays can be up to 10 kΩ/□ with minimal retarding effect on the display refresh rate.[154] Because there is limited current through voltage-driven displays, the device will operate as long as effective voltage is applied to the active layer. In this section, we will focus on current-driven applications such as OLEDs and touch screens. Polymer and small molecule-based organic light-emitting diodes (OLEDs) are rapidly approaching large-scale commercialization, driven by attractions such as low cost, fast response, applications in large-area flexible displays, and propelled by advances in efficiencies and operational lifetimes.[387−390] OLEDs are "dual-injection" devices in which holes and electrons are injected from the anode and cathode, respectively, into an active molecular/macromolecular medium to produce, via exciton decay, light emission.[390]

Demonstration of working OLED devices including small molecules and polymers has been done with transparent and conductive CNT electrodes.[7,35,38,44,218,329,384−386] Figure 28a shows the device structure by Martel et al. In this device, small molecule Alq_3 was used as the active emission layer, and LiF/Al is the cathode. Transparent CNTs on glass is used as the anode. The CNTs were fabricated by pulsed laser vaporization. As pointed out, the interface between CNTs and Alq_3 is a key element for an efficient OLED device. The considerable surface roughness of CNT films imposes a problem for the thickness of the organic layer. In this study, parylene was chosen to be used as the buffer layer due to its conformable coating quality. The parylene layer also helps the wetting of the organic layer onto the CNT thin films, which is important for charge transport in the devices. Figure 28a also shows an SEM of the cross section in the OLED device. The current density and luminance characteristics of devices based on ITO and CNT anodes were displayed in Figure 28b and c. Because of the rough surface of CNT films, thicker organic layers were used. However, the turn-on voltage for CNT-based OLEDs (6.4 eV) is only slightly

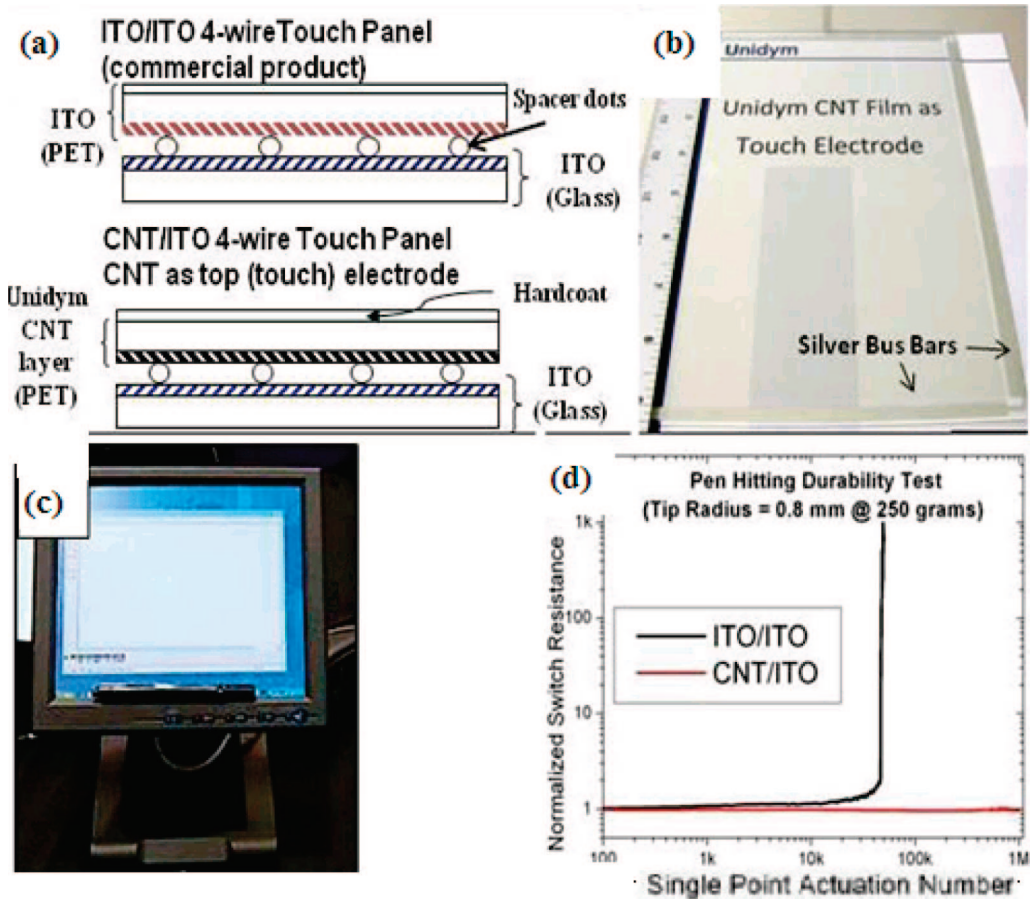

Figure 29. (a) Schematic of ITO/ITO (top) and CNT/ITO (bottom) touch panel used for mechanical testing; (b) photograph of CNT on PET film as touch electrode (ITO on glass bottom electrode) in a 10.4" diagonal functional touch panel. (c) Touch panel integrated with a full color LCD. (d) Pen touch actuation data demonstrating CNT touch electrode working long after ITO touch electrode has failed. (Reprinted with permission from ref 299. Copyright 2009 The Society of Information Display.)

higher than that measured for ITO-based OLEDs (6.2 eV). The maximum brightness achieved is 2800 Cd/m^2, approaching that of ITO-based OLED (6000 Cd/m^2). The difference of the light output is due to the optical transmittance between CNTs (44%) and ITO (90%) in this study.

Marks et al. have demonstrated a working polymer-based OLED device using laser ablation CNT thin films with the filtration and transfer printing method.[35,218] Figure 28d shows the device structure. In this study, three difference cases were studied: without PEDOT, with PEDOT, and with PEDOT/MeOH. MeOH was used to improve the wetting between PEDOT and CNTs. Surface roughness plays a significant role in the OLED device performance. The surface roughness is significantly improved after the PEDOT coating, from ~10 to ~4 nm. Furthermore, we found that incorporation of MeOH has significantly lowered the roughness to 0.96 nm. Surface modification improved the OLED device performance, as confirmed in the device curves in Figure 28e,f. The PEDOT device shows poor performance, which may be mainly due to the high surface roughness of the CNT films. The best OLED device with the structure has a maximum luminance of 1000 cd/m^2, a turn-on voltage of ~5.0 V, and a maximum current efficiency of ~0.85 Cd/A. We further improve the OLED device performance by incorporating an electron-dominated emission (BT) layer, and the maximum brightness achieved is 3500 Cd/m^2. The lifetime of OLED devices using CNT anodes was measured and compared to ITO-based OLEDs. The lifetime of CNT-based OLEDs is 55 h, comparable with ITO-based OLEDs with 52 h. The outstanding device performance, together with the supreme mechanical properties, means that CNT electrodes have strong potential for thin film OLED displays, especially for flexible OLED displays.

Another current-driven application for transparent CNT films is touch screens. Fewer display technologies are as omnipresent as touch screen technology in everyday life. There are various types of touch screens: four, five, or eight wire resistive touch screens, capacitive touch screens, acoustic touch screens, infrared touch screen, and others. Transparent and conductive electrodes are an essential component in most types of touch screen. Extremely high optical transmittance (>90%) and low R_s (<300 OPS) are normally needed for touch screens. Besides the optoelectronic performance of transparent electrodes, the mechanical durability under single point indentation is critical, because a commercial touch screen panel is normally exposed to up to a million touches at a single point.[259] Also, the transparent conductor should have strong adhesion to the substrate, and therefore may require an additional encapsulation or binder layer; however, that binder layer should not decrease the electrical conductivity nor the optical transmittance.[393] Meanwhile, the electrical conductivity uniformity needs to be high, and the variation of resistance needed to be less than 5% for accurate position sensing.[299] Figure 29a shows the device structure for a four-wire touch panel.[299] The bottom glass electrode is ITO due to its high transmittance. The four-wire resistive touch panel architecture is shown in the bottom portion of Figure 29a. A CNT/PET

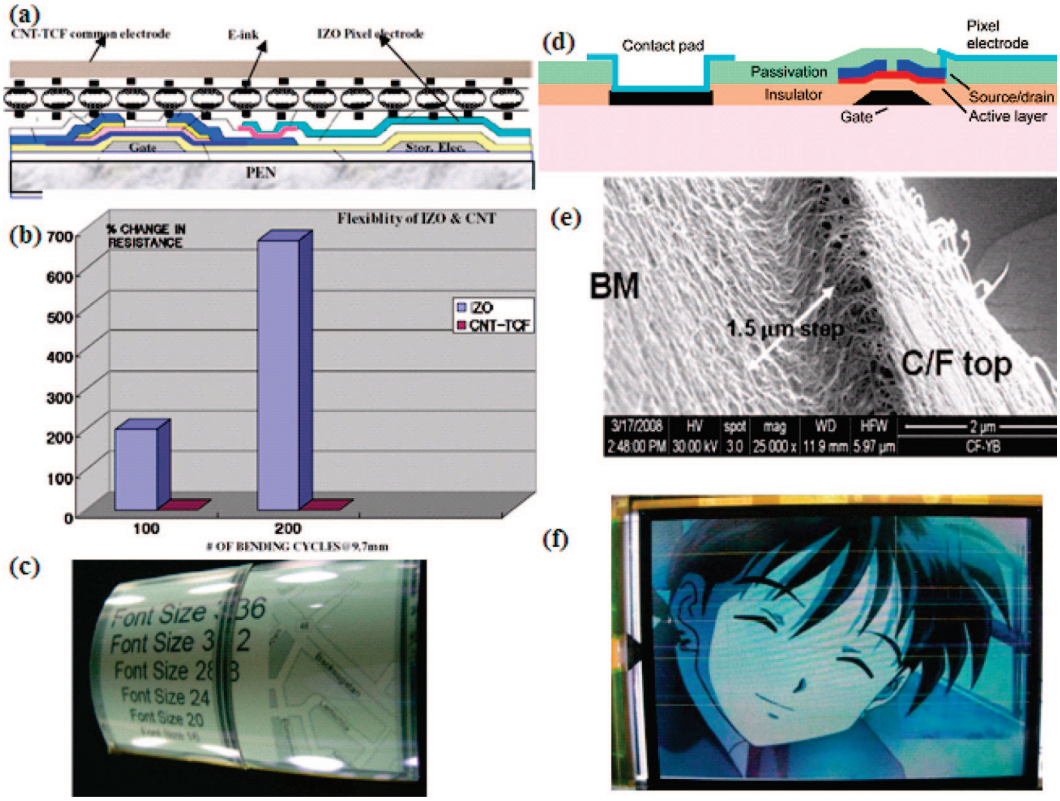

Figure 30. (a) Schematic of display structure using IZO on TFT side and CNT on TFT electrode. (b) The bending data of CNT vs IZO. (c) The flexible CNT-EPD panel exhibited in SID 2008. (d) Conventional 5 mask process architecture for TFT-LCD. (e) CNT-coated color filter showing excellent step coverage of substrate.[399] (f) A working LCD prototype with transparent CNT film on color filter side. (Reprinted with permission from ref 399. Copyright 2009 The Society of Information Display.)

film with a clear hard coat was placed over ITO/glass with spacer dots, and assembled into a touch panel. The final touch panel is shown in Figure 29b, and the touch panel integrated with a full color LCD is shown in Figure 29c. The mechanical robustness of the touch panel was measured using a single point actuation tap test using a 0.8 mm stylus and 250*g* of force. A similar test was also performed on a commercial ITO touch panel. The curvature induced by the stylus creates high tensile and compressive stress, which, in the case of ITO, leads to cracking of the conductive film, and an asymptotic rise in the switch resistance. The end result is a panel that is inaccurate, unresponsive, and has poor resolution. The flexible, web-like topology of a CNT film provides natural stress relief, making it almost impossible to crack or break by such mechanical tapping. Figure 29d shows that a panel with a CNT touch electrode continues to operate with negligible change in switch resistance, long after an ITO panel has failed. The mechanical robustness demonstrated by CNT touch panels promises to increase the lifetime and durability of current touch screens, while opening future applications in flexible and curved touch screens. The next step for resistive touch screens is to replace both the top and the bottom transparent electrodes. The touch resistance of CNT−CNT versus CNT−ITO could be better due to the absence of the possible heterojunction between CNT and ITO. Although CNT and ITO have very similar work functions, the difference of one being n-type and the other being p-type could cause some potential problem for use in resistive touch screens.

5.3.3. Voltage-Driven Displays

There are a few types of voltage-driven displays: electrowetting displays where droplets of liquid move, electrochromic displays where polymers change color, electrophoretic displays (EPD), capacitive touch screens, and liquid crystal displays (LCDs).[154,392,394−398] In these applications, an applied voltage across the device drives some change in the device. The sheet conductance requirement for voltage-driven displays is much less than in current driven displays.[154] The applications of transparent CNT films in all of these applications have been demonstrated by different groups.[154,392] Different issues arise and are solved. For example, for electrowetting displays, the conductive surface should be hydrophobic, and a thin layer of Teflon was deposited using vacuum deposition for this purpose. The hydrophobic surface can help move the liquid droplet with lower voltages.[154] For EPD applications, flexibility is critical. A schematic is shown in Figure 30a. Here, the CNT films on a PEN substrate show much better bending properties as compared to an IZO film (Figure 30b). There is no change of R_s observed for CNT films on PEN after 200 bending cycles, while the resistance of IZO films on a PEN substrate increases by 700% after 200 bending cycles using a 1 cm radius mandrel. With the use of transparent and conductive CNT films, flexible EPD devices have been demonstrated. CNT films are used here on the color filter side (Figure 30c). The reflectance response to voltage is the same as in an IZO-based device, with a slightly higher turn-on voltage. Lower "black" reflectivity is seen in a CNT panel, which improves the black reflectivity and enhances the readability of the printed text. The CNT-

TCF used holds superior optical-electrical properties, which greatly enhance the display performance by providing a better contrast ratio and higher readability, essential requirements for e-paper-based applications in the fast-spreading area of e-readers. These results greatly indicate the usage of CNT-based electrodes as a successful ITO replacement technology in the display area.

CNT thin films for LCD applications have also been demonstrated, as in Figure 30d−f. Beyond the performance of transmittance and sheet conductance, other properties such as the color, the contact resistance with metals, the ability to form a conformal coating on a step structure, device patterning techniques, and other device integration issues are all critical for successful adoption of transparent CNTs in commercialization. Figure 30d shows the 5-mask process device structure for LCD applications. CNTs are used on the color filter side on top of the TFT. Because of the mechanical flexibility and strong binding energy between CNTs and the LCD substrate, conformal coating of CNTs on the color filter step was observed (Figure 30e). This step coverage ensures the electrical conductance across the step, which is critical for addressing the pixels. Figure 30f shows the working LCD prototypes where CNT films were used on the color filter side. Usually, step height in a TFT backplane is 0.2−0.5 μm and 1.5 μm in the color filter. Efforts to minimize this step height to improve display quality have been investigated. The planarization of overall uneven surface feature requires additional processes and higher material cost. ITO can cover this step even though it is deposited by physical vapor deposition (PVD), but there exist yield loss and reliability issues from overhanging structures in via and contact PAD open regions. The step coverage of the CNT film on various steps and geometries was examined by Park et al.[399] Figure 30e shows the step coverage on the color filter side. The step height is 1.0−1.5 μm high depending on the resin color. The CNT films have adequate coverage across all step heights and surface topologies. In this application, the films were patterned with photolithography combined with plasma etching, which is fully compatible with LCD materials and fabrication processes.

The application demonstration of transparent CNT films on LCDs and EPD prototypes confirms the use of CNT films for voltage-driven displays. Even though the R_s (200 Ω/□) with a transmittance above 80% for CNTs is much higher than for ITO (∼20 Ω/□), it has been demonstrated that the high R_s does not prohibit the use of CNT films in voltage-driven devices. The response time in electrowetting displays, EPDs, and LCDs is not significantly larger than that for ITO- or IZO-based devices. The mechanical properties, ease of patterning, and process compatibility with device fabrication lines make transparent CNT films close to commercialization.

5.3.4. Electrostatic and EMI Shielding

Electrostatic charge (ESC) dissipation is needed for many applications such as advanced spacecrafts and roll-to-roll manufacturing facilities. The building up of ESC without appropriate dissipation could be extremely dangerous. As well, the ability to be ultralight weight, transparent, and flexible is important for ESC dissipation materials. The R_s requirement for ESC dissipation is in the range of 10^6-10^{10} Ω/□. Because of the extreme high conductivity of CNT films, a transparent and conductive CNT coating is useful for this particular application, and easily fulfills the requirement. The R_s of CNT thin films can be tuned by varying the film thickness.[26] For better mechanical integrity, CNTs are incorporated into a polymer to be applied as a thin film coating for ESC dissipation applications.[63,280,400−404] Charge decay was tested for high voltages up to 3000 V. It was found that the surface conductivity of a CNT coating is sufficient for ESC mitigation with negligible degradation in the optical properties. The films exhibit a high degree of flexibility and mechanical robustness through harsh manipulation tests.

Electromagnetic interference (EMI) is a serious problem for our society, considering the pervasiveness of electronic devices. In certain circumstances, the leakage of EM radiation could cause catastrophic damages. For shielding, the major mechanism is by reflection. Metal foils and metal grids are two common shielding materials. Recently conductive polymers have been tested for EMI shielding applications, but the intrinsic degradation is problematic. A matrix containing conductive fillers is an attractive alternative for shielding.[405,406] Composites incorporating CNTs have extremely low electrical percolation threshold due to the high aspect ratio. The total EMI shielding effectiveness (SE) is the sum of contributions from absorption and reflection. SE is calculated as SE (dB) $= -10 \log(P_t/P_0)$, where P_t and P_0 are the transmitted and the incident intensities of the EM wave, respectively.[403] When reflection is the main mechanism of shielding, it is directly related to the material conductivity. For materials with frequency-independent conductivity, the shielding can easily be calculated from the dc conductivity and the SE scaled as SE $\approx \log(\sigma/fd)$, where σ is the dc conductivity, f is the frequency, and d is the film thickness.[280] The SE can be experimentally measured or calculated on the basis of the quasi-optics formula. Highly conducting CNTs have been incorporated into composites for EMI shielding purposes, and a 49 dB shielding effectiveness at 10 MHz has been measured for 15% NT loading of a polymer composite.[403] Different SEs were achieved for the same CNT loading due to differences in conductivity. Figure 31a shows the data for CNTs incorporated into polymers with different CNT lengths and heat treatments. It is obvious that longer CNTs lead to better SE, which is consistent with the dc conductivity results. The SE data show clear dependence on the EM frequency. High frequency leads to larger skin depth, which needs a larger thickness to achieve the same SE. Also, the high temperature annealing of CNTs in inner gas or vacuum can remove the defects and improve the dc conductivity. As in Figure 31a, the annealing also improves the SE, which is again consistent with the dc conductivity increase (from 0.12 to 0.14 S/cm). Lim et al. have measured a SE in the terahertz range using time-domain terahertz spectroscopy on thin layers of CNTs coated on flexible substrates.[140] The data are in good agreement with the Drude free-electron model. The SE data are plotted in Figure 31b. The transmittance data are much larger and the SE data are much smaller than those in the microwave range, which is reasonable given the fact that higher frequency leads to large penetration of EMI waves. These films demonstrated good shielding of electromagnetic waves in the terahertz range, while transparency to visible light was maintained. They also found that the shielding efficiency can be engineered by thickness control of the CNT layer and/or by additional chemical treatment. The amount of terahertz transmission reduces dramatically after acid treatments. Note that the chemical treatment and acid doping do not change the spectra of CNT thin films in the visible range. For CNT thin films without the incorporation of polymer, the frequency-

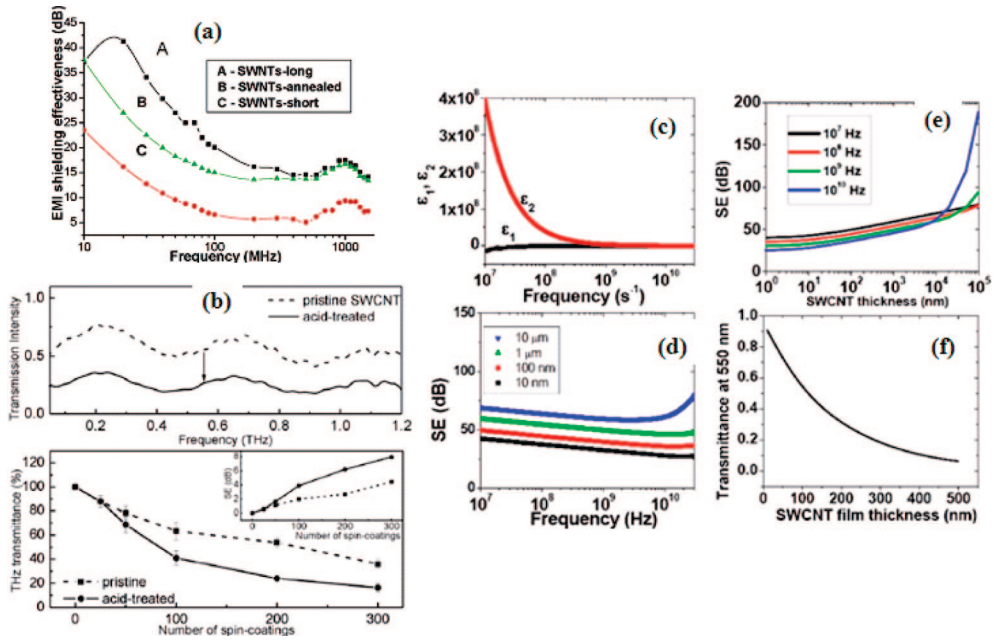

Figure 31. (a) Impact of wall integrity and aspect ratio on the EMI shielding effectiveness of the composites containing 10 wt % CNTs. (Reprinted with permission from ref 403. Copyright 2006 American Chemical Society.) (b) Transmission spectra vs frequency and number of coating for spin coated CNT (dashed line is for pristine CNT, and solid line is for acid treated CNT). The inset shows the calculated SE data. (Reprinted with permission from ref 140. Copyright 2008 American Institute of Physics.) (c) Dielectric constant vs frequency for CNT thin films. (d) EMI shielding effectiness (SE) vs frequency in microwave frequency range. (e) SE vs CNT film thickness. (f) Calculated optical transmittance vs CNT thickness. (Reprinted with permission from ref 280. Copyright 2007 American Institute of Physics.)

dependent conductivity in the 10−30 GHz range is measured using the Corbino reflection technique over temperatures of 20−400 K.[407] The SE for various film thicknesses is calculated on the basis of the real and imaginary parts of the microwave conductivity. Microwave was treated as quasi-optics, and the formula for standard optics are applied here, on the basis of the fact that the wavelength of microwave is much larger than our film thickness (~30 nm). Based on the two parts of the conductivity, the dielectric constants in this frequency range are plotted in Figure 31c. The SE versus films thickness and frequency are also plotted in Figure 31d and e. The transmittance data in the visible range were calculated on the basis of the data from Diegio and are plotted in Figure 31f. Shielding effectiveness of 43 dB at 10 MHz and 28 dB at 10 GHz are found for films with 90% optical transmittance, which suggests that SWCNT films are promising as a type of transparent microwave shielding material.

5.3.5. Stretchable Electrode for Actuators

Dielectric elastomers and compliant electrode materials have exhibited extraordinarily high performance, which shows great potential as use in a wide range of novel applications including robotics and artificial muscles. However, the local breakdown initiated at defects causes terminal failure of the entire actuator, frequently setting the device on fire. Fault-tolerant compliant electrode materials are thus essential to dielectric elastomers as it greatly enhances the performance and lifetime of packaged actuators while improving safety. Fault tolerance has been studied in polypropylene thin film capacitors via a technique called self-clearing or self-healing.[322] The region around the breakdown site in the film is the cleared area, and it consequently isolates the defects from electrical contact. This self-clearing technique prolongs the lifetime of large-area polymer thin film capacitors. Metallic thin film electrodes, however, are not compliant with dielectric elastomers. Because of the extreme mechanical flexibility and stretchability as discussed in the previous section,[106,186,300,408] CNT films were potentially useful for stretchable and self-cleaning electrodes for actuator applications. The degradation of SWCNTs has been reported under high current in a field emitter,[230,409,410] under high temperature as a light bulb filament,[410] or under plasma. The fluffy CNT can even be ignited in air with a 100 mW/cm^2 photographic flash.[411] In the fault tolerance experiment described above, the current rose to 35 μA. Much of this current passed through a very small area over which the electrical heating may be significant because of the high voltage applied. The temperature was sufficiently high to cause arcing and degradation of the CNTs. Figure 32a and b shows the setup of Pei's study.[408] Two CNT films were sprayed onto the elastomer substrate through shadow masks on both sides. The circular areas are overlapping each other, and the high voltages were applied through the black lines of CNT films. Figure 32c shows the current−voltage curve for three actuations. The first peak corresponds to the clearing event from the fault, and the self-cleaning process is fast. SEM in Figure 32d shows the morphology after the self-cleaning. The CNTs were burned away in the empty areas where the short between the cathode and anode could potentially short the entire actuator device. They observed that the actuator device works fine after the self-cleaning event. The lifetime of the actuator with CNT electrode is prolonged as compared to a carbon grease electrode-based device, as shown in Figure 32e, which is due to the self-cleaning of the CNT electrode in the devices. For this type of actuator device application, the outstanding stretchable property of CNT film is also very important.

5.3.6. Other Applications

There are many other applications where transparent and conductive CNT films can be used, especially for flexible electronics. The applications include use as interconnects in

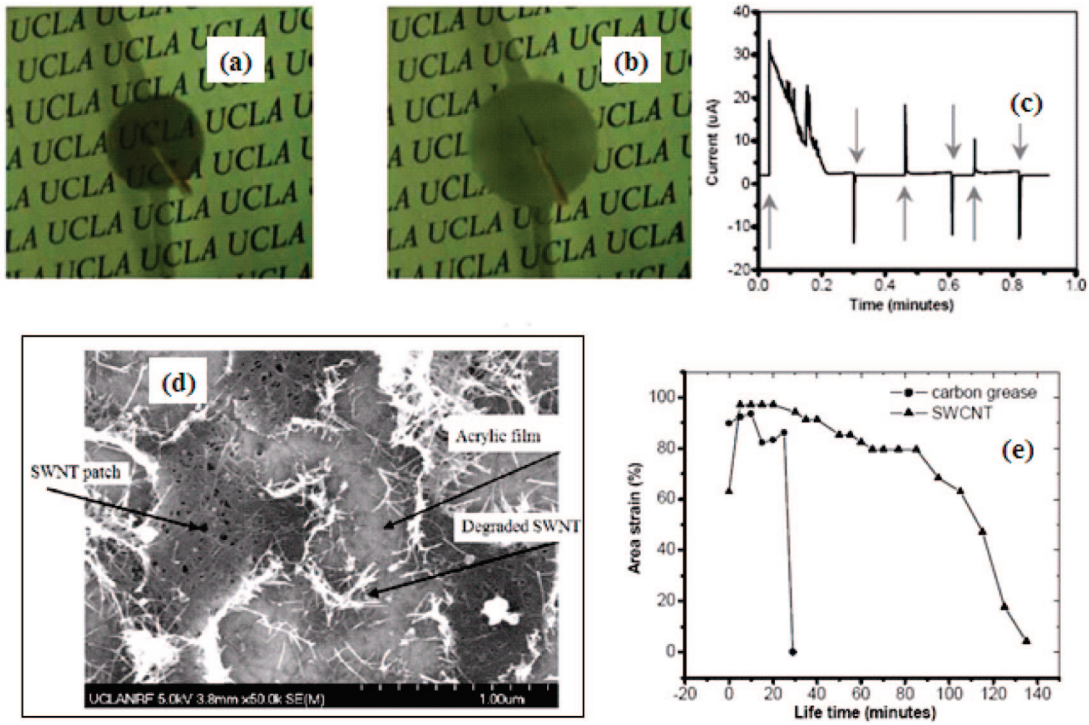

Figure 32. (a and b) 80% strain was obtained on the film with SWCNT electrodes through self-clearing albeit a fault has been introduced. (c) The current−voltage curve for the film with CNT electrodes for three actuations. The upward arrows indicate voltage application; the downward arrows indicate voltage turned off. (d) Self-cleaned CNT electrode surface near the fault. The CNT patches are isolated from each other by the degraded, nonconductive path. Electrically induced strain alteration during the actuator lifetime test of a 300% biaxially prestrained 4905 film coated with either carbon grease or CNT electrodes under 0−3 kV square wave driving at 80 MHz frequency. (e) Electrically induced strain alteration during the actuator lifetime test of 100% biaxially prestrained CNT films. (Reprinted with permission from ref 408. Copyright 2008 Wiley-VCH.)

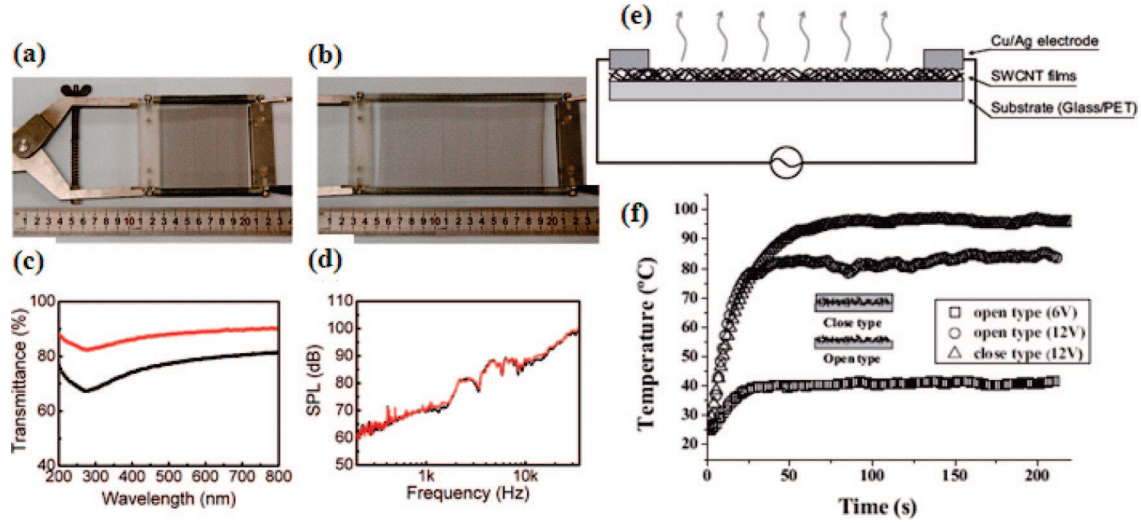

Figure 33. (a) Stretchable CNT thin film loud speaker. (a) A one-layer CNT thin film is put on two springs that serve also as electrodes. The CNTs are aligned perpendicular to the two spring electrodes. (b) The CNT thin film was stretched to 200% of its original width. (c) Transmittance spectra of the one-layer CNT thin film before (black) and after (red) being stretched to 200% of its original width, measured by using a UV−vis spectrophotometer. (d) Measured SPLs versus frequency for a one-layer CNT thin film before (black) and after (red) being stretched to 200% of its original width. Both input powers are 2.5 W. (Reprinted with permission from ref 413. Copyright 2008 American Chemical Society.) (e) Schematic diagram of a SWCNT film heater on a substrate with an electrode pair. (f) Temperature response of the SWCNT film surface on a PET substrate. The area of the SWCNT film was 4 × 4 cm^2. The film thickness of the open configuration was 188 lm, while the thickness was 250 lm in the closed configuration. (Reprinted with permission from ref 414. Copyright 2007 Wiley-VCH.)

electronics, general electrode application as source or drain electrode in thin film transistors, electrodes in LEDs to provide ohmic contact, and IR imaging/communication.[412] Figure 33 shows novel applications as in transparent loudspeakers and transparent heaters. The working mechanism is based on the thermoacoustic effect, which has been studied for more than 200 years. In loudspeaker applications, the ability to be stretched is important.[413] In Fan's study, the CNT films were pulled out from a superaligned CNT array. The transmittance is 80% and 90% for as-is and 200% stretched films. The CNT film loudspeaker can produce sounds as loud as a commercial voice-coil loudspeaker. The

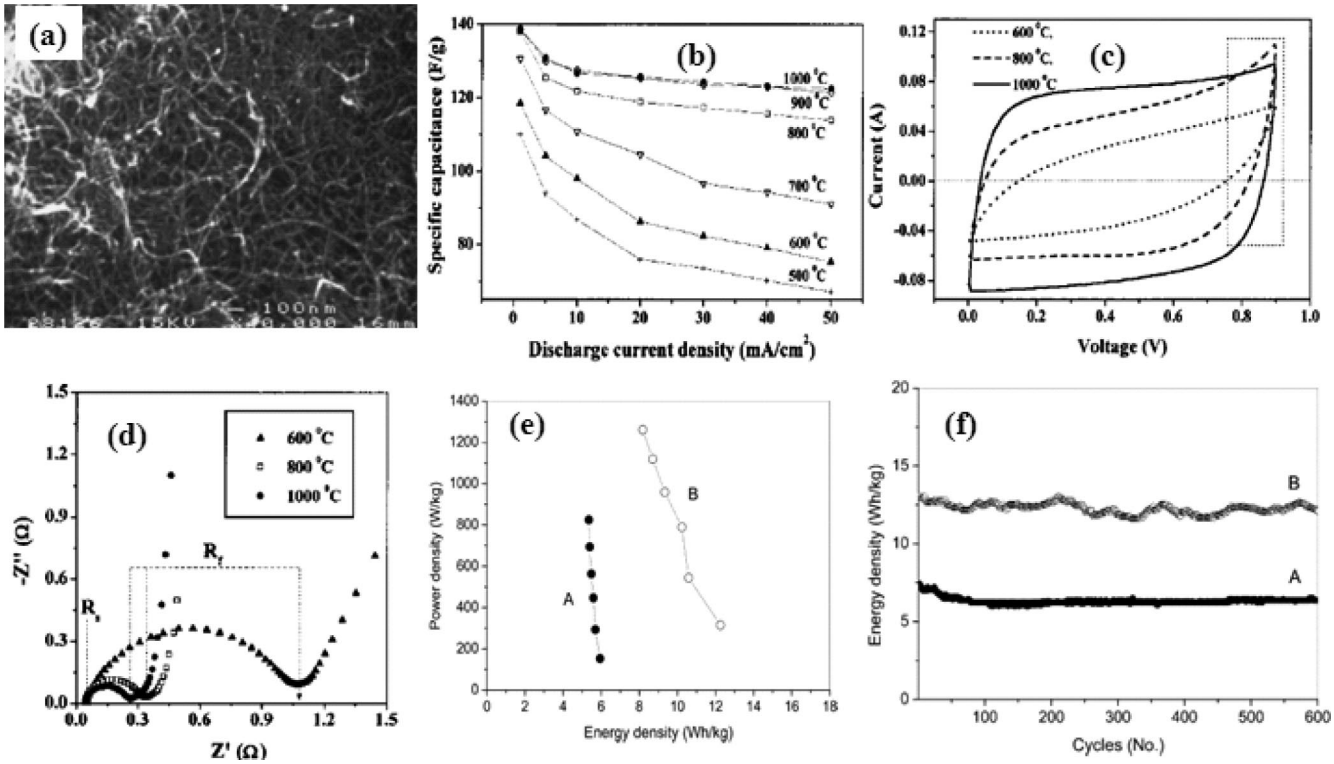

Figure 34. (a) SEM micrograph of a nanotube electrode. The electrode consists of randomly entangled and cross-linked carbon nanotubes, which have uniform diameters of 8 nm. (Reprinted with permission from ref 156. Copyright 1997 American Institute of Physics.) (b) The specific capacitances of the heat-treated electrodes at various temperatures as a function of the discharging current density at a charging voltage of 0.9 V for 10 min. (c) The cyclic voltammetric (CV) behaviors (sweep rate, 100 mV/s) for the CNT electrodes at various heat-treatment temperatures. (d) The complex-plane impedance plots for the CNT electrodes for various heat-treatment temperatures at an ac-voltage amplitude of 5 mV; Z'', imaginary impedance, Z', real impedance. (Reprinted with permission from ref 178. Copyright 2001 Wiley-VCH.) (e) Ragone plots of power density versus energy density for (A) CNT−CNT supercapacitor; (B) CNT−TNW supercapacitor. (f) Variation of the energy density with the number of cycles for CNT−CNT supercapacitor and CNT−TNW supercapacitor at a rate of 10 °C. (Reprinted with permission from ref 92. Copyright 2006 Wiley-VCH.)

resistance of CNT films in this study can be tuned to meet the requirements of the driving circuit, from 500 to 8 Ω s. The speakers are enabled by two major properties of CNT thin films: the mechanical stretchability and optical visibility. They have made loudspeakers to mount on a 17 in. LCD screen and an 8 cm × 14.5 cm flexible transparent loudspeaker that is mounted over a waving flag. San et al. have applied CNT films as a transparent heater, which can be used to defrost windows for automobile applications.[414] In this application, optimized R_s is needed for generating the most heat with an applied voltage. Additionally, optical transmittance is needed for window applications. Figure 33e shows their test setup. The CNT thin films were connected by Cu/Ag to apply the electrical field. Figure 33f shows the quick temperature response of the CNT film surface after application of different voltages. The temperature rose up to ∼100 °C in less than a minute in a closed system with 12 V applied. A defrosting study was carried out for a CNT film with an R_s of 1190 Ω/□ and a transparency of 91.3%. The frost on the surface was removed completely after supplying the CNT film heater with 0.12 W for 1 min.

5.4. Nanoporous Electrodes for Energy Storage

The third major type of application for CNT thin films is using its nanoporous structure with high surface area for an electrochemical capacitor. An electrochemical capacitor is also called a supercapacitor due to its large capacitance. The capacitance is proportional to A/d, where A is the effective surface area and d is the distance between two electrodes. The electrochemical double layer structure with thickness of ∼1 nm leads to a large capacitance.[415] Another major factor leading to high capacitance is to use an electrode with high surface area. CNT films have large surface area, up to 1000 cm^2/g, which is attractive for this application.[309] The large surface area of CNT films is due to the pores with high density. For supercapacitor applications, the pores need to be accessible to the mobile ions. There are three major categories of pores in materials according to IUPAC classification: (i) micropores of <2 nm; (ii) mesopores of 2−5 nm; and (iii) macropores of >5 nm.[178] In general, pore size in the range of 3−5 nm is required for improved double layer capacitors. For supercapacitor applications, the total capacitance includes two components: the electrostatic component and the pseudocapacitance. The SEM in Figure 34a reveals the highly porous structure of CNT films, which is ideal for supercapacitor applications. There are several studies on the application of porous CNT electrodes for supercapacitor applications.[34,40,45,50,52,92,156,318−320,416] Niu et al. used MWCNTs and found pores of 9.2 nm with 8 nm diameter CNTs.[156] The specific capacitance was measured to be 102 and 49 F/g at 1 and 100 Hz, respectively. The electrolyte in their device is 38% H_2SO_4, and a power density of 8000 W/kg has been achieved. The equivalent series resistance (ESR) is low, 0.094 Ω. Impedance measurement indicates that the stored energy is accessible at a frequency of 100 Hz. In this study, there is no pseudocapacitance involved. Lee et al. made supercapacitors using SWCNTs and achieved a maximum specific capacitance of 180 F/g and a measured

power density of 20 kW/kg at an energy density of 7 Wh/kg in a solution of 7.5 M KOH.[178] The capacitance increases with the annealing time and the charge time, which is correlated to the R_s of CNT films after heat treatment. As shown in the charge curve, the capacitance increases dramatically and reaches its 80% value in the first 10 min. Continued increase in the capacitance over a long time is generally observed from the porous electrodes and is attributed to the existence of various forms of pores and pore diameters in the electrode. Figure 34b shows the discharge curve for CNT films with different annealing temperature. For the 1000 °C sample, the capacitance decreases by 10%, while for the 700 °C sample, the capacitance decreases by 30%. Note that the existence of the long flat region in the discharging is useful for practical applications. The cyclic voltammetry (CV) behavior with a sweep rate of 100 mV/s at various temperatures is shown in Figure 34c. The power density increases with increasing heat-treatment temperature. Note that the CV curve at 1000 °C is close to the ideal rectangular shape due to the small ESR of CNT electrodes. The complex-plane impedance plots were show Figure 34d. In this study, the contact resistance and the electrolyte resistance are identical for all of the samples. Therefore, the difference in impedance comes from the CNT electrode resistance. The ideally polarizable capacitance will give rise to a straight line along the imaginary axis. In real capacitors with a series resistance, this line has a finite slope, representing the diffusive resistivity of the electrolyte within the pore of the electrode. With increasing heat-treatment temperatures, the diffusive line comes closer to an ideally straight line. The contact resistance between CNT electrodes and the current collector is also critical. They studied this effect by choosing different current collectors, which cause different contact resistance. The data in the Ragone plots agree well with the impedance data. As discussed, another method to improve the overall capacitance is to introduce pesudocapacitance by bringing in active groups on the CNTs. These materials could be transition metal oxides or conductive polymers.[26,34,40,52,319] Frackowiak et al. have studied the modification of CNT films with polypyrrole (PPy). The pesodocapacitance by a quick faradaic reaction greatly enhances the overall capacitance. The choice of PPy has the advantage of being electrically conductive and maintaining the porous structure for high ion conductivity. The capacitance increases from 50 F/g to 163 F/g after 5 nm PPy modification. Tour et al. obtained 7 times increase of capacitance using a pyrrole coating on a CNT surface.[26] The pyrrole coating on CNT films increases the capacitance of CNT films dramatically. The data for power density and energy density in Ragone plots show dramatic improvement after the pyrrole coating on CNT films. Note that the double layer capacitance for bare CNT electrode is 10 F/cm^2 and pyrrole-modified CNT electrode is 145 F/cm^2. At 10 mA discharge current, the power density of pyrrole treated samples is almost 25 times that of the controlled bulky paper. Li et al. reported a new supercapacitor structure, using CNT electrode as cathode and TiO_2−B nanowires as anode.[92] As compared to CNT−CNT supercapacitor, CNT−NW doubles the energy density while maintaining the cycle stability. They conclude that CNT−CNT supercapacitors are energy limited while CNT−NWs are power limited, as shown in Figure 34e. In the Nyquist plots for CNT−CNT and CNT−NW

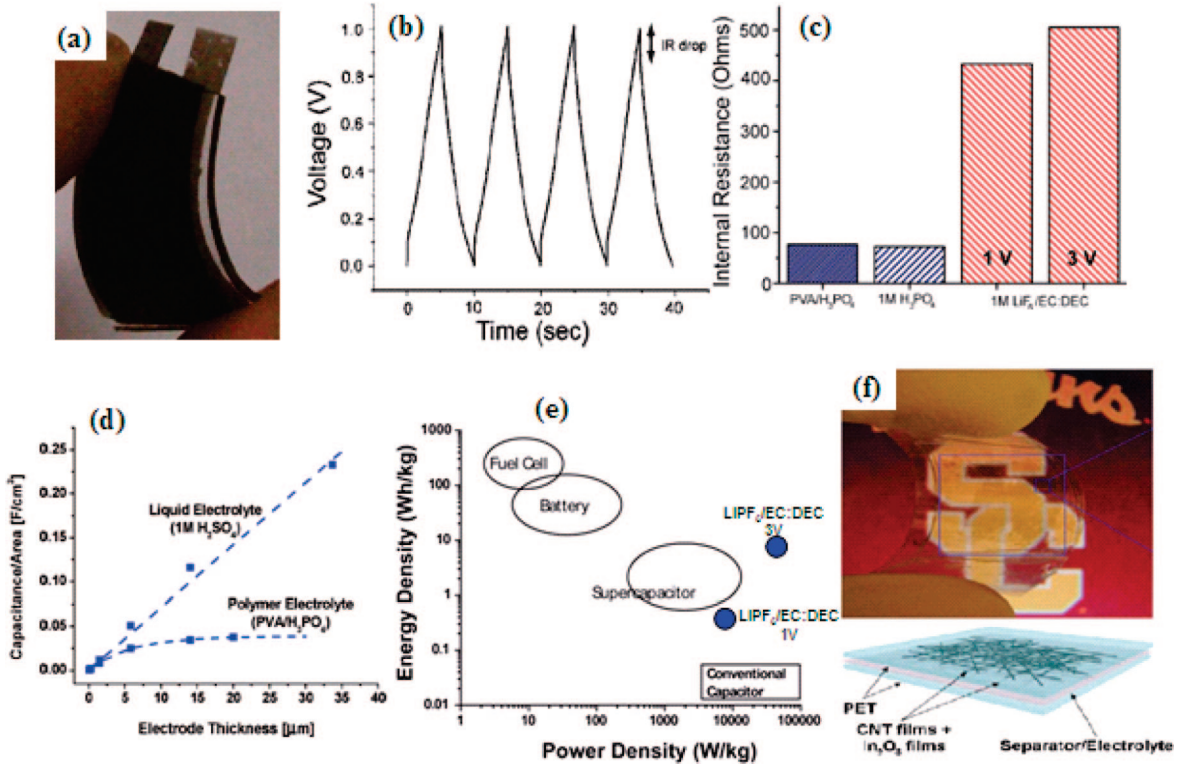

Figure 35. (a) Thin film supercapacitor using spraying SWCNT films on PET as electrodes and a PVA/H_3PO_4-based polymer electrolyte as both electrolyte and separator. (b) Charge/discharge curves measured with a 1 mA/cm^2 current density for a thin film SWCNT supercapacitor using PVA/H_3PO_4 polymer electrolyte. (c) Internal resistance obtained from the charge−discharge curve using 1 mA/cm^2 current density. (d) Thickness dependence of the capacitance per area for SWCNT thin film comparing a liquid (1 M H_2SO_4) and a gel electrolyte (PVA/H_3PO_4). (Reprinted with permission from ref 7. Copyright 2009 American Chemical Society.) (e) A Ragone plot showing the SWCNT electrode in capacitance, along with other energy storage device. (After ref 8.) (f) A flexible and transparent supercapacitor using CNT films and In_2O_3 nanowires. (Reprinted with permission from ref 419. Copyright 2009 American Institute of Physics.)

Table 3. Summary of Various Types of Transparent Electrodes and Their Potential Applications

	advantages	disadvantages	applications
carbon nanotube	highly flexible	relatively high sheet resistance for solar cell and large-scale display applications	touch screen
	neutral color		EPD
	low haze		flexible OLED
	low reflection		LCD
	can be doped		IR devices
	solution processable		EC, EL displays
	cheap in bulk		
	chemically stable		
graphene	flexible, neutral color	relatively high sheet resistance for solar cell and large-scale display applications	touch screen
	potentially low cost, continuous improvement of conductivity		flexible OLED
	can be doped		
	potentially solution processable		
	low surface roughness		
metal nanowire or thin film (i.e., Ag or Au)	low sheet resistance	relatively high haze value	mainly solar cells
	large light scattering	high surface roughness	
	mechanically flexible	poor chemical stability	
	surfactant-free processing		
	solution processable		
PEDOT	flexible	relative high sheet resistance	surface modification for nanowire or nanotube network electrode
	mature	chemically sensitive	
	solution processable	color	
ITO, AZO	mature	costly	optoelectronic devices on rigid substrates
	low sheet resistance	poor mechanical properties	
	high transparency	high reflection	
	solution processed ITO particle or ITO nanowires are under study		

supercapacitors before and after 600 cyclings, there are some interesting differences between the two sets of curves. The charge transfer between electrolyte and the electrode changed noticeably for the CNT−NW supercapacitor, which contributed to the decrease of the NW conductivity after the 600 cyclings. Figure 34f shows the cycling stability up to 600 cycles. For commercial applications, cycling up to 100 000 cycles is generally needed.[415,417] A more recent study by Wei et al. reveals that the supercapacitor with SWCNT film electrodes yields cycling of over 200 000 cycles in a coin cell structure with a constant density of 20 A/g at 25 and 100, respectively, while maintaining 80% efficiency.[418]

Along with the "printed power" concept, Grüner et al. have successfully demonstrated that porous CNT films can be used as both the current collector and the electrode for supercapacitor applications.[320] CNT films and the gel electrolytes can be printed on the basis of CNT inks. Because of the high conductivity, CNT electrodes can also replace the metal current collector to serve as a bifunctional material in supercapacitors. Figure 35a shows a flexible supercapacitor using a CNT film as both electrode and current collector, and a printable polymer electrolyte is used. Various types of electrolytes, including aqueous and polymer electrolytes, were tested in such devices. The internal resistance (IR), the specific capacitance, and the cycling were studied. From the IR drop in the charge/discharge curve, the internal resistance is calculated (Figure 35b and c). The CNT film is fabricated by spraying to a R_s of 40−50 Ω/□. Such resistance is relative high for a current collector, and further development is needed to decrease the R_s. By applying thicker materials, improving the dispersion quality, and optimizing the coating method, the sheet conductance could be improved. The internal resistance found in this study shows that the aqueous-based devices have much lower internal resistance than organic electrolyte-based devices, due to the significant difference in electrolyte conductivity. In this study, the $LiPF_6$/EC:DEC conductivity is 10 mS/cm, while the aqueous H_3PO_4 conductivity is 100−300 mS/cm. The energy and power density were calculated from the charge/discharge curve using a simple formula. The power density is $V_i^2/4RM$, where V_i is the initial voltage, R is the equivalent series resistance, and M is the total mass of CNT coating on both electrodes. The maximum energy storage is $CV_i^2/2M$, where C is the total capacitance. The data were plotted along with the other types of energy storage devices. They pointed out that increasing the voltage used to 3 V from 1 V increases both the power density and the energy density by roughly 1 order of magnitude. In a separate study, Zhou et al. have made a supercapacitor with the features of optical transparency and mechanical flexibility using metal nanowires/carbon nanotube heterogeneous films.[419] The device structure is shown in Figure 35e. The CNT films were fabricated by the filtration method, and the In_2O_3 nanowires were deposited and transferred to CNTs. Both CNTs and In_2O_3 nanowire films were fabricated by a solution-based method. The supercapacitor performance greatly improves by the incorporation of In_2O_3 nanowires due to their redox transitions. Rinzler et al. have recently reported a simple method to further increase the porosity of CNT films by an engineering method.[39] The strategy is to use a CNT dispersion with sacrificial nano-

particles to form a CNT/nanoparticles composite film. The sacrificial nanoparticles are subsequently eliminated by a process that does not change the film framework. This leads to CNT films with a pore size of ~200 nm with an increase of surface area of 2.5×. The porous and conductive CNT film has many other application potentials. For example, Grüner et al. have also tested porous CNT electrodes for a battery electrode.[420] Haddon et al. have used porous support for Pt catalysis for fuel cell applications.[42] There is much potential for applications to use porous and conductive CNT film by filling the porous with other materials to bring in new functionality for device application.

6. Summary and Outlook

We have reviewed the various aspects of CNT thin films, including film fabrication, patterning, properties, and various device applications. One of the major remaining roadblocks to commercializing device applications is to find a scalable and reliable method to separate metallic and semiconducting CNTs. The separation of CNTs will benefit two major applications. Semiconducting CNTs will benefit thin film transistors, and metallic CNTs will benefit highly conductive electrodes for transparent conductor applications. These two immediate applications areas of CNT thin films will be the dominant applications. There is much industrial interest in commercializing these two applications. For this, development with manufacturing in mind is a must. Further understanding of the physics and chemistry of CNTs will benefit development. As in the silicon industry, much effort has been spent to improve the purity of the materials as well as to control doping. When compared to silicon or ITO, CNT thin film technology is still at its early stage. Although the performance of transparent electrodes using CNTs has been demonstrated in the lab for applications such as touch screens and OLEDs, the material stability, the scalability, and the reproducibility still need to be improved. Applications of CNT thin films in solar cells and thin film transistors for flexible electronics will require continued development. The performance as a transparent electrode is still 2 times worse than the best flexible ITO electrodes. For thin film transistors, the on/off is normally in the range of 10^3, but an improvement to 10^5 is needed. For all applications, a full material examination and process flow needed to be examined before serious commercialization. The commercialization prospects will continue to affect the research direction. There is much more to understand regarding CNT thin films, such as control of tube purity and doping, scalable tube separation methods, and integration challenges into commercial devices. However, despite the remaining questions, CNT films will soon be an essential component in commercial device applications, especially as transparent electrodes for various devices. Within the next couple of years, CNT films will be realized as electrodes for touch panels, soon followed by integration into display and photovoltaic applications, and potentially for energy storage applications. In the race with transparent and conductive oxides, CNT thin films will certainly find their applications in flexible electronic devices. Table 3 summarizes the advantages and disadvantages of the emerging candidates. Although these emerging candidates will preferably be fabricated through solution based, roll-to-roll processing, with the potential of being low cost, they have dramatically fundamental differences in certain properties. For example, metal nanowire networks show intrinsic, high haze value, which is beneficial for solar cell applications, while the neutral color of CNT or graphene films is preferred for displays. In the long run, each candidate may find its application in certain devices as a replacement for ITO.

7. Acknowledgments

We acknowledge E. Artukovic, Y. Zhou, M. Kaempgen, and M. Briman from George Gruner's group, X. Hua from S. Anlage's group at the University of Maryland, J. Li and J. Liu from T. Marks's group at Northwestern University, W. Yuan and Z. Yu from Q. Pei's group at UCLA, Y. Zhao and R. Ramirez from F. Stoddart's group at Northwestern University, and M. Rowell and M. Topinka from M. McGehee's group at Stanford University. We also acknowledge the scientists at Unidym Inc.

8. References

(1) Shipway, A. K., E.; Willner, I. *ChemPhysChem* **2001**, *1*, 18.
(2) Johnson, J. C.; Choi, H. J.; Knutsen, K. P.; Schaller, R. D.; Yang, P. D.; Saykally, R. J. *Nat. Mater.* **2002**, *1*, 106.
(3) Chen, B. H.; Lin, H. C.; Huang, T. Y.; Wei, J. H.; Wang, H. H.; Tsai, M. J.; Chao, T. S. *Appl. Phys. Lett.* **2006**, *88*, 093502.
(4) Duan, X. F.; Huang, Y.; Agarwal, R.; Lieber, C. M. *Nature* **2003**, *421*, 241.
(5) Yu, X.; Rajamani, R.; Stelson, K. A.; Cui, T. *J. Nanosci. Nanotechnol.* **2006**, *6*, 1939.
(6) Cui, Y.; Zhong, Z. H.; Wang, D. L.; Wang, W. U.; Lieber, C. M. *Nano Lett.* **2003**, *3*, 149.
(7) Kaempgen, M.; Chan, C. K.; Ma, J.; Cui, Y.; Gruner, G. *Nano Lett.* **2009**, *9*, 1872.
(8) Stankovich, S.; Dikin, D. A.; Dommett, G. H. B.; Kohlhaas, K. M.; Zimney, E. J.; Stach, E. A.; Piner, R. D.; Nguyen, S. T.; Ruoff, R. S. *Nature* **2006**, *442*, 282.
(9) Jackson, R.; Domercq, B.; Jain, R.; Kippelen, B.; Graham, S. *Adv. Funct. Mater.* **2008**, *18*, 2548.
(10) Saito, R.; Fujita, M.; Dresselhaus, G.; Dresselhaus, M. S. *Phys. Rev. B* **1992**, *46*, 1804.
(11) Ohta, T.; Bostwick, A.; Seyller, T.; Horn, K.; Rotenberg, E. *Science* **2006**, *313*, 951.
(12) Novoselov, K. S.; Jiang, Z.; Zhang, Y.; Morozov, S. V.; Stormer, H. L.; Zeitler, U.; Maan, J. C.; Boebinger, G. S.; Kim, P.; Geim, A. K. *Science* **2007**, *315*, 1379.
(13) Novoselov, K. S.; Geim, A. K.; Morozov, S. V.; Jiang, D.; Katsnelson, M. I.; Grigorieva, I. V.; Dubonos, S. V.; Firsov, A. A. *Nature* **2005**, *438*, 197.
(14) Meyer, J. C.; Geim, A. K.; Katsnelson, M. I.; Novoselov, K. S.; Booth, T. J.; Roth, S. *Nature* **2007**, *446*, 60.
(15) Gusynin, V. P.; Sharapov, S. G. *Phys. Rev. Lett.* **2005**, *95*, 146801.
(16) Geim, A. K.; Novoselov, K. S. *Nat. Mater.* **2007**, *6*, 183.
(17) Berger, C.; Song, Z. M.; Li, X. B.; Wu, X. S.; Brown, N.; Naud, C.; Mayou, D.; Li, T. B.; Hass, J.; Marchenkov, A. N.; Conrad, E. H.; First, P. N.; de Heer, W. A. *Science* **2006**, *312*, 1191.
(18) Berger, C.; Song, Z. M.; Li, T. B.; Li, X. B.; Ogbazghi, A. Y.; Feng, R.; Dai, Z. T.; Marchenkov, A. N.; Conrad, E. H.; First, P. N.; de Heer, W. A. *J. Phys. Chem. B* **2004**, *108*, 19912.
(19) Durkop, T. G., S.; Cobas, E.; Fuhrer, M. S. *Nano Lett.* **2004**, *4*, 35.
(20) Wintmire, J. W. W., C. T. *Phys. Rev. Lett.* **1998**, *81*, 2506.
(21) Kane, C. M., E. *Phys. Rev. Lett.* **1997**, *78*, 1932.
(22) Snow, E. S.; Novak, J. P.; Campbell, P. M.; Park, D. *Appl. Phys. Lett.* **2003**, *82*, 2145.
(23) Bekyarova, E.; Itkis, M. E.; Cabrera, N.; Zhao, B.; Yu, A. P.; Gao, J. B.; Haddon, R. C. *J. Am. Chem. Soc.* **2005**, *127*, 5990.
(24) Kaiser, A. B.; Skakalova, V.; Roth, S. *Physica E* **2008**, *40*, 2311.
(25) Vaillancourt, J.; Zhang, H. Y.; Vasinajindakaw, P.; Xia, H. T.; Lu, X. J.; Han, X. L.; Janzen, D. C.; Shih, W. S.; Jones, C. S.; Stroder, M.; Chen, M. Y. H.; Subbaraman, H.; Chen, R. T.; Berger, U.; Renn, M. *Appl. Phys. Lett.* **2008**, *93*, 243301.
(26) Zhou, C. F.; Kumar, S.; Doyle, C. D.; Tour, J. M. *Chem. Mater.* **2005**, *17*, 1997.
(27) Fukao, T.; Nakamura, S.; Kataura, H.; Shiraishi, M. *Jpn. J. Appl. Phys., Part 1* **2006**, *45*, 6524.
(28) Gulyaev, Y. V.; Sinitsyn, N. I.; Torgashov, G. V.; Mevlyut, S. T.; Zhbanov, A. I.; Zakharchenko, Y. F.; Kosakovskaya, Z. Y.; Chernozatonskii, L. A.; Glukhova, O. E.; Torgashov, I. G. *J. Vac. Sci. Technol., B* **1997**, *15*, 422.
(29) Cheah, J. W.; Shi, Y. M.; Ong, H. G.; Lee, C. W.; Li, L. J.; Wang, J. L. *Appl. Phys. Lett.* **2008**, *93*, 082103.

(30) Artukovic, E.; Kaempgen, M.; Hecht, D. S.; Roth, S.; Gruner, G. *Nano Lett.* **2005**, *5*, 757.
(31) Cao, Q.; Hur, S. H.; Zhu, Z. T.; Sun, Y. G.; Wang, C. J.; Meitl, M. A.; Shim, M.; Rogers, J. A. *Adv. Mater.* **2006**, *18*, 304.
(32) Unalan, H. E.; Fanchini, G.; Kanwal, A.; Du Pasquier, A.; Chhowalla, M. *Nano Lett.* **2006**, *6*, 677.
(33) Hecht, D.; Hu, L. B.; Gruner, G. *Appl. Phys. Lett.* **2006**, 89.
(34) Ham, H. T.; Choi, Y. S.; Jeong, N.; Chung, I. J. *Polymer* **2005**, *46*, 6308.
(35) Li, J.; Hu, L.; Wang, L.; Zhou, Y.; Gruner, G.; Marks, T. J. *Nano Lett.* **2006**, *6*, 2472.
(36) Takenobu, T.; Takahashi, T.; Kanbara, T.; Tsukagoshi, K.; Aoyagi, Y.; Iwasa, Y. *Appl. Phys. Lett.* **2006**, *88*, 033511.
(37) Behnam, A.; Noriega, L.; Choi, Y.; Wu, Z. C.; Rinzler, A. G.; Ural, A. *Appl. Phys. Lett.* **2006**, *89*, 093107.
(38) Zhang, D. H.; Ryu, K.; Liu, X. L.; Polikarpov, E.; Ly, J.; Tompson, M. E.; Zhou, C. W. *Nano Lett.* **2006**, *6*, 1880.
(39) Das, R. N.; Liu, B.; Reynolds, J. R.; Rinzler, A. G. *Nano Lett.* **2009**, *9*, 677.
(40) Lee, J. Y.; Liang, K.; An, K. H.; Lee, Y. H. *Synth. Met.* **2005**, *150*, 153.
(41) Ramesh, P.; Itkis, M. E.; Tang, J. M.; Haddon, R. C. *J. Phys. Chem. C* **2008**, *112*, 9089.
(42) Tang, J. M.; Jensen, K.; Waje, M.; Li, W.; Larsen, P.; Pauley, K.; Chen, Z.; Ramesh, P.; Itkis, M. E.; Yan, Y.; Haddon, R. C. *J. Phys. Chem. C* **2007**, *111*, 17901.
(43) Trancik, J. E.; Barton, S. C.; Hone, J. *Nano Lett.* **2008**, *8*, 982.
(44) Liu, D.; Fina, M.; Guo, J. H.; Chen, X. B.; Liu, G.; Johnson, S. G.; Mao, S. S. *Appl. Phys. Lett.* **2009**, *94*, 013110.
(45) Du, C. S.; Pan, N. *Nanotechnology* **2006**, *17*, 5314.
(46) Krstic, V.; Duesberg, G. S.; Muster, J.; Burghard, M.; Roth, S. *Chem. Mater.* **1998**, *10*, 2338.
(47) Maeda, Y.; Kimura, S.; Kanda, M.; Hirashima, Y.; Hasegawa, T.; Wakahara, T.; Lian, Y. F.; Nakahodo, T.; Tsuchiya, T.; Akasaka, T.; Lu, J.; Zhang, X. W.; Gao, Z. X.; Yu, Y. P.; Nagase, S.; Kazaoui, S.; Minami, N.; Shimizu, T.; Tokumoto, H.; Saito, R. *J. Am. Chem. Soc.* **2005**, *127*, 10287.
(48) Mukhopadhyay, I.; Touhara, H. *J. Solid State Electrochem.* **2008**, *12*, 715.
(49) Behnam, A.; Bosman, G.; Ural, A. *Phys. Rev. B* **2008**, *78*, 085431.
(50) Taberna, P. L.; Chevallier, G.; Simon, P.; Plee, D.; Aubert, T. *Mater. Res. Bull.* **2006**, *41*, 478.
(51) Fan, S. S.; Chapline, M. G.; Franklin, N. R.; Tombler, T. W.; Cassell, A. M.; Dai, H. J. *Science* **1999**, *283*, 512.
(52) An, K. H.; Kim, W. S.; Park, Y. S.; Moon, J. M.; Bae, D. J.; Lim, S. C.; Lee, Y. S.; Lee, Y. H. *Adv. Funct. Mater.* **2001**, *11*, 387.
(53) Chiang, I. W.; Brinson, B. E.; Smalley, R. E.; Margrave, J. L.; Hauge, R. H. *J. Phys. Chem. B* **2001**, *105*, 1157.
(54) Dillon, A. C.; Gennett, T.; Jones, K. M.; Alleman, J. L.; Parilla, P. A.; Heben, M. J. *Adv. Mater.* **1999**, *11*, 1354.
(55) Bozhko, A. D.; Sklovsky, D. E.; Nalimova, V. A.; Rinzler, A. G.; Smalley, R. E.; Fischer, J. E. *Appl. Phys. A: Mater. Sci. Process.* **1998**, *67*, 75.
(56) Shelimov, K. B.; Esenaliev, R. O.; Rinzler, A. G.; Huffman, C. B.; Smalley, R. E. *Chem. Phys. Lett.* **1998**, *282*, 429.
(57) Liu, P.; Sun, Q.; Zhu, F.; Liu, K.; Jiang, K.; Liu, L.; Li, Q.; Fan, S. *Nano Lett.* **2008**, *8*, 647.
(58) Javey, A.; Kim, H.; Brink, M.; Wang, Q.; Ural, A.; Guo, J.; McIntyre, P.; McEuen, P.; Lundstrom, M.; Dai, H. J. *Nat. Mater.* **2002**, *1*, 241.
(59) Deheer, W. A.; Chatelain, A.; Ugarte, D. *Science* **1995**, *270*, 1179.
(60) Choi, W. B.; Chung, D. S.; Kang, J. H.; Kim, H. Y.; Jin, Y. W.; Han, I. T.; Lee, Y. H.; Jung, J. E.; Lee, N. S.; Park, G. S.; Kim, J. M. *Appl. Phys. Lett.* **1999**, *75*, 3129.
(61) Nilsson, L.; Groening, O.; Emmenegger, C.; Kuettel, O.; Schaller, E.; Schlapbach, L.; Kind, H.; Bonard, J. M.; Kern, K. *Appl. Phys. Lett.* **2000**, *76*, 2071.
(62) Futaba, D. N.; Hata, K.; Yamada, T.; Hiraoka, T.; Hayamizu, Y.; Kakudate, Y.; Tanaike, O.; Hatori, H.; Yumura, M.; Iijima, S. *Nat. Mater.* **2006**, *5*, 987.
(63) Saini, P.; Choudhary, V.; Singh, B. P.; Mathur, R. B.; Dhawan, S. K. *Mater. Chem. Phys.* **2009**, *113*, 919.
(64) Xie, S. S.; Chang, B. H.; Li, W. Z.; Pan, Z. W.; Sun, L. F.; Mao, J. M.; Chen, X. H.; Qian, L. X.; Zhou, W. Y. *Adv. Mater.* **1999**, *11*, 1135.
(65) Liu, X. L.; Han, S.; Zhou, C. W. *Nano Lett.* **2006**, *6*, 34.
(66) Zhang, M.; Fang, S. L.; Zakhidov, A. A.; Lee, S. B.; Aliev, A. E.; Williams, C. D.; Atkinson, K. R.; Baughman, R. H. *Science* **2005**, *309*, 1215.
(67) Gruner, G. *J. Mater. Chem.* **2006**, *16*, 3533.
(68) Strano, M. S.; Dyke, C. A.; Usrey, M. L.; Barone, P. W.; Allen, M. J.; Shan, H. W.; Kittrell, C.; Hauge, R. H.; Tour, J. M.; Smalley, R. E. *Science* **2003**, *301*, 1519.
(69) Matarredona, O.; Rhoads, H.; Li, Z. R.; Harwell, J. H.; Balzano, L.; Resasco, D. E. *J. Phys. Chem. B* **2003**, *107*, 13357.
(70) Islam, M. F.; Rojas, E.; Bergey, D. M.; Johnson, A. T.; Yodh, A. G. *Nano Lett.* **2003**, *3*, 269.
(71) Gong, L. X.; Wei, C. M.; Hu, J. B.; Li, Q. L. *Chin. J. Anal. Chem.* **2008**, *36*, 1121.
(72) Bachilo, S. M.; Strano, M. S.; Kittrell, C.; Hauge, R. H.; Smalley, R. E.; Weisman, R. B. *Science* **2002**, *298*, 2361.
(73) Stahl, H.; Appenzeller, J.; Martel, R.; Avouris, P.; Lengeler, B. *Phys. Rev. Lett.* **2000**, *85*, 5186.
(74) Bergin, S. D.; Nicolosi, V.; Cathcart, H.; Lotya, M.; Rickard, D.; Sun, Z. Y.; Blau, W. J.; Coleman, J. N. *J. Phys. Chem. C* **2008**, *112*, 972.
(75) Strano, M. S.; Moore, V. C.; Miller, M. K.; Allen, M. J.; Haroz, E. H.; Kittrell, C.; Hauge, R. H.; Smalley, R. E. *J. Nanosci. Nanotechnol.* **2003**, *3*, 81.
(76) Bandyopadhyaya, R.; Nativ-Roth, E.; Regev, O.; Yerushalmi-Rozen, R. *Nano Lett.* **2002**, *2*, 25.
(77) Shin, J. Y.; Premkumar, T.; Geckeler, K. E. *Chem. A* **2008**, *14*, 6044.
(78) Eda, G.; Fanchini, G.; Kanwal, A.; Chhowalla, M. *J. Appl. Phys.* **2008**, *103*, 093118.
(79) White, B.; Banerjee, S.; O'Brien, S.; Turro, N. J.; Herman, I. P. *J. Phys. Chem. C* **2007**, *111*, 13684.
(80) Ishikawa, F. N.; Chang, H. K.; Ryu, K.; Chen, P. C.; Badmaev, A.; De Arco, L. G.; Shen, G. Z.; Zhou, C. W. *ACS Nano* **2009**, *3*, 73.
(81) O'Connell, M. J.; Bachilo, S. M.; Huffman, C. B.; Moore, V. C.; Strano, M. S.; Haroz, E. H.; Rialon, K. L.; Boul, P. J.; Noon, W. H.; Kittrell, C.; Ma, J. P.; Hauge, R. H.; Weisman, R. B.; Smalley, R. E. *Science* **2002**, *297*, 593.
(82) Chen, Z. H.; Du, X.; Du, M. H.; Rancken, C. D.; Cheng, H. P.; Rinzler, A. G. *Nano Lett.* **2003**, *3*, 1245.
(83) Furtado, C. A.; Kim, U. J.; Gutierrez, H. R.; Pan, L.; Dickey, E. C.; Eklund, P. C. *J. Am. Chem. Soc.* **2004**, *126*, 6095.
(84) Giordani, S.; Bergin, S.; Nicolosi, V.; Lebedkin, S.; Blau, W. J.; Coleman, J. N. *Phys. Status Solidi B* **2006**, *243*, 3058.
(85) Giordani, S.; Bergin, S. D.; Nicolosi, V.; Lebedkin, S.; Kappes, M. M.; Blau, W. J.; Coleman, J. N. *J. Phys. Chem. B* **2006**, *110*, 15708.
(86) Beecher, P.; Servati, P.; Rozhin, A.; Colli, A.; Scardaci, V.; Pisana, S.; Hasan, T.; Flewitt, A. J.; Robertson, J.; Hsieh, G. W.; Li, F. M.; Nathan, A.; Ferrari, A. C.; Milne, W. I. *J. Appl. Phys.* **2007**, 102.
(87) Bae, E. J.; Min, Y. S.; Kim, U. J.; Park, W. J. *Nanotechnology* **2007**, *18*, 495203.
(88) Lau, K. T.; Lu, M.; Lam, C. K.; Cheung, H. Y.; Sheng, F. L.; Li, H. L. *Compos. Sci. Technol.* **2005**, *65*, 719.
(89) Maeda, Y.; Kimura, S.; Hirashima, Y.; Kanda, M.; Lian, Y. F.; Wakahara, T.; Akasaka, T.; Hasegawa, T.; Tokumoto, H.; Shimizu, T.; Kataura, H.; Miyauchi, Y.; Maruyama, S.; Kobayashi, K.; Nagase, S. *J. Phys. Chem. B* **2004**, *108*, 18395.
(90) Liu, Z. F.; Shen, Z. Y.; Zhu, T.; Hou, S. F.; Ying, L. Z.; Shi, Z. J.; Gu, Z. N. *Langmuir* **2000**, *16*, 3569.
(91) Rahy, A.; Bajaj, P.; Musselman, I. H.; Hong, S. H.; Sun, Y. P.; Yang, D. J. *Appl. Surf. Sci.* **2009**, *255*, 7084.
(92) Wang, Q.; Wen, Z. H.; Li, J. H. *Adv. Funct. Mater.* **2006**, *16*, 2141.
(93) Bahr, J. L.; Mickelson, E. T.; Bronikowski, M. J.; Smalley, R. E.; Tour, J. M. *Chem. Commun.* **2001**, 193.
(94) Hwang, J. Y.; Nish, A.; Doig, J.; Douven, S.; Chen, C. W.; Chen, L. C.; Nicholas, R. J. *J. Am. Chem. Soc.* **2008**, *130*, 3543.
(95) Jung, Y. C.; Sahoo, N. G.; Cho, J. W. *Macromol. Rapid Commun.* **2006**, *27*, 126.
(96) Valentini, L.; Armentano, I.; Kenny, J. M.; Cantalini, C.; Lozzi, L.; Santucci, S. *Appl. Phys. Lett.* **2003**, *82*, 961.
(97) O'Connell, M. J.; Boul, P.; Ericson, L. M.; Huffman, C.; Wang, Y. H.; Haroz, E.; Kuper, C.; Tour, J.; Ausman, K. D.; Smalley, R. E. *Chem. Phys. Lett.* **2001**, *342*, 265.
(98) Satake, A.; Miyajima, Y.; Kobuke, Y. *Chem. Mater.* **2005**, *17*, 716.
(99) Kauffman, D. R.; Star, A. *Nano Lett.* **2007**, *7*, 1863.
(100) Steuerman, D. W.; Star, A.; Narizzano, R.; Choi, H.; Ries, R. S.; Nicolini, C.; Stoddart, J. F.; Heath, J. R. *J. Phys. Chem. B* **2002**, *106*, 3124.
(101) Yan, Y. H.; Chan-Park, M. B.; Zhang, Q. *Small* **2007**, *3*, 24.
(102) Fu, K. F.; Sun, Y. P. *J. Nanosci. Nanotechnol.* **2003**, *3*, 351.
(103) Star, A.; Stoddart, J. F.; Steuerman, D.; Diehl, M.; Boukai, A.; Wong, E. W.; Yang, X.; Chung, S. W.; Choi, H.; Heath, J. R. *Angew. Chem., Int. Ed.* **2001**, *40*, 1721.
(104) Nish, A.; Hwang, J. Y.; Doig, J.; Nicholas, R. J. *Nat. Nanotechnol.* **2007**, *2*, 640.
(105) Landi, B. J.; Raffaelle, R. P.; Heben, M. J.; Alleman, J. L.; VanDerveer, W.; Gennett, T. *Nano Lett.* **2002**, *2*, 1329.
(106) Trottier, C. M.; Glatkowski, P.; Wallis, P.; Luo, J. *J. Soc. Inf. Disp.* **2005**, *13*, 759.
(107) Tsai, Y. C.; Li, S. C.; Chen, J. M. *Langmuir* **2005**, *21*, 3653.

(108) Zheng, M.; Jagota, A.; Semke, E. D.; Diner, B. A.; McLean, R. S.; Lustig, S. R.; Richardson, R. E.; Tassi, N. G. *Nat. Mater.* **2003**, *2*, 338.
(109) Cohen, E.; Gutoff, E. *Modern Coating and Drying Technology*; VCH Publishers: New York, 1992.
(110) Tracton, A. A. *Coatings Technology Handbook*; C.H.I.P.S.: New York, 2005.
(111) Eley, R. R.; Schwartz, L. W. *J. Coat. Technol.* **2002**, *74*, 43.
(112) Gunther, L.; Peukert, W. *Colloids Surf., A* **2003**, *225*, 49.
(113) Nisogi, H.; Bousfield, D. W.; Lepoutre, P. F. *Tappi J.* **2000**, *83*, 100.
(114) Washo, B. D. *IBM J. Res. Dev.* **1977**, *21*, 190.
(115) Willenbacher, N.; Hanciogullari, H.; Wagner, H. G. *Chem. Eng. Technol.* **1997**, *20*, 557.
(116) Hobbie, E. K.; Fry, D. J. *J. Chem. Phys.* **2007**, *126*, 124907.
(117) Kinloch, I. A.; Roberts, S. A.; Windle, A. H. *Polymer* **2002**, *43*, 7483.
(118) Lin-Gibson, S.; Pathak, J. A.; Grulke, E. A.; Wang, H.; Hobbie, E. K. *Phys. Rev. Lett.* **2004**, 92.
(119) Dan, B.; Irvin, G. C.; Pasquali, M. *ACS Nano* **2009**, *3*, 835.
(120) Saiyard, A. H. B., A. G.; Rakshit, A. K. *Colloid Polym. Sci.* **1998**, *276*, 913.
(121) Lin, Z. G., J. J.; Scriven, L. E.; Davis, H. T. *J. Phys. Chem.* **1994**, *98*, 5984.
(122) Raghavan, S. R. F., G.; Kaler, E. W. *Langmuir* **2002**, *18*, 3797.
(123) Lim, S. C.; Jeong, H. J.; Kim, K. S.; Lee, I. B.; Bae, D. J.; Lee, Y. H. *Carbon* **2005**, *43*, 2801.
(124) Yang, P. D. *Nature* **2003**, *425*, 243.
(125) Kim, Y.; Minami, N.; Zhu, W. H.; Kazaoui, S.; Azumi, R.; Matsumoto, M. *Jpn. J. Appl. Phys., Part 1* **2003**, *42*, 7629.
(126) Armitage, N. P.; Gabriel, J. C. P.; Gruner, G. *J. Appl. Phys.* **2004**, *95*, 3228.
(127) Li, W.; Wang, X.; Chen, Z.; Waje, M.; Yan, Y. *Langmuir* **2005**, *21*, 9386.
(128) Liu, K.; Roth, S.; Duesberg, G.; Wagenhals, M.; Journet, C.; Bernier, P. *Synth. Met.* **1999**, *103*, 2513.
(129) Hazani, M.; Hennrich, F.; Kappes, M.; Naaman, R.; Peled, D.; Sidorov, V.; Shvarts, D. *Chem. Phys. Lett.* **2004**, *391*, 389.
(130) Liang, F.; Sadana, A. K.; Peera, A.; Chattopadhyay, J.; Gu, Z. N.; Hauge, R. H.; Billups, W. E. *Nano Lett.* **2004**, *4*, 1257.
(131) Long, D. P.; Lazorcik, J. L.; Shashidhar, R. *Adv. Mater.* **2004**, *16*, 814.
(132) Mamedov, A. A.; Kotov, N. A.; Prato, M.; Guldi, D. M.; Wicksted, J. P.; Hirsch, A. *Nat. Mater.* **2002**, *1*, 190.
(133) Rao, S. G.; Huang, L.; Setyawan, W.; Hong, S. H. *Nature* **2003**, *425*, 36.
(134) Seemann, L.; Stemmer, A.; Naujoks, N. *Nano Lett.* **2007**, *7*, 3007.
(135) Shimoda, H.; Fleming, L.; Horton, K.; Zhou, O. *Physica B* **2002**, *323*, 135.
(136) Vijayaraghavan, A.; Blatt, S.; Weissenberger, D.; Oron-Carl, M.; Hennrich, F.; Gerthsen, D.; Hahn, H.; Krupke, R. *Nano Lett.* **2007**, *7*, 1556.
(137) Xue, W.; Cui, T. H. *Nanotechnology* **2007**, *18*, 145709.
(138) Saran, N.; Parikh, K.; Suh, D. S.; Munoz, E.; Kolla, H.; Manohar, S. K. *J. Am. Chem. Soc.* **2004**, *126*, 4462.
(139) LeMieux, M. C.; Roberts, M.; Barman, S.; Jin, Y. W.; Kim, J. M.; Bao, Z. N. *Science* **2008**, *321*, 101.
(140) Seo, M. A.; Yim, J. H.; Ahn, Y. H.; Rotermund, F.; Kim, D. S.; Lee, S.; Lim, H. *Appl. Phys. Lett.* **2008**, *93*, 231905.
(141) Lay, M. D.; Novak, J. P.; Snow, E. S. *Nano Lett.* **2004**, *4*, 603.
(142) Sharma, R.; Lee, C. Y.; Choi, J. H.; Chen, K.; Strano, M. S. *Nano Lett.* **2007**, *7*, 2693.
(143) Degennes, P. G. *Rev. Mod. Phys.* **1985**, *57*, 827.
(144) Kamat, P. V.; Thomas, K. G.; Barazzouk, S.; Girishkumar, G.; Vinodgopal, K.; Meisel, D. *J. Am. Chem. Soc.* **2004**, *126*, 10757.
(145) Lima, M. D.; de Andrade, M. J.; Bergmann, C. P.; Roth, S. *J. Mater. Chem.* **2008**, *18*, 776.
(146) Krupke, R.; Linden, S.; Rapp, M.; Hennrich, F. *Adv. Mater.* **2006**, *18*, 1468.
(147) Hsieh, Y. P.; Hofmann, M.; Son, H. B.; Jia, X. T.; Chen, Y. F.; Liang, C. T.; Dresselhaus, M. S.; Kong, J. *Nanotechnology* **2009**, *20*, 065601.
(148) Kwon, J. H.; Lee, K. S.; Lee, Y. H.; Ju, B. K. *Electrochem. Solid-State Lett.* **2006**, *9*, 85.
(149) Ulbricht, R.; Lee, S. B.; Jiang, X. M.; Inoue, K.; Zhang, M.; Fang, S. L.; Baughman, R. H.; Zakhidov, A. A. *Sol. Energy Mater. Sol. Cells* **2007**, *91*, 416.
(150) Ramasamy, E.; Lee, W. J.; Lee, D. Y.; Song, J. S. *Electrochem. Commun.* **2008**, *10*, 1087.
(151) Schindler, A.; Brill, J.; Fruehauf, N.; Novak, J. P.; Yaniv, Z. *Physica E* **2007**, *37*, 119.
(152) Zhao, X.; Chu, B. T. T.; Ballesteros, B.; Wang, W. L.; Johnston, C.; Sykes, J. M.; Grant, P. S. *Nanotechnology* **2009**, *20*, 065605.
(153) Kaempgen, M.; Duesberg, G. S.; Roth, S. *Appl. Surf. Sci.* **2005**, *252*, 425.
(154) Hu, L. B.; Gruner, G.; Gong, J.; Kim, C. J.; Hornbostel, B. *Appl. Phys. Lett.* **2007**, *90*, 093124.
(155) Hu, L. G., G.; Jenkins, J.; Kim, C. J. *J. Mater. Chem.* **2009**, *19*, 5845.
(156) Niu, C. M.; Sichel, E. K.; Hoch, R.; Moy, D.; Tennent, H. *Appl. Phys. Lett.* **1997**, *70*, 1480.
(157) Lawrence, R. C., A.; Dabasis, M. U.S. Patent Application no. 20061088723, 2006.
(158) Wei, J. Q.; Jia, Y.; Shu, Q. K.; Gu, Z. Y.; Wang, K. L.; Zhuang, D. M.; Zhang, G.; Wang, Z. C.; Luo, J. B.; Cao, A. Y.; Wu, D. H. *Nano Lett.* **2007**, *7*, 2317.
(159) Kordas, K.; Mustonen, T.; Toth, G.; Jantunen, H.; Lajunen, M.; Soldano, C.; Talapatra, S.; Kar, S.; Vajtai, R.; Ajayan, P. M. *Small* **2006**, *2*, 1021.
(160) Mustonen, T.; Kordas, K.; Saukko, S.; Toth, G.; Penttilla, J. S.; Helisto, P.; Seppa, H.; Jantunen, H. *Phys. Status Solidi B* **2007**, *244*, 4336.
(161) Mustonen, T.; Maklin, J.; Kordas, K.; Halonen, N.; Toth, G.; Saukko, S.; Vahakangas, J.; Jantunen, H.; Kar, S.; Ajayan, P. M.; Vajtai, R.; Helisto, P.; Seppa, H.; Moilanen, H. *Phys. Rev. B* **2008**, 77.
(162) Panhuis, M. I. H.; Heurtematte, A.; Small, W. R.; Paunov, V. N. *Soft Matter* **2007**, *3*, 840.
(163) Sainz, R.; Small, W. R.; Young, N. A.; Valles, C.; Benito, A. M.; Maser, W. K.; Panhuis, M. I. H. *Macromolecules* **2006**, *39*, 7324.
(164) Liu, J.; Casavant, M. J.; Cox, M.; Walters, D. A.; Boul, P.; Lu, W.; Rimberg, A. J.; Smith, K. A.; Colbert, D. T.; Smalley, R. E. *Chem. Phys. Lett.* **1999**, *303*, 125.
(165) Cai, D. Y.; Song, M.; Xu, C. X. *Adv. Mater.* **2008**, *20*, 1706.
(166) Song, J. W.; Kim, J.; Yoon, Y. H.; Choi, B. S.; Kim, J. H.; Han, C. S. *Nanotechnology* **2008**, 19.
(167) Hines, D. R.; Mezhenny, S.; Breban, M.; Williams, E. D.; Ballarotto, V. W.; Esen, G.; Southard, A.; Fuhrer, M. S. *Appl. Phys. Lett.* **2005**, *86*, 163101.
(168) Hur, S. H.; Khang, D. Y.; Kocabas, C.; Rogers, J. A. *Appl. Phys. Lett.* **2004**, *85*, 5730.
(169) Menard, E.; Meitl, M. A.; Sun, Y. G.; Park, J. U.; Shir, D. J. L.; Nam, Y. S.; Jeon, S.; Rogers, J. A. *Chem. Rev.* **2007**, *107*, 1117.
(170) Xu, H.; Zhang, S. X.; Anlage, S. M.; Hu, L. B.; Gruner, G. *Phys. Rev. B* **2008**, 77.
(171) Zhou, Y. X.; Gaur, A.; Hur, S. H.; Kocabas, C.; Meitl, M. A.; Shim, M.; Rogers, J. A. *Nano Lett.* **2004**, *4*, 2031.
(172) Fanchini, G.; Unalan, H. E.; Chhowalla, M. *Appl. Phys. Lett.* **2006**, *88*, 191919.
(173) Zhou, Y. X.; Hu, L. B.; Gruner, G. *Appl. Phys. Lett.* **2006**, *88*, 123109.
(174) Allen, A. C.; Sunden, E.; Cannon, A.; Graham, S.; King, W. *Appl. Phys. Lett.* **2006**, *88*, 083112.
(175) Chang-Jian, S. K.; Ho, J. R.; Cheng, J. W. J.; Sung, C. K. *Nanotechnology* **2006**, *17*, 1184.
(176) Sunden, E.; Moon, J. K.; Wong, C. P.; King, W. P.; Graham, S. *J. Vac. Sci. Technol., B* **2006**, *24*, 1947.
(177) Irvin, G. M., D.; Anderson, C.; Rowley, L. U.S. Patent Application no. 0188721, 2006.
(178) An, K. H.; Kim, W. S.; Park, Y. S.; Choi, Y. C.; Lee, S. M.; Chung, D. C.; Bae, D. J.; Lim, S. C.; Lee, Y. H. *Adv. Mater.* **2001**, *13*, 497.
(179) Peng, H. R., T.; Schurmann, G.; King, G.; Yoon, J.; Narayanamuti, V.; Golovchenko, J. *Appl. Phys. Lett.* **2003**, *83*, 4238.
(180) Xu, X. P.; Brandes, G. R. *Appl. Phys. Lett.* **1999**, *74*, 2549.
(181) Ago, H.; Murata, K.; Yumura, M.; Yotani, J.; Uemura, S. *Appl. Phys. Lett.* **2003**, *82*, 811.
(182) Kind, H.; Bonard, J. M.; Emmenegger, C.; Nilsson, L. O.; Hernadi, K.; Maillard-Schaller, E.; Schlapbach, L.; Forro, L.; Kern, K. *Adv. Mater.* **1999**, *11*, 1285.
(183) Lim, C. H.; Min, D. H.; Lee, S. B. *Appl. Phys. Lett.* **2007**, *91*, 243117.
(184) Kumar, S.; Pimparkar, N.; Murthy, J. Y.; Alam, M. A. *Appl. Phys. Lett.* **2006**, *88*, 123505.
(185) Cao, Q.; Rogers, J. A. *Adv. Mater.* **2009**, *21*, 29.
(186) Cao, Q.; Kim, H. S.; Pimparkar, N.; Kulkarni, J. P.; Wang, C. J.; Shim, M.; Roy, K.; Alam, M. A.; Rogers, J. A. *Nature* **2008**, *454*, 495.
(187) Castro, M. R. S.; Lasagni, A. F.; Schmidt, H. K.; Mucklich, F. *Appl. Surf. Sci.* **2008**, *254*, 5874.
(188) Chae, J. H.; Ho, X. N.; Rogers, J. A.; Jain, K. *Appl. Phys. Lett.* **2008**, 92.
(189) Behnam, A.; Choi, Y.; Noriega, L.; Wu, Z. C.; Kravchenko, I.; Rinzler, A. G.; Ural, A. *J. Vac. Sci. Technol.* **2007**, *25*, 348.
(190) Vaillancourt, J.; Lu, X.; Han, X.; Janzen, D. C. *Electron. Lett.* **2006**, *42*, 1365.
(191) Blanchet, G. B.; Loo, Y. L.; Rogers, J. A.; Gao, F.; Fincher, C. R. *Appl. Phys. Lett.* **2003**, *82*, 463.
(192) Arthur, D. G., P. U.S. Patent Application, 2006.
(193) Park, J. U.; Meitl, M. A.; Hur, S. H.; Usrey, M. L.; Strano, M. S.; Kenis, P. J. A.; Rogers, J. A. *Angew. Chem., Int. Ed.* **2006**, *45*, 581.

(194) Jung, M. S.; Jung, S. O.; Jung, D. H.; Ko, Y. K.; Jin, Y. W.; Kim, J.; Jung, H. T. *J. Phys. Chem. B* **2005**, *109*, 10584.
(195) Hu, L. P., Y.; Hecht, D.; Ladous, C.; O'Connell, M.; Thomas, D.; Gruner, G.; Irvin, G.; Drzaic, P. *MRS. Proc.* **2009**, 1109-B10−07.
(196) Gandhi, S. U.S. Patent Application US2008128397.
(197) Ou, E.; Hu, L.; Raymond, G.; Soo, O.; Pan, J.; Zheng, Z.; Park, Y.; Hecht, D.; Irvin, G.; Drzaic, P.; Gruner, G. *ACS Nano* **2009**, *3*, 2258.
(198) Takai, M.; Bollmann, D.; Haberger, K. *Appl. Phys. Lett.* **1994**, *64*, 2560.
(199) Yavas, O.; Takai, M. *J. Appl. Phys.* **1999**, *85*, 4207.
(200) Tracton, A. A. *Coatings Technology: Fundamentals, Testing, and Processing Techniques*; CRC Press, Taylor & Francis Group: Boca Raton, FL, 2007.
(201) Banerjee, S.; Hemraj-Benny, T.; Wong, S. S. *Adv. Mater.* **2005**, *17*, 17.
(202) Zhao, J. J.; Xie, R. H. *J. Nanosci. Nanotechnol.* **2003**, *3*, 459.
(203) Jhi, S. H.; Louie, S. G.; Cohen, M. L. *Phys. Rev. Lett.* **2000**, *85*, 1710.
(204) Geng, H. Z.; Kim, K. K.; So, K. P.; Lee, Y. S.; Chang, Y.; Lee, Y. H. *J. Am. Chem. Soc.* **2007**, *129*, 7758.
(205) Fischer, J. E.; Dai, H.; Thess, A.; Lee, R.; Hanjani, N. M.; Dehaas, D. L.; Smalley, R. E. *Phys. Rev. B* **1997**, *55*, 4921.
(206) Tselev, A.; Woodson, M.; Qian, C.; Liu, J. *Nano Lett.* **2008**, *8*, 152.
(207) Tombler, T. W.; Zhou, C. W.; Alexseyev, L.; Kong, J.; Dai, H. J.; Lei, L.; Jayanthi, C. S.; Tang, M. J.; Wu, S. Y. *Nature* **2000**, *405*, 769.
(208) Ruzicka, B.; Degiorgi, L.; Gaal, R.; Thien-Nga, L.; Bacsa, R.; Salvetat, J. P.; Forro, L. *Phys. Rev. B* **2000**, *61*, 2468.
(209) Kazaoui, S.; Minami, N.; Jacquemin, R.; Kataura, H.; Achiba, Y. *Phys. Rev. B* **1999**, *60*, 13339.
(210) Kazaoui, S.; Minami, N.; Matsuda, N.; Kataura, H.; Achiba, Y. *Appl. Phys. Lett.* **2001**, *78*, 3433.
(211) Rao, A. M.; Eklund, P. C.; Bandow, S.; Thess, A.; Smalley, R. E. *Nature* **1997**, *388*, 257.
(212) Takenobu, T.; Kanbara, T.; Akima, N.; Takahashi, T.; Shiraishi, M.; Tsukagoshi, K.; Kataura, H.; Aoyagi, Y.; Iwasa, Y. *Adv. Mater.* **2005**, *17*, 2430.
(213) Ulbricht, H.; Moos, G.; Hertel, T. *Phys. Rev. B* **2002**, *66*, 075404.
(214) Jackson, R.; Graham, S. *Appl. Phys. Lett.* **2009**, *94*, 012109.
(215) Moon, J. S.; Park, J. H.; Lee, T. Y.; Kim, Y. W.; Yoo, J. B.; Park, C. Y.; Kim, J. M.; Jin, K. W. *Diamond Relat. Mater.* **2005**, *14*, 1882.
(216) Pan, J. Y.; Zhu, C. C.; Gao, Y. L. *Appl. Surf. Sci.* **2008**, *254*, 3787.
(217) Rowell, M. W.; Topinka, M. A.; McGehee, M. D.; Prall, H. J.; Dennler, G.; Sariciftci, N. S.; Hu, L. B.; Gruner, G. *Appl. Phys. Lett.* **2006**, 88.
(218) Li, J. F.; Hu, L. B.; Liu, J.; Wang, L.; Marks, T. J.; Gruner, G. *Appl. Phys. Lett.* **2008**, *93*, 083306.
(219) Chiba, K.; Futagami, A. *Appl. Phys. Lett.* **2008**, *93*, 013114.
(220) Marsh, D. H.; Rance, G. A.; Whitby, R. J.; Giustiniano, F.; Khlobystov, A. N. *J. Mater. Chem.* **2008**, *18*, 2249.
(221) Unger, E.; Duesberg, G. S.; Liebau, M.; Graham, A. P.; Seidel, R.; Kreupl, F.; Hoenlein, W. *Appl. Phys. A: Mater. Sci. Process.* **2003**, *77*, 735.
(222) Hu, L.; Zhao, Y. L.; Ryu, K.; Zhou, C.; Stoddart, J. F.; Gruner, G. *Adv. Mater.* **2008**, *20*, 939.
(223) Kong, B. S.; Jung, D. H.; Oh, S. K.; Han, C. S.; Jung, H. T. *J. Phys. Chem. C* **2007**, *111*, 8377.
(224) D'Yachkov, P. N.; Hermann, H. *J. Appl. Phys.* **2004**, *95*, 399.
(225) McEuen, P. L.; Fuhrer, M. S.; Park, H. K. *IeEEE Trans. Nanotechnol.* **2002**, *1*, 78.
(226) Wildoer, J. W. G.; Venema, L. C.; Rinzler, A. G.; Smalley, R. E.; Dekker, C. *Nature* **1998**, *391*, 59.
(227) Saito, S. D. D., M. S. *Physics Properties of Carbon Nanotubes*; Imperial College Press: London, 1998.
(228) Nosho, Y.; Ohno, Y.; Kishimoto, S.; Mizutani, T. *Nanotechnology* **2007**, *18*, 415202.
(229) Matsuda, Y.; Deng, W. Q.; Goddard, W. A. *J. Phys. Chem. C* **2007**, *111*, 11113.
(230) Bachtold, A.; Henny, M.; Terrier, C.; Strunk, C.; Schonenberger, C.; Salvetat, J. P.; Bonard, J. M.; Forro, L. *Appl. Phys. Lett.* **1998**, *73*, 274.
(231) Lan, C.; Zakharov, D. N.; Reifenberger, R. G. *Appl. Phys. Lett.* **2008**, *92*, 213112.
(232) Jackson, R.; Graham, S. *Appl. Phys. Lett.* **2009**, *94*, 012109.
(233) Woo, Y.; Duesberg, G. S.; Roth, S. *Nanotechnology* **2007**, *18*, 095203.
(234) Kay Hyeok, A.; Won Seok, K.; Young Soo, P.; Jeong-Mi, M.; Dong Jae, B.; Seong Chu, L.; Young Seak, L.; Young Hee, L. *Adv. Funct. Mater.* **2001**, *11*, 387.
(235) Nosho, Y.; Ohno, Y.; Kishimoto, S.; Mizutani, T. *Nanotechnology* **2006**, *17*, 3412.
(236) Nosho, Y.; Ohno, Y.; Kishimoto, S.; Mizutani, T. *Appl. Phys. Lett.* **2005**, *86*, 073105.
(237) Leonard, F.; Tersoff, J. *Phys. Rev. Lett.* **2000**, *84*, 4693.
(238) Xu, Z.; Bai, X. D.; Wang, E. G.; Wang, Z. L. *Appl. Phys. Lett.* **2005**, *87*, 163106.
(239) Shiraishi, M.; Ata, M. *Carbon* **2001**, *39*, 1913.
(240) Gao, R. P.; Pan, Z. W.; Wang, Z. L. *Appl. Phys. Lett.* **2001**, *78*, 1757.
(241) Suzuki, S.; Bower, C.; Watanabe, Y.; Zhou, O. *Appl. Phys. Lett.* **2000**, *76*, 4007.
(242) Su, W. S.; Leung, T. C.; Li, B.; Chan, C. T. *Appl. Phys. Lett.* **2007**, *90*, 163103.
(243) Zhao, J. J.; Han, J.; Lu, J. P. *Phys. Rev. B* **2002**, *65*, 193401.
(244) Ago, H.; Kugler, T.; Cacialli, F.; Salaneck, W. R.; Shaffer, M. S. P.; Windle, A. H.; Friend, R. H. *J. Phys. Chem. B* **1999**, *103*, 8116.
(245) Baumgartner, G.; Carrard, M.; Zuppiroli, L.; Bacsa, W.; deHeer, W. A.; Forro, L. *Phys. Rev. B* **1997**, *55*, 6704.
(246) Salvato, M.; Cirillo, M.; Lucci, M.; Orlanducci, S.; Ottaviani, I.; Terranova, M. L.; Toschi, F. *Phys. Rev. Lett.* **2008**, *101*, 246804.
(247) Kwon, Y. K.; Saito, S.; Tomanek, D. *Phys. Rev. B* **1998**, *58*, 13314.
(248) Li, S. D.; Yu, Z.; Rutherglen, C.; Burke, P. J. *Nano Lett.* **2004**, *4*, 2003.
(249) McEuen, P. L.; Park, J. Y. *Mater. Res. Bull.* **2004**, *29*, 272.
(250) Sundqvist, P.; Garcia-Vidal, F. J.; Flores, F.; Moreno-Moreno, M.; Gomez-Navarro, C.; Bunch, J. S.; Gomez-Herrero, J. *Nano Lett.* **2007**, *7*, 2568.
(251) Yao, Z.; Postma, H. W. C.; Balents, L.; Dekker, C. *Nature* **1999**, *402*, 273.
(252) Farajian, A. A.; Esfarjani, K.; Kawazoe, Y. *Phys. Rev. Lett.* **1999**, *82*, 5084.
(253) Stadermann, M.; Papadakis, S. J.; Falvo, M. R.; Novak, J.; Snow, E.; Fu, Q.; Liu, J.; Fridman, Y.; Boland, J. J.; Superfine, R.; Washburn, S. *Phys. Rev. B* **2004**, *69*, 201402.
(254) Martin, C. A.; Sandler, J. K. W.; Shaffer, M. S. P.; Schwarz, M. K.; Bauhofer, W.; Schulte, K.; Windle, A. H. *Compos. Sci. Technol.* **2004**, *64*, 2309.
(255) Grunlan, J. C.; Mehrabi, A. R.; Bannon, M. V.; Bahr, J. L. *Adv. Mater.* **2004**, *16*, 150.
(256) Sandler, J. K. W.; Kirk, J. E.; Kinloch, I. A.; Shaffer, M. S. P.; Windle, A. H. *Polymer* **2003**, *44*, 5893.
(257) Kymakis, E.; Alexandou, I.; Amaratunga, G. A. J. *Synth. Met.* **2002**, *127*, 59.
(258) Flahaut, E.; Peigney, A.; Laurent, C.; Marliere, C.; Chastel, F.; Rousset, A. *Acta Mater.* **2000**, *48*, 3803.
(259) Hu, L.; Hecht, D. S.; Gruner, G. *Nano Lett.* **2004**, *4*, 2513.
(260) Pike, G. E.; Seager, C. H. *Phys. Rev. B* **1974**, *10*, 1421.
(261) Kirkpatr, S. *Rev. Mod. Phys.* **1973**, *45*, 574.
(262) Simien, D.; Fagan, J. A.; Luo, W.; Douglas, J. F.; Migler, K.; Obrzut, J. *ACS Nano* **2008**, *2*, 1879.
(263) Du, F. M.; Fischer, J. E.; Winey, K. I. *Phys. Rev. B* **2005**, 72.
(264) Hecht, D. S.; Ramirez, R. J. A.; Briman, M.; Artukovic, E.; Chichak, K. S.; Stoddart, J. F.; Gruner, G. *Nano Lett.* **2006**, *6*, 2031.
(265) Venkateswaran, U. D.; Rao, A. M.; Richter, E.; Menon, M.; Rinzler, A.; Smalley, R. E.; Eklund, P. C. *Phys. Rev. B* **1999**, *59*, 10928.
(266) Skakalova, V. K., A. B.; Woo, Y. S.; Roth, S. *Phys. Rev. B* **2006**, *74*, 085403.
(267) Kaiser, A. B. *Rep. Prog. Phys.* **2001**, *64*, 1.
(268) Kaiser, A. B.; Dusberg, G.; Roth, S. *Phys. Rev. B* **1998**, *57*, 1418.
(269) Itkis, M. E.; Borondics, F.; Yu, A. P.; Haddon, R. C. *Science* **2006**, *312*, 413.
(270) Zhang, H. L.; Li, J. F.; Zhang, B. P.; Yao, K. F.; Liu, W. S.; Wang, H. *Phys. Rev. B* **2007**, 75.
(271) Dyre, J. C.; Schroder, T. B. *Rev. Mod. Phys.* **2000**, *72*, 873.
(272) Yu, Z.; Rutherglen, C.; Burke, R. J. *Appl. Phys. Lett.* **2006**, 88.
(273) Rosenblatt, S.; Yaish, Y.; Park, J.; Gore, J.; Sazonova, V.; McEuen, P. L. *Nano Lett.* **2002**, *2*, 869.
(274) Pesetski, A. A.; Baumgardner, J. E.; Folk, E.; Przybysz, J. X.; Adam, J. D.; Zhang, H. *Appl. Phys. Lett.* **2006**, 88.
(275) Li, S. D.; Yu, Z.; Yen, S. F.; Tang, W. C.; Burke, P. J. *Nano Lett.* **2004**, *4*, 753.
(276) Hu, L. B.; Hecht, D. S.; Gruner, G. *Appl. Phys. Lett.* **2009**, *94*, 081103.
(277) Kilbride, B. E.; Coleman, J. N.; Fraysse, J.; Fournet, P.; Cadek, M.; Drury, A.; Hutzler, S.; Roth, S.; Blau, W. J. *J. Appl. Phys.* **2002**, *92*, 4024.
(278) Jeon, T. I.; Kim, K. J.; Kang, C.; Maeng, I. H.; Son, J. H.; An, K. H.; Lee, J. Y.; Lee, Y. H. *J. Appl. Phys.* **2004**, *95*, 5736.
(279) Ugawa, A.; Rinzler, A. G.; Tanner, D. B. *Ferroelectrics* **2001**, *249*, 145.
(280) Xu, H.; Anlage, S. M.; Hu, L. B.; Gruner, G. *Appl. Phys. Lett.* **2007**, *90*, 183119.
(281) McLachlan, D. S.; Chiteme, C.; Park, C.; Wise, K. E.; Lowther, S. E.; Lillehei, P. T.; Siochi, E. J.; Harrison, J. S. *J. Polym. Sci., Part B: Polym. Phys.* **2005**, *43*, 3273.

(282) Kaiser, A. B.; Challis, K. J.; McIntosh, G. C.; Kim, G. T.; Yu, H. Y.; Park, J. G.; Jhang, S. H.; Park, Y. W. *Curr. Appl Phys.* **2002**, *2*, 163.
(283) Fuhrer, M. S.; Holmes, W.; Richards, P. L.; Delaney, P.; Louie, S. G.; Zettl, A. *Synth. Met.* **1999**, *103*, 2529.
(284) Parikh, K.; Cattanach, K.; Rao, R.; Suh, D. S.; Wu, A. M.; Manohar, S. K. *Sensors Actuators, B* **2006**, *113*, 55.
(285) Yang, Y.; Wang, L.; Yan, H.; Jin, S.; Marks, T. J.; Li, S. Y. *Appl. Phys. Lett.* **2006**, *89*, 051116.
(286) Barnes, T. M.; Van de Lagemaat, J.; Levi, D.; Rumbles, G.; Coutts, T. J.; Weeks, C. L.; Britz, D. A.; Levitsky, I.; Peltola, J.; Glatkowski, P. *Phys. Rev. B* **2007**, *75*, 235410.
(287) Nishimura, H.; Minami, N.; Shimano, R. *Appl. Phys. Lett.* **2007**, *91*, 011108.
(288) Kamaras, K.; Rinzler, A. G.; Tanner, D. B.; Walters, D. A. *Phys. Status Solidi B* **2006**, *243*, 3126.
(289) Fanchini, G.; Miller, S.; Parekh, L. B.; Chhowalla, M. *Nano Lett.* **2008**, *8*, 2176.
(290) Kang, M. G.; Kim, M. S.; Kim, J. S.; Guo, L. J. *Adv. Mater.* **2008**, *20*, 4624.
(291) Lee, J. Y.; Connor, S. T.; Cui, Y.; Peumans, P. *Nano Lett.* **2008**, *8*, 689.
(292) Taft, E. A.; Philipp, H. R. *Phys. Rev.* **1965**, *138*, A197.
(293) Yakobson, B. I.; Brabec, C. J.; Bernholc, J. *Phys. Rev. Lett.* **1996**, *76*, 2511.
(294) Iijima, S.; Brabec, C.; Maiti, A.; Bernholc, J. *J. Chem. Phys.* **1996**, *104*, 2089.
(295) Nardelli, M. B.; Fattebert, J. L.; Orlikowski, D.; Roland, C.; Zhao, Q.; Bernholc, J. *Carbon* **2000**, *38*, 1703.
(296) Avouris, P.; Hertel, T.; Martel, R.; Schmidt, T.; Shea, H. R.; Walkup, R. E. *Appl. Surf. Sci.* **1999**, *141*, 201.
(297) Hertel, T.; Walkup, R. E.; Avouris, P. *Phys. Rev. B* **1998**, *58*, 13870.
(298) Sreekumar, T. V.; Liu, T.; Kumar, S.; Ericson, L. M.; Hauge, R. H.; Smalley, R. E. *Chem. Mater.* **2003**, *15*, 175.
(299) Hecht, S.; Thomas, D.; Hu, L.; C., L.; Irvin, G.; P., D. *Inf. Disp.* **2009**, *17*, 941.
(300) Hu, L. B.; Yuan, W.; Brochu, P.; Gruner, G.; Pei, Q. B. *Appl. Phys. Lett.* **2009**, *94*, 161108.
(301) Ou, E. H., L.; Raymond, G.; Soo, O.; Pan, J.; Zheng, Z.; Park, Y.; Hecht, D.; Irvin, G.; Drzaic, P.; Gruner, G. *ACS Nano* **2009**, *3*, 2258.
(302) Zhang, X. W. *Adv. Mater.* **2008**, *20*, 4140.
(303) Chen, C. L.; Lopez, E.; Jung, Y. J.; Muftu, S.; Selvarasah, S.; Dokmeci, M. R. *Appl. Phys. Lett.* **2008**, 93.
(304) Li, J.; Lu, Y. J.; Ye, Q.; Cinke, M.; Han, J.; Meyyappan, M. *Nano Lett.* **2003**, *3*, 929.
(305) Snow, E. S.; Perkins, F. K. *Nano Lett.* **2005**, *5*, 2414.
(306) Fu, Q.; Liu, J. *Langmuir* **2005**, *21*, 1162.
(307) Gordon, R. G. *Mater. Res. Bull.* **2000**, *25*, 52.
(308) Stupp, S.; Messsmore, G.; Arnold, M.; Zubarev, E. U.S. Patent 6890654, 2005.
(309) Pandolfo, A. G.; Hollenkamp, A. F. *J. Power Sources* **2006**, *157*, 11.
(310) Morgan, C.; Alemipour, Z.; Baxendale, M. *Physica Status Solidi A* **2008**, *205*, 1394.
(311) Engel, M.; Small, J. P.; Steiner, M.; Freitag, M.; Green, A. A.; Hersam, M. C.; Avouris, P. *ACS Nano* **2008**, *2*, 2445.
(312) Lee, C. W.; Weng, C. H.; Wei, L.; Chen, Y.; Chan-Park, M. B.; Tsai, C. H.; Leou, K. C.; Poa, C. H. P.; Wang, J. L.; Li, L. J. *J. Phys. Chem. C* **2008**, *112*, 12089.
(313) Tsukagoshi, K.; Sekiguchi, M.; Ayagi, Y.; Kanbara, T.; Takenobu, T.; Iwasa, Y. *Jpn. J. Appl. Phys., Part 2* **2007**, *46*, L571.
(314) Gruner, G. *Anal. Bioanal. Chem.* **2006**, *384*, 322.
(315) Bradley, K.; Davis, A.; Gabriel, J. C. P.; Gruner, G. *Nano Lett.* **2005**, *5*, 841.
(316) Blackburn, J. L.; Barnes, T. M.; Beard, M. C.; Kim, Y. H.; Tenent, R. C.; McDonald, T. J.; To, B.; Coutts, T. J.; Heben, M. J. *ACS Nano* **2008**, *2*, 1266.
(317) Wu, Z. C.; Chen, Z. H.; Du, X.; Logan, J. M.; Sippel, J.; Nikolou, M.; Kamaras, K.; Reynolds, J. R.; Tanner, D. B.; Hebard, A. F.; Rinzler, A. G. *Science* **2004**, *305*, 1273.
(318) An, K. H.; Jeon, K. K.; Heo, J. K.; Lim, S. C.; Bae, D. J.; Lee, Y. H. *J. Electrochem. Soc.* **2002**, *149*, A1058.
(319) Gupta, V.; Miura, N. *Electrochim. Acta* **2006**, *52*, 1721.
(320) Kaempgen, M.; Chan, C. K.; Ma, J.; Cui, Y.; Gruner, G. *Nano Lett.* **2009**, *9*, 1872.
(321) Dimitrakopoulos, C. D.; Malefant, P. R. L. *Adv. Mater.* **2002**, *14*, 99.
(322) Tortai, J. H.; Bonifaci, N.; Denat, A.; Trassy, C. *J. Appl. Phys.* **2005**, *97*, 053304.
(323) Shim, M.; Javey, A.; Kam, N. W. S.; Dai, H. J. *J. Am. Chem. Soc.* **2001**, *123*, 11512.
(324) Siddons, G. P.; Merchin, D.; Back, J. H.; Jeong, J. K.; Shim, M. *Nano Lett.* **2004**, *4*, 927.
(325) Manohara, H. M.; Wong, E. W.; Schlecht, E.; Hunt, B. D.; Siegel, P. H. *Nano Lett.* **2005**, *5*, 1469.
(326) Topinka, M. A.; Rowell, M. W.; Goldhaber-Gordon, D.; McGehee, M. D.; Hecht, D. S.; Gruner, G. *Nano Lett.* **2009**, *9*, 1866.
(327) Appenzeller, J.; Knoch, J.; Radosavljevic, M.; Avouris, P. *Phys. Rev. Lett.* **2004**, *92*, 226802.
(328) Koswatta, S. O.; Lundstrom, M. S.; Nikonov, D. E. *Nano Lett.* **2007**, *7*, 1160.
(329) Schindler, A.; Spiessberger, S.; Hergert, S.; Fruehauf, N.; Novak, J. P.; Yaniv, Z. *Physica E* **2007**, *37*, 119.
(330) Tans, S. J.; Verschueren, A. R. M.; Dekker, C. *Nature* **1998**, *393*, 49.
(331) Bachtold, A.; Hadley, P.; Nakanishi, T.; Dekker, C. *Science* **2001**, *294*, 1317.
(332) Chattopadhyay, D.; Galeska, L.; Papadimitrakopoulos, F. *J. Am. Chem. Soc.* **2003**, *125*, 3370.
(333) Krupke, R.; Hennrich, F.; von Lohneysen, H.; Kappes, M. M. *Science* **2003**, *301*, 344.
(334) An, L.; Fu, Q. A.; Lu, C. G.; Liu, J. *J. Am. Chem. Soc.* **2004**, *126*, 10520.
(335) Li, Y. M.; Mann, D.; Rolandi, M.; Kim, W.; Ural, A.; Hung, S.; Javey, A.; Cao, J.; Wang, D. W.; Yenilmez, E.; Wang, Q.; Gibbons, J. F.; Nishi, Y.; Dai, H. J. *Nano Lett.* **2004**, *4*, 317.
(336) Kanungo, M.; Lu, H.; Malliaras, G. G.; Blanchet, G. B. *Science* **2009**, *323*, 234.
(337) Wong, W. S.; Salleo, A. *Flexible Electronics*; Springer: New York, 2009,.
(338) Snow, E. S. C., P. M.; Ancona, M. G. *Appl. Phys. Lett.* **2005**, *86*, 033105.
(339) Hur, S. H.; Yoon, M. H.; Gaur, A.; Shim, M.; Facchetti, A.; Marks, T. J.; Rogers, J. A. *J. Am. Chem. Soc.* **2005**, *127*, 13808.
(340) Estrada, D.; Dutta, S.; Liao, A.; Pop, E. *Nanotechnology* **2010**, *21*, 5702.
(341) Kim, W.; Javey, A.; Vermesh, O.; Wang, O.; Li, Y. M.; Dai, H. J. *Nano Lett.* **2003**, *3*, 193.
(342) McGill, S. A.; Rao, S. G.; Manandhar, P.; Xiong, P.; Hong, S. *Appl. Phys. Lett.* **2006**, *89*, 163123.
(343) Artukovic, E. K., M.; Hecht, D. S.; Roth, S.; Gruner, G. *Nano Lett.* **2005**, *5*, 757.
(344) Shiraishi, M.; Nakamura, S.; Fukao, T.; Takenobu, T.; Kataura, H.; Iwasa, Y. *Appl. Phys. Lett.* **2005**, *87*, 093107.
(345) Bradley, K.; Gabriel, J. C. P.; Gruner, G. *Nano Lett.* **2003**, *3*, 1353.
(346) Besteman, K.; Lee, J. O.; Wiertz, F. G. M.; Heering, H. A.; Dekker, C. *Nano Lett.* **2003**, *3*, 727.
(347) Han, L.; Wu, W.; Kirk, F. L.; Luo, J.; Maye, M. M.; Kariuki, N. N.; Lin, Y. H.; Wang, C. M.; Zhong, C. J. *Langmuir* **2004**, *20*, 6019.
(348) Staii, C.; Johnson, A. T. *Nano Lett.* **2005**, *5*, 1774.
(349) Robinson, J. A.; Snow, E. S.; Badescu, S. C.; Reinecke, T. L.; Perkins, F. K. *Nano Lett.* **2006**, *6*, 1747.
(350) Snow, E. S.; Perkins, F. K.; Houser, E. J.; Badescu, S. C.; Reinecke, T. L. *Science* **2005**, *307*, 1942.
(351) Allen, B. L.; Kichambare, P. D.; Star, A. *Adv. Mater.* **2007**, *19*, 1439.
(352) Bradley, K.; Briman, M.; Star, A.; Gruner, G. *Nano Lett.* **2004**, *4*, 253.
(353) Kauffman, D. R.; Star, A. *Chem. Soc. Rev.* **2008**, *37*, 1197.
(354) Tasis, D.; Tagmatarchis, N.; Bianco, A.; Prato, M. *Chem. Rev.* **2006**, *106*, 1105.
(355) Ferrer-Anglada, N.; Kaempgen, M.; Roth, S. *Phys. Status Solidi B* **2006**, *243*, 3519.
(356) Cattanach, K.; Kulkarni, R. D.; Kozlov, M.; Manohar, S. K. *Nanotechnology* **2006**, *17*, 4123.
(357) Ginley, D. S.; Bright, C. *Mater. Res. Bull.* **2000**, *25*, 15.
(358) Lewis, B. G.; Paine, D. C. *Mater. Res. Bull.* **2000**, *25*, 22.
(359) Gordon, R. *Mater. Res. Bull.* **2000**, *25*, 52.
(360) Fortunato, E.; Ginley, D.; Hosono, H.; Paine, D. C. *Mater. Res. Bull.* **2007**, *32*, 242.
(361) Kumar, A.; Welsh, D. M.; Morvant, M. C.; Piroux, F.; Abboud, K. A.; Reynolds, J. R. *Chem. Mater.* **1998**, *10*, 896.
(362) Kim, J. Y.; Jung, J. H.; Lee, D. E.; Joo, J. *Synth. Met.* **2002**, *126*, 311.
(363) Kirchmeyer, S.; Reuter, K. *J. Mater. Chem.* **2005**, *15*, 2077.
(364) Zhu, W.; Bower, C.; Zhou, O.; Kochanski, G.; Jin, S. *Appl. Phys. Lett.* **1999**, *75*, 873.
(365) Cao, Q.; Zhu, Z. T.; Lemaitre, M. G.; Xia, M. G.; Shim, M.; Rogers, J. A. *Appl. Phys. Lett.* **2006**, 88.
(366) Wu, J. B.; Becerril, H. A.; Bao, Z. N.; Liu, Z. F.; Chen, Y. S.; Peumans, P. *Appl. Phys. Lett.* **2008**, *92*, 263302.
(367) Eda, G.; Fanchini, G.; Chhowalla, M. *Nat. Nanotechnol.* **2008**, *3*, 270.
(368) Wang, X.; Zhi, L. J.; Mullen, K. *Nano Lett.* **2008**, *8*, 323.
(369) Kang, M. G.; Guo, L. J. *Adv. Mater.* **2007**, *19*, 1391.
(370) Pode, R. B.; Lee, C. J.; Moon, D. G.; Han, J. I. *Appl. Phys. Lett.* **2004**, *84*, 4614.

(371) Kang, M. G.; Guo, L. J. *J. Vac. Sci. Technol., B* **2007**, *25*, 2637.
(372) Park, J. U.; Hardy, M.; Kang, S. J.; Barton, K.; Adair, K.; Mukhopadhyay, D. K.; Lee, C. Y.; Strano, M. S.; Alleyne, A. G.; Georgiadis, J. G.; Ferreira, P. M.; Rogers, J. A. *Nat. Mater.* **2007**, *6*, 782.
(373) Hong, W. J.; Xu, Y. X.; Lu, G. W.; Li, C.; Shi, G. Q. *Electrochem. Commun.* **2008**, *10*, 1555.
(374) Becerril, H. A.; Mao, J.; Liu, Z.; Stoltenberg, R. M.; Bao, Z.; Chen, Y. *ACS Nano* **2008**, *2*, 463.
(375) Sgobba, V.; Guldi, D. M. *J. Mater. Chem.* **2008**, *18*, 153.
(376) Guldi, D. M.; Rahman, G. M. A.; Prato, M.; Jux, N.; Qin, S. H.; Ford, W. *Angew. Chem., Int. Ed.* **2005**, *44*, 2015.
(377) Landi, B. J.; Raffaelle, R. P.; Castro, S. L.; Bailey, S. G. *Prog. Photovolt.* **2005**, *13*, 165.
(378) Jia, Y.; Wei, J. Q.; Wang, K. L.; Cao, A. Y.; Shu, Q. K.; Gui, X. C.; Zhu, Y. Q.; Zhuang, D. M.; Zhang, G.; Ma, B. B.; Wang, L. D.; Liu, W. J.; Wang, Z. C.; Luo, J. B.; Wu, D. *Adv. Mater.* **2008**, *20*, 4594.
(379) Hatton, R. A.; Blanchard, N. P.; Tan, L. W.; Latini, G.; Cacialli, F.; Silva, S. R. P. *Org. Electron.* **2009**, *10*, 388.
(380) Miller, A. J.; Hatton, R. A.; Chen, G. Y.; Silva, S. R. P. *Appl. Phys. Lett.* **2007**, *90*, 023105.
(381) Miller, A. J.; Hatton, R. A.; Silva, S. R. P. *Appl. Phys. Lett.* **2006**, *89*, 133117.
(382) van de Lagemaat, J.; Barnes, T. M.; Rumbles, G.; Shaheen, S. E.; Coutts, T. J.; Weeks, C.; Levitsky, I.; Peltola, J.; Glatkowski, P. *Appl. Phys. Lett.* **2006**, *88*, 233503.
(383) Contreras, M. B., T.; van de Lagemaat, J.; Rumbles, G.; Coutts, T. J. 2006 IEEE 4th World Conference on Photovoltaic Energy Conversion (WCPEC-4) Waikoloa, Hawaii, May 7−12, 2006.
(384) Williams, C. D.; Robles, R. O.; Zhang, M.; Li, S.; Baughman, R. H.; Zakhidov, A. A. *Appl. Phys. Lett.* **2008**, 93.
(385) Chhowalla, M. *J. Soc. Inf. Disp.* **2007**, *15*, 1085.
(386) Aguirre, C. M.; Auvray, S.; Pigeon, S.; Izquierdo, R.; Desjardins, P.; Martel, R. *Appl. Phys. Lett.* **2006**, *88*, 183104.
(387) Veinot, J. G. C.; Marks, T. J. *Acc. Chem. Res.* **2005**, *38*, 632.
(388) Chen, C. T. *Chem. Mater.* **2004**, *16*, 4389.
(389) Shim, H. K.; Jin, J. I. *Polym. Electron. Photonic Appl.* **2002**, 158.
(390) Mitschke, U.; Bauerle, P. *J. Mater. Chem.* **2000**, *10*, 1471.
(391) Pickering, J. A. *Int. J. Man-Mach. Stud.* **1986**, *25*, 249.
(392) King, R. C. Y.; Roussel, F. *Appl. Phys. A: Mater. Sci. Process.* **2007**, *86*, 159.
(393) Luo, J.; Glatkowski, P.; Wallis, P. U.S. Patent 0209392, 2005.
(394) Pauluth, D.; Tarumi, K. *J. Mater. Chem.* **2004**, *14*, 1219.
(395) Hayes, R. A.; Feenstra, B. J. *Nature* **2003**, *425*, 383.
(396) Rogers, J. A.; Bao, Z.; Baldwin, K.; Dodabalapur, A.; Crone, B.; Raju, V. R.; Kuck, V.; Katz, H.; Amundson, K.; Ewing, J.; Drzaic, P. *Proc. Natl. Acad. Sci. U.S.A.* **2001**, *98*, 4835.
(397) Schadt, M. *Annu. Rev. Mater. Sci.* **1997**, *27*, 305.
(398) Sarkar, P.; Nicholson, P. S. *J. Am. Ceram. Soc.* **1996**, *79*, 1987.
(399) Park, Y. H., L.; Gruner, G.; Irvin, G.; Drzaic, P. *SID Digest* **2008**, *37*, 537.
(400) Al-Salehi, M. H.; Sundararaj, U. *Carbon* **2009**, *47*, 1738.
(401) Das, N. C.; Maiti, S. *J. Mater. Sci.* **2008**, *43*, 1920.
(402) Liu, Z. F.; Bai, G.; Huang, Y.; Ma, Y. F.; Du, F.; Li, F. F.; Guo, T. Y.; Chen, Y. S. *Carbon* **2007**, *45*, 821.
(403) Li, N.; Huang, Y.; Du, F.; He, X. B.; Lin, X.; Gao, H. J.; Ma, Y. F.; Li, F. F.; Chen, Y. S.; Eklund, P. C. *Nano Lett.* **2006**, *6*, 1141.
(404) Watson, K. A.; Ghose, S.; Delozier, D. M.; Smith, J. G.; Connell, J. W. *Polymer* **2005**, *46*, 2076.
(405) Lee, B. O.; Woo, W. J.; Kim, M. S. *Macromol. Mater. Eng.* **2001**, *286*, 114.
(406) Das, N. C.; Khastgir, D.; Chaki, T. K.; Chakraborty, A. *Composites, Part A* **2000**, *31*, 1069.
(407) Booth, J. C.; Wu, D. H.; Qadri, S. B.; Skelton, E. F.; Osofsky, M. S.; Pique, A.; Anlage, S. M. *Phys. Rev. Lett.* **1996**, *77*, 4438.
(408) Yuan, W.; Hu, L. B.; Yu, Z. B.; Lam, T. L.; Biggs, J.; Ha, S. M.; Xi, D. J.; Chen, B.; Senesky, M. K.; Gruner, G.; Pei, Q. B. *Adv. Mater.* **2008**, *20*, 621.
(409) Bonard, J. M.; Klinke, C.; Dean, K. A.; Coll, B. F. *Phys. Rev. B* **2003**, *67*, 115406.
(410) Zhao, Z. G.; Li, F.; Liu, C.; Cheng, H. M. *J. Appl. Phys.* **2005**, *98*, 044306.
(411) Ajayan, P. M.; Ramanath, G.; Terrones, M.; Ebbesen, T. W. *Science* **2002**, *297*, 192.
(412) Lee, K.; Wu, Z.; Chen, Z.; Ren, F.; Pearton, S. J.; Rinzler, A. G. *Nano Lett.* **2004**, *4*, 911.
(413) Xiao, L.; Chen, Z.; Feng, C.; Liu, L.; Bai, Z. Q.; Wang, Y.; Qian, L.; Zhang, Y. Y.; Li, Q. Q.; Jiang, K. L.; Fan, S. S. *Nano Lett.* **2008**, *8*, 4539.
(414) Yoo, Y. H.; Song, J. W.; Kim, J.; Park, J. K.; Oh, S. K.; Han, C. S. *Adv. Mater.* **2007**, *19*, 4284.
(415) Conway, B. E. *Electrochemical Supercapacitors: Scientific Fundamentals and Technological Applications*; Springer: New York, 1999.
(416) Frackowiak, E.; Beguin, F. *Carbon* **2002**, *40*, 1775.
(417) Mayer, S. T.; Pekala, R. W.; Kaschmitter, J. L. *J. Electrochem. Soc.* **1993**, *140*, 446.
(418) Masarapu, C. Z., H. F.; Hung, K. H.; Wei, B. *ACS Nano* **2009**, *3*, 2199.
(419) Chen, P. S., G.; Sukcharoenchoke, S.; Zhou, C. *Appl. Phys. Lett.* **2009**, *94*, 43313.
(420) Kiebele, A.; Gruner, G. *Appl. Phys. Lett.* **2007**, *91*, 144104.

CR9002962